Archeomagnetic intensity investigations of French medieval ceramic workshops: Contribution to regional field modeling and archeointensity-based dating

Agnès Genevey, Yves Gallet, Erwan Thébault, Philip W. Livermore, Alexandre Fournier, Sébastien Jesset, Annie Lefèvre, Nadine Mahé-Hourlier, Emmanuel Marot, Stéphane Regnard

▶ **To cite this version:**

Agnès Genevey, Yves Gallet, Erwan Thébault, Philip W. Livermore, Alexandre Fournier, et al.. Archeomagnetic intensity investigations of French medieval ceramic workshops: Contribution to regional field modeling and archeointensity-based dating. Physics of the Earth and Planetary Interiors, 2021, 318, pp.106750. 10.1016/j.pepi.2021.106750 . hal-03284542

HAL Id: hal-03284542
https://hal.science/hal-03284542v1

Submitted on 8 Nov 2021

HAL is a multi-disciplinary open access archive for the deposit and dissemination of scientific research documents, whether they are published or not. The documents may come from teaching and research institutions in France or abroad, or from public or private research centers.

L'archive ouverte pluridisciplinaire **HAL**, est destinée au dépôt et à la diffusion de documents scientifiques de niveau recherche, publiés ou non, émanant des établissements d'enseignement et de recherche français ou étrangers, des laboratoires publics ou privés.

Distributed under a Creative Commons Attribution - NonCommercial - NoDerivatives 4.0 International License

Archeomagnetic intensity investigations of French Medieval ceramic workshops: Contribution to regional field modeling and archeointensity-based dating

A. Genevey[1], Y Gallet[2], E. Thébault[3], P. W. Livermore[4], A. Fournier[2], S. Jesset[5], A. Lefèvre[6], N. Mahé-Hourlier[7], E. Marot[8], S. Regnard[9]

[1]Sorbonne Université, CNRS, Laboratoire d'Archéologie Moléculaire et Structurale, LAMS, F-75005 Paris, France

[2]Université de Paris, Institut de Physique du Globe de Paris, CNRS, F-75005 Paris, France

[3]Université Clermont Auvergne, CNRS, IRD, OPGC, Laboratoire Magmas et Volcans, F-63000 Clermont-Ferrand, France

[4]School of Earth & Environment, University of Leeds, Leeds, UK

[5]Pôle d'Archéologie Ville d'Orléans, F-45000 Orléans, France

[6]Institut national de recherches archéologiques préventives, Centre de recherches archéologiques de la Courneuve, F-93126 La Courneuve, France

[7]Institut national de recherches archéologiques préventives, Centre de recherches archéologiques de Passy, F-89510 Passy, France

[8]Bourges Plus, Service d'archéologie préventive, F-18000 Bourges, France

[9]Centre de recherches archéologiques du Vexin français, F-95450 Guiry-en-Vexin, France

Keywords

Archeointensity, Medieval period, Western Europe, Field intensity modeling, Archeointensity dating

Highlights

- 7 new Triaxe archeointensity data are obtained from French medieval pottery workshops
- They allow a refinement of the evolution of intensities during the High Middle Ages
- A set of available intensity data is re-examined based on cooling rate correction
- We illustrate the sensitivity of regional intensity models to modeling strategies
- We discuss two different procedures for archeointensity dating

Abstract

Seven new archeointensity data are obtained through the analysis of groups of pottery and kiln fragments from ceramic workshops unearthed in France, precisely dated from the High Middle Ages. The measurements are carried out using the Triaxe magnetometer, following a dedicated experimental protocol that takes into account the effects of anisotropy and cooling rate (CR) on thermoremanent magnetization acquisition. The new data are consistent with the evolution of intensity variations described by our previous data obtained in France and Northern Italy, which display between the 5th and 10th c. a pronounced camel-back shape. In particular, they provide supporting evidence of an intensity minimum that occurred around the transition between the 7th and 8th century. These data, combined with a selection of previously published results within a 700 km radius of Beaune and re-examined based on CR correction, formed the basis of new regional mean intensity variation curves based on two independent modeling approaches. The first algorithm developed by Thébault and Gallet (2010) based on bootstrapping and now irregularly spaced knots according to the data distribution gives rather smooth intensity variations, while the second approach proposed by Livermore et al (2018) based on a transdimensional Bayesian technique shows more abrupt variations with sometimes stronger amplitudes. We explore the dating potential of these two

variations curves, which have an unprecedented resolution, by studying two medieval pottery workshops. Six fragment groups (three per workshop) are analyzed using the Triaxe protocol, providing mean archeointensity values for each of the two sites. Two different procedures are used for their dating, either by comparing the intensity value to be dated with the reference intensity variation curves obtained from the two modeling techniques or by analyzing the marginal posterior probability distribution of the age values derived from the method of Livermore et al (2018). For France, the two techniques yield very similar results. The archeointensity dating results combined with archeological arguments and radiocarbon data, make it possible to better constrain the age of the end of activity of the two workshops. Archeointensity investigation of displaced materials thus appears as an effective means to obtain original chronological constraints on the age of their production, paving the way for a wide range of complementary research on Medieval pottery.

1. Introduction

Archeomagnetism is a method now commonly implemented in the field of archeology throughout the European area to provide chronological constraints on fired clay artifacts whose dating requires refinement. This tool is based on the use of local reference curves of the temporal variations of the geomagnetic field in direction and/or intensity, either directly obtained from the analysis of numerous dated structures in the region of interest, or, when not available, deduced from regional or even global time-dependent geomagnetic field models. In Europe, one may rely on the regional SCHA-DIF.4K field model covering the past four millennia recently constructed by Pavón-Carrasco et al. (2021), which updates and extends the previous SCHA-DIF.3K model (Pavón-Carrasco et al. 2009). The following studies indicate the breadth of existing research and interests in a variety of European countries: Belgium, Ech-Chakrouni et al. (2013); Bulgaria, Herries et al. (2008); England, Batt et al.

(2017); France, Gallet et al. (2009) and Hervé and Lanos (2017); Austria, Schnepp et al. (2015); Greece, Aidona et al. (2017); Italy, Tema et al. (2014) and Principe et al. (2018); Spain, Gómez-Paccard and Beamud (2008) and Catanzariti et al. (2007).

In France, archeomagnetism is so well integrated into the archeological fabric that this method is now included in the prescription files of preventive (rescue) excavations when heating structures are detected in situ at the time of archeological diagnosis prior to excavation. In the archeomagnetic laboratory founded in the 1930s by Emile Thellier in Saint-Maur, for instance, several hundred pottery and domestic kilns have been studied since the early 1990s, and the results used for dating purposes based on the reference directional variation curve available for the past two millennia (i.e. Thellier, 1981, Bucur, 1994, Gallet et al. 2002, Le Goff et al., 2002; 2020 in this volume).

Compared to in-situ burnt structures, the materials discovered displaced from the location where they were fired have been much less investigated archeomagnetically, in particular with the purpose of providing chronological constraints. However, archeomagnetic studies of large ensembles of architectural bricks or tiles have made it possible to refine the age of buildings from the inclination information (e.g. Lanos, 2019). On the other hand, the possibility of using the archeointensity as the only dating element for displaced objects has not yet been really exploited (Gallet et al., 2014a; Shaar et al., 2020). There are two main reasons for this: firstly, intensity data have long remained much less numerous than directional data and knowledge of intensity variations was thus very fragmentary. Secondly, and despite significant progress in intensity data acquisition all over Europe, the available data often show a dispersion that de facto limits their application for dating. A recent study by Casas and Tema (2019) explored the dating potential in Europe of the SCHA-DIF.3K model and highlighted the low added value of intensity measurements for dating. France, however, benefits from a relatively dense archeointensity dataset covering the past 1600 years, showing

101 little dispersion (Genevey et al., 2009; 2013; 2016; 2019). These results describe smooth
102 millennial-scale variations punctuated by a pseudo-periodic (~260 years) succession of
103 intensity peaks of roughly the same amplitude and each lasting ~200 years (Genevey et al.,
104 2016; Livermore et al., 2018). Maxima are observed at the beginning of the 7th c., during the
105 9th c., the 12th c., at the end of the 14th c. and at the beginning of the 17th century. Genevey et
106 al. (2016) suggested that this recurrence in intensity peaks could be related to a wave motion
107 at the top of the core, for example due to stable stratification (see discussion in, e.g., Buffett et
108 al., 2016). Although the reality of these peaks seems now well established, their description
109 needs to be improved through the acquisition of new data. A densification of the
110 archeointensity database is therefore still required, with the same effort being made for the
111 archeomagnetic directions (see for instance Le Goff et al., 2020 in this volume).
112 With this objective, we present seven new Medieval archeointensity results obtained
113 from the analysis of precisely dated groups of pottery and kiln fragments. These results allow
114 a refinement of the reference intensity variation curve available in France. We then explore
115 the potential of this curve for dating purposes through the study of two ceramic production
116 sites of the High Middle Ages located in the Centre and Ile-de-France regions. The
117 construction of the reference curve of geomagnetic field intensities and archeomagnetic
118 dating are both carried out using two different techniques (Thébault and Gallet, 2010;
119 Livermore et al., 2018), which allows us to compare them and to illustrate the implications of
120 selecting one single regional modeling and/or dating option rather than the other.
121
122 **2. Description of the collected archeological fragments.**
123 **2.1 Dated ceramic sets**
124 Among the new groups of fragments, five come from two ceramic production areas largely
125 exploited in our previous intensity studies i.e. Saran in the Centre region of France and

126 Vanves located close to Paris, in the Ile de France region (Fig. 1a). At Saran, the analysis of
127 groups SAR19 and SAR21 completes the archeointensity study of the material from the
128 excavation zone known as La Guignace (Bouillon, 2015). Another group (SAR36) is
129 associated with a small production unit known as “la voie nouvelle”, which was discovered
130 more recently and dated from the first half of the 7th century (Jesset, to be published). The two
131 groups from Vanves, referred to as VAN03 and VAN09, come from the excavations
132 conducted in Rue Gaudray (Lefèvre and Peixoto, 2015), from which some materials were
133 already studied for archeointensity (Gallet et al. 2009; Genevey et al. 2016). The VAN03
134 group has been re-sampled with fragments taken from almost complete pots isolated by A.
135 Lefèvre because they have a morphology typical of the production of the associated kiln. The
136 numbering of the fragments from this group thus starts at number 23 (Supp. Table1). The
137 dating of these five groups is mainly based on typo-chronological constraints previously
138 described in Genevey et al. (2016). For that reason, we exclusively collected fragments of
139 pottery lips whose shape is clearly identified and characteristic of the production.
140 The other groups are associated with two ceramic production sites recently unearthed
141 and both located in the Ile-de-France region, at Hermé (c. 85 km south-east of Paris) and
142 Chamigny (c. 60 km east of Paris, Fig. 1a). The rescue excavations at the site known as
143 “Hermé Les Malletons (S.P.M. carrière)” were carried out in 2014 by the French National
144 Institute for Preventive Archeological Research (INRAP), being motivated by the
145 establishment of a new quarry. These excavations revealed a discontinuous occupation of the
146 site from Prehistory to the beginning of the 11th c. (Chaudriller, 2019). Focusing on the High
147 Middle Ages period, the site was a rural settlement during the 7th c. with a husbandry activity.
148 Towards the middle of the 9th c. the site evolved and two types of workshop were developed,
149 linked to metallurgical and ceramic productions. Four pottery kilns document this later
150 activity. Three phases of production were evidenced: during the second half of the 9th c., at

151 the beginning of the 10th c., and finally around the end of the 10th century. Only the last two
152 phases were sampled for archeointensity analysis. Three groups of ceramic fragments (called
153 HERME01 to HERME03) are respectively associated with the productions of kilns F1621
154 and F3160 of the intermediate phase (beginning of the 10th c.) and with kiln F3060 of the last
155 phase (end of the 10th c.). Unfortunately, none of these pottery fragments provided
156 archeointensity results (*infra.*). For the last phase, we doubled the sampling with a group of
157 fragments collected from Kiln 3060 (HERME04). The fragments were taken all along the
158 central tongue support of the kiln particularly well preserved and made of limestone covered
159 with a thin clay layer (Fig. 1b). The potsherds that were found inside the kiln show a clear
160 rupture with respect to the previous productions of the site, whether it concerns the profile,
161 the edge, or the handle of the pots. Based on the form of the pottery, all fragments were dated
162 prior to the end of the 10th century and a dating between c. 970 and 1000 is thus retained for
163 the last activity of the kiln (and thus for the HERME04 group). It should be noted that
164 archeomagnetic dating based on directions was conducted on the same kiln (N. Warmé in
165 Chaudriller, 2019). A 95%-confidence level dating between 900 and 1080 was obtained using
166 the new reference curve determined by Le Goff et al. (2020 in this volume). Within this time
167 window, the interval [940-990] appears however as being the most probable with a maximum
168 probability c. 960 (see description of the method in Le Goff et al., 2002), which is in good
169 agreement with the ceramological constraints.

170 At Chamigny, the excavations at the place called "la grande maison" are recent,
171 carried out in the summer of 2017. Conducted by INRAP, they were prescribed following a
172 project for the construction of individual houses. Two distinct occupation phases have been
173 observed on this site: The first is dated to the Neolithic period, then, after a long period of
174 abandonment, a re-occupation is documented from the end of the 6th-early 7th c. until the end
175 of the 10th century (Mahé, 2020). It is mainly characterized by metallurgical and pottery

activities. Several groups of fragments from the different pottery production units (five kilns in total) were sampled for archeointensity measurements but only one group (CHAM03) has provided successful results so far. This group consists of fragments from the working area of kiln 2629 (Fig. 1c). The dating of this production is constrained by morphological and stylistic elements given by the numerous fragments found inside the kiln. Among other elements, one may mention the absence of carinated bowls, the importance of deep shapes with short collar and re-entrant rim or jugs with a shamrock-shaped tubular spout. They indicate a dating around the end of the 7th c. - very beginning of the 8th century (Mahé, 2020).

2.2 Sets of ceramics collected in order to provide chronological constraints

The first site studied was excavated during the fall-winter of 2015-2016 by the archeological service of the urban community of the city of Bourges (in the center of France, Fig. 1a). These excavations were carried out before the construction of a housing estate in the city La Chapelle Saint Ursin (Bourges's suburbs) at the place called "l'angoulaire, chemin des vallées aux fruscades" (Marot, 2017). This site mainly revealed the existence of a Roman villa constructed *ex nihilo* at the beginning of the 1st century AD. The villa remained in activity until the 6th c. with successive modifications and enlargements. The last phase saw the installation of a small ceramic production unit for the inhabitants of the villa and surrounding area. The objective of our work was to provide chronological constraints about the end of this pottery activity. To this purpose, we sampled fragments of pottery characteristic of the production found in the kiln, as well as fragments of the kiln itself. For the pottery, two groups were collected corresponding to pottery wasters showing deformations for the first set (BOUR01), and evidence of overfiring for the second (BOUR02). The samples from the kiln itself correspond to fired clay fragments from the dome that were found in the filling

(BOUR03). It may be stressed that no archeomagnetic directional study was carried out at the time of the excavations.

The second site was excavated in 1997 after the fortuitous discovery of a burial site on private land in Vienne-en-Arthies in the hamlet of Chaudry (50 km northwest of Paris, Fig. 1a). The excavations, made over a small area, were entrusted to the Centre de Recherches Archéologiques du Vexin Français (CRAVF; Regnard 1999). They revealed the existence of a pottery kiln of which only the heating chamber was unearthed (the rest of the kiln being located outside the excavated area). It was filled by a largely standardized ceramic production of pots for cooking, with a mainly sandy and, to a lesser extent, granular paste. This site is the only witness currently known of a production in the Vexin Français region (Fig. 1a: area in yellow) during the Carolingian period, although archeologists presume the existence of a more important pottery production in this region. Three groups of potsherds were selected with the objective of better constraining the period of activity of this pottery production, especially its end. The first two groups consist of fragments with a grey sandy paste (CHAU01) and grey-brown sandy paste (CHAU02) which are typical of this production, while the last group comprises fragments with red granular re-baked paste (CHAU03). These later potsherds were most probably used for the construction of the kiln. We note that this kiln, only partially excavated, was not sampled for archeomagnetic directional analysis.

3. Measurements workflow

The workflow in this study is identical in all respects to the one used in our previous archeointensity studies conducted on Western European artifacts (Genevey et al. 2009, 2013, 2016, 2019). All experiments were carried out at the paleomagnetic laboratory of the Institut de Physique du Globe de Paris (IPGP).

The evolution of magnetic susceptibility in weak field was first measured for each fragment during heating-cooling cycles between room temperature and c. 500°C. These measurements were performed using an Agico Kappabridge KLY3-S coupled with a CS3 furnace. The reversibility of the susceptibility curves, evaluated visually, allowed the selection of the fragments that are *a priori* most favorable for intensity measurements (carried out over the same temperature range).

For each fragment, a first specimen was then measured for intensity determination using the Triaxe protocol. If the observed behavior met our quality criteria or was promising for intensity determination, other specimens were then measured. This is also the case if the chosen temperature range was not adequate for the first specimen. The Triaxe experimental method and our quality criteria have been extensively detailed in previous publications (e.g. Le Goff and Gallet, 2004, Gallet and Le Goff, 2006, Genevey et al., 2009, Hartmann et al., 2010, Gallet et al. 2014b) and recently by Troyano et al. (2021 in this volume). We remind the reader that the magnetization measurements are performed automatically at high temperatures following a protocol that takes into account the anisotropy and cooling rate effects on thermoremanent remanent magnetization (TRM) acquisition, and minimizes possible effect related to the presence of multidomain grains (Genevey et al., 2009, Hartmann et al., 2010; 2011, Hervé et al., 2017, Shaar et al., 2020). As for the quality criteria, they aim to test the stability on heating of the magnetic mineralogy (thanks in particular to magnetic susceptibility vs. temperature curves), the quality of the individual determination and the consistency of the results both at the fragment (with a minimum of two specimens per fragment and an error between them of less than 5%) and fragment group levels. A minimum of three fragments successfully analyzed per group and an error on the mean intensity value of less than 10% and 5μT are required. The purpose of the 5%-coherence test is to exclude fragments for which we can suspect a reliability problem in the recording of the geomagnetic

signal. At the site level, our quality criteria aim mainly at assessing the temporal homogeneity of the fragments forming a group.

After the archeointensity experiments, a fragment from each retained group was subjected to Lowrie's (1990) test to provide further constraints on the magnetic mineralogy of the archeological collection. The three orthogonal IRM were acquired in a field of 1.5T, 0.4T and 0.2T using a pulse magnetometer MMPM10.

4. Results

We analyzed 157 ceramic shards and two groups of kiln fragments. Applying our quality criteria, three groups (SAR19, SAR21 and HERME04) yield a reasonable success rate between 50% and 60%. For the rest of the collection, the rate is lower, ranging between 16% and 36%, the lowest percentages being obtained for the groups studied for dating (i.e. BOUR# and CHAU#). It should be noted that these rates were calculated in relation to the number of fragments actually measured on the Triaxe. Several fragments were indeed too weakly magnetized (<~30 10^{-8} Am^2) with respect to the sensitivity of this magnetometer (Supp. Table 1).

The mean intensity values obtained for the different groups of fragments are reported in Table 1. Here the groups BOUR01 and BOUR02 on one hand, and CHAU01 and CHAU02 on the other hand have been merged for the computation of a mean value as these pairs are representative of the same pottery production. The eleven mean values hence determined are well defined with a maximum standard deviation of 2.9μT (or 3.9% of the corresponding mean; BOUR01/02 group). The consistency of the intensity results for each group of fragments is further shown in Figure 2, which presents the data at the specimen level obtained for six different groups of pottery (SAR36, CHAM03, BOUR01/02 and CHAU01/02) and kiln fragments (HERME04; BOUR03). Concerning the BOUR03 group, which consists of

fired clay fragments from the kiln dome, significant variations in colour were observed at the fragment scale, from bright red, to wine-red and brown. Of the 33 specimens tested, only the browns provided suitable results. For HERME04, the 30 specimens analyzed were taken exclusively from the limestone part of the fragments. The thin clay layer was indeed too weakly magnetized to allow analyses using the Triaxe. Such weak magnetization appears to be a characteristic of the majority of the potsherds collected at Hermé. Other shards from this site were further discarded due to strong alteration detected during the magnetic susceptibility measurements with the consequence, as previously mentioned, that no intensity results were obtained for the Hermé pottery production.

The alteration of the magnetic mineralogy revealed by the non-reversibility between the heating and cooling magnetic susceptibility curves is one of the reasons for the exclusion of several fragments (Figs. 3a,b). In almost equal proportions (i.e., 16% versus 14%), fragments were also discarded when it was impossible to isolate reliably their primary magnetization component. This is illustrated in Figure 3c where the thermal demagnetization of specimen CHAU01-10A reveals two magnetization components with widely overlapping unblocking temperature spectra, which prevented the ancient TRM from being clearly isolated. In the intensity diagram, this results in complex evolutions in the R'(Ti) data between T1 (or T1') and T2, with significantly varying values (Fig. 3d). In general, however, most failures in intensity determination at the specimen level (70%) are related to "non-ideal" Triaxe behavior, as defined by our quality criteria, observed in the intensity diagrams, i.e., with non-constant R'(Ti) ratios over the temperature range where the primary magnetization is isolated. Specimen HERM04-08A illustrates this problem with a single component demagnetized between 150°C to 520°C (Fig. 3e) while decreasing R'(Ti) ratios are observed over the same temperature range (Fig. 3f). In rare other cases, the R'(Ti) ratios have a concave shape, also leading to the rejection of the specimen.

The thermal demagnetization of the 3-axis IRMs (recall that one fragment among those successfully analyzed was chosen for each group) shows a very classical magnetic mineralogy for baked clay artifacts (Fig. 4). The latter is first characterized by the predominance of low coercivity minerals (less than 0.2 T) with unblocking temperatures of less than 600 °C. These minerals are likely from the magnetite family with a different level of impurities. The thermal demagnetization of the hard component (1.25 T) also indicates the presence in various proportions of a high-coercivity magnetic phase with unblocking temperatures lower than 200-250 °C. These properties are compatible with those of the epsilon iron oxide, which is widespread in the materials analyzed in archeomagnetism (e.g. Chauvin et al. 2000; Hartmann et al. 2011; Genevey et al. 2016; López-Sánchez et al. 2017; 2020 in this volume). Note that the presence of hematite is not clearly attested in our collection. Finally, Figure 4 shows several examples of magnetic susceptibility vs temperatures curves. Although these measurements do not provide additional information on the magnetic mineralogy (since the heating is only conducted up to 500-520 °C), they illustrate the reversibility criterion applied on magnetic susceptibilities which is taken into account in our archeomagnetic studies.

5. Selection of data available within a 700 km radius of Beaune with a focus on the cooling rate effect

Our seven precisely-dated new results are reported in Figure 5 together with our previous data obtained mainly in France, but also in Belgium (for one datum) and more recently in Tuscany in northern Italy. As in our last publication, all data have been reduced to the common site of Beaune in Burgundy (47.02°N, 4.84°E). At this stage, we observe that the new results are consistent with the intensity variations described from our previous datasets which display between the 5th and 10th c. a pronounced camel-back shape (Genevey et al., 2016). They make

it possible to better define the hump that occurred during the 7th and 8th c., with a maximum reached around 600 AD followed by a decrease until the beginning of the 8th century. Moreover, Hermé's result dating from the end of the 10th c. helps to trace more precisely the strong and remarkable decrease in intensities, by ~20 μT, which occurred between the beginning of the 9th c. and the end of the 10th century.

Other archeointensity results dating from the past 1700 years were previously obtained within the 700 km-radius of Beaune. As in our previous publications, these data were examined through a set of selection criteria, retaining only those obtained using Thellier and Thellier (1959) derived protocols including at least two pTRM-checks or with the Shaw (1974) method. The number of intensity results used to derive the mean is required to be greater or equal to three and the errors around the mean value must be of less than 15% (this threshold is therefore less restrictive than the one used for our own data). The TRM anisotropy must also be taken into account when objects more sensitive to this effect are analyzed (such as pottery or tiles). An additional criterion concerns the age uncertainties, which must be less than or equal to ±50 years. Applying these criteria, the remaining dataset comprises results obtained by Chauvin et al. (2000) and Gómez-Paccard et al. (2012) with respectively seven and four data from France, Casas et al. (2005) (one English result), Donadini et al. (2008) and Donadini et al. (2012) with respectively one and two data from Switzerland, and Schnepp et al. (2020 in this volume) with four data from Germany. Eleven of these data were derived from the study of in-situ burnt structures, i.e., kilns or fireplaces, with analyzed samples from bricks (five data) and baked clay (five data), while baked rocks were collected in one case. The eight other results were obtained from the analysis of artifacts discovered displaced from the location where they were produced: bricks in seven cases and tiles in the last one.

The cooling rate (CR) effect is another parameter whose importance has been discussed in several studies (for a general discussion see Brown et al. (2021) in this volume, but also Genevey et al. 2003, 2008, Hervé et al., 2019; Kostadinova-Avramova and Jordanova, 2019; Jones-Cervantes et al., 2020). With regard to the correction of this effect, different strategies were implemented for the 19 data above. In particular, it was not considered by Casas et al. (2005), whereas it was evaluated for each analyzed fragment by Chauvin et al. (2000). The mean values per group of fragments were then computed using only CR-corrected data. The situation is more complex for the other studies. For the data obtained by Gómez-Paccard et al. (2012), the CR effect is evaluated for each fragment but a correction is applied only when the percentage of alteration is lower than the percentage of CR correction. We recall that the alteration percentage is calculated from a loop-back test identical to a pTRM-check. It allows us to ascertain the stability of the magnetic mineralogy from measurements specifically dedicated to the evaluation of the CR effect. The average per group of fragments was then calculated combining both uncorrected and CR-corrected intensity determinations. The values concerned are reported in Supplementary Figure 1. For the result obtained at Angers, the majority of the values (86%) were CR-corrected and the general mean calculated by Gómez-Paccard et al. (2012) (81.3±10.8μT) is consistent with the average obtained using only the CR-corrected data (82.7±11.3μT). For the other three groups, only 33 to 38% of the collection were CR-corrected, leading to three different situations. For the Mont-Saint-Michel site, the CR-corrected values show the same distribution as the uncorrected ones (supp. Fig. 1). Therefore, the mean value calculated with all the data or with only the CR-corrected data is fairly similar (69.9±7.0μT versus 70.0±7.4μT). At Pierrefitte-sur-Sauldre, the CR-corrected data are in the middle of the distribution of all the values (supp. Fig. 1), and the mean calculated using only these data (83.6±1.1μT) presents an error much smaller but within the uncertainty interval of the mean derived from all data (89.3±8.7μT).

373 Finally, for the fragment group at Saran, the CR-corrected values are all much lower than the
374 uncorrected ones (supp. Fig. 1). The mean obtained from the CR-corrected values has a
375 smaller error (67.8±3.6μT) but, above all, it is not compatible with the average calculated
376 using all the data (79.9±8.3μT). It is interesting to note that this group corresponds to
377 fragments from a kiln sampled at Saran, whose filling has already been analyzed by Genevey
378 et al. (2016) (A36/SAR08 group) who found a mean intensity of 72.0 ± 3.6μT. Genevey et al.
379 (2016) proposed a possible time gap between the last use of the kiln and its filling to explain
380 the difference between the results, although there is no archeological evidence to support this
381 option. Considering only the CR-corrected data obtained by Gómez-Paccard et al. (2012) now
382 leads to a mean intensity value (67.8±3.6μT) compatible with that of Genevey et al. (2016). It
383 thus appears that the strategy used by Gómez-Paccard and co-authors is not adequate in
384 certain circumstances, in particular when the distributions of the CR-corrected and non-
385 corrected values are different. Below, for the results of Gómez-Paccard et al. (2012), we
386 chose to retain only the mean values computed using the CR-corrected data.
387 We also analyzed in more detail the result obtained by Donadini et al. (2008). Here
388 again the situation is different with fragments from the same medieval kiln analyzed both in
389 the paleomagnetic laboratory at Helsinki and Sofia. At Helsinki, small (volume 1 cm^3) and
390 larger (volume 8 cm^3) samples were measured, and a fan was used for cooling the fragments
391 during the Thellier experiments. At Sofia, only large samples (volume 8 cm^3) were studied
392 and the oven used for the Thellier experiments was left cooled without a fan. As expected, the
393 mini-samples systematically gave higher values (Supp. Fig. 1). An arbitrary decrease of 10%
394 accounting for the CR effect was thus applied to those data by Donadini et al. (2008), which
395 *de facto* reduced the difference with the other results, but still with higher values (Supp. Fig.
396 1). The mean intensity value for this medieval kiln was computed by combining the data from
397 the large samples (Helsinki and Sofia) without changes and those from the mini samples

corrected by 10%. This leads to a mean value with a small error (86.85±1.49μT) which likely does not express the real uncertainties associated with this determination. We have preferred to keep only the results from the Sofia analyses (large samples, no fan, 83.9±3.9μT), assuming they are less affected by the CR effect although a residual CR effect is possible.

The next set of two data was acquired by Donadini et al. (2012) from Medieval fireplaces unearthed in Zurich. The sample's volume is 8 cm^3, therefore corresponding to that of the big samples in the 2008 study (i.e. those for which no CR correction was applied). No CR experiment was performed; instead, an educated-guess decrease of 10% was applied to both data. Given the uncertainty about the relevance of this arbitrary correction, we have preferred not to retain these two values.

The last data set recently acquired by Schnepp et al. (2020) includes four data obtained by the Thellier method, in its original version or in the version modified by Coe (1967), but only three of them were CR-corrected, with an experimental evaluation of this effect for each specimen. We therefore retained these three data, while the fourth result for which the CR-effect was not explored was discarded. For the same reason, we also did not retain the result of Casas et al. (2005). In our region of interest, Schnepp et al. (2020) also obtained several intensity results using the multi-specimen method (Biggin and Poidras, 2006; Dekkers and Böhnel, 2006) according to the so-called MSP-DSC technique developed by Fabian and Leonhardt (2010). Without prejudging their reliability nor consistency with the other data, we chose at this stage not to consider them because the CR-effect on the multi-specimen results would still deserve further investigation (Schnepp et al., 2020).

This leaves us with the original dataset of Chauvin et al. (2000), four mean results from the Gómez-Paccard et al. (2012) study calculated using only the CR-corrected data, one result from Donadini et al. (2008) derived from the analysis of big samples at Sofia laboratory where no fan was used and the three CR-corrected data from Schnepp et al. (2020 in this

423 volume). These twelve data are reported in Figure 5. They are all consistent with our own
424 dataset (e.g., Genevey et al., 2019), thus entering in the same evolutionary trend, albeit often
425 showing either higher or lower intensity values.
426
427 **6. Construction of a secular variation curve**
428 In our previous studies focused on the field intensity variations in Western Europe
429 over the past 1600 years, we successively applied two modeling strategies to derive a mean
430 variation curve. Genevey et al. (2013; 2016) used the approach developed by Thébault and
431 Gallet (2010) based on an iteratively reweighted least-squares inverse technique combined
432 with a bootstrap algorithm exploring the intensity and dating uncertainties of each data point.
433 It allows the computation of a large set of individual models using cubic B-splines whose
434 knots are evenly spaced, according to the average of the time intervals between data. The time
435 interval between two knots was equal to 70 years in Genevey et al. (2013) and 50 years in
436 Genevey et al. (2016). A master curve is then provided in the form of probability density
437 function (pdf) as a function of time. One of the objectives of this approach is to reduce the
438 effects of possible outliers. This is achieved thanks to the use of Huber weights for the
439 experimental data errors, the latter being normally distributed within one standard deviation
440 and less steeped beyond, and a re-weighted least-squares scheme. An important point is that
441 the algorithm now includes uneven knot positions, according to the temporal distribution of
442 the data, which allows us to provide a more robust and detailed determination of the intensity
443 field variations.
444 More recently, Genevey et al. (2019) used the transdimensional Bayesian method
445 developed by Livermore et al. (2018), which is based on piecewise linear regression of the
446 available data. The number and temporal distribution of the linear segments are imposed by
447 the data according to their experimental and dating uncertainties, without a priori hypothesis

448 on the complexity of the intensity variations to be determined (i.e. with a minimum level of
449 regularization). A perturbation procedure called AH-RJMCMC (for Age Hyperparameter -
450 Reverse Jump Monte Carlo Markov Chain; see explanations in Livermore et al., 2018) allows
451 the determination of a large ensemble of models whose distribution (pdf), mean, median,
452 mode and 95% credible interval are provided, as well as the posterior intensity and age
453 distributions of each individual datum (Livermore et al., 2018, 2021 in this volume; see also
454 Lanos, 2004; Hellio and Gillet, 2014; Hervé and Lanos, 2017). All calculations are made
455 using a wide prior distribution of the intensity values for each knot common to two
456 consecutive segments, which has been here chosen between 35 μT and 95 μT; the maximum
457 number of knots over the entire documented time interval is conservatively set to 150.
458 Finally, it should be noted that both techniques allow us to take into account a possible time-
459 order relationship between subsets of the data.

460 The two approaches above were used to calculate the intensity variations within the
461 700 km-radius of the city of Beaune in France. The computations are carried out using either
462 our own dataset alone (Figs. 6a,c; supp. Table 2), which has the advantage of being very
463 homogeneous from an experimental point of view, or our data combined with those described
464 in Section 5 (Figs. 6b,d; supp. Table 2), the latter being modified along the lines discussed in
465 this section. A good agreement is observed between the different variation curves displayed in
466 Figure 6, which all show the same evolution mainly characterized by a series of century-scale
467 intensity maxima. Such an agreement is not surprising given the density of the data and their
468 overall good consistency. In detail, however, some differences are observed which are
469 intimately linked to the methods used for the computations.

470 Firstly, the intensity variations are smooth when derived from the Thébault and Gallet
471 (2010) method which considers a certain level of regularization and for which each model is
472 constructed using cubic-B-splines, whereas the use of linear segments in the case of the

473 method developed by Livermore et al. (2018) gives more abrupt variations. Secondly, the pdf
474 calculated from the two datasets using the Thébault and Gallet (2010) algorithm are fairly
475 similar, which is expected as they differ by the addition of only twelve results. It is also worth
476 recalling that the bootstrap algorithm tends to attenuate the effect of deviant results, and thus
477 to determine the most robust intensity variations. Conversely, in the method developed by
478 Livermore et al. (2018), a single result can have a significant effect on the pdf, especially if its
479 uncertainty is small. This is well illustrated by a result at the $6^{th}/7^{th}$ c. transition obtained by
480 Gómez-Paccard et al. (2012), with quite small experimental (1.1μT) and dating (65 years)
481 uncertainties, which is higher in intensity than the other data available in the same period.
482 When incorporated in the calculations (compare Figs. 6c and 6d), it significantly increases the
483 amplitude of the intensity peak, whereas its effect is very minor with the Thébault and Gallet
484 (2010) method (compare Figs. 6a and 6b). Similarly, three results obtained by Chauvin et al.
485 (2000) between the end of the 14^{th} c. and the first half of the 15^{th} c. appear higher than the
486 other data documenting this period, while one result from Schnepp et al. (2020) dated to the
487 middle of the 13^{th} c. is significantly lower. Here again, the incorporation of these data in the
488 computations based on the bootstrap algorithm has little effect on the pdf (Figs. 6a,b). On the
489 other hand, these results significantly modify the pdf obtained from the AH-RJMCMC
490 method (compare Fig. 6c and 6d). When the data are not taken into account in the calculations
491 (Fig. 6c), the mode of the pdf shows a linear evolution between ~1000 and ~1500, while two
492 intensity peaks during the 11^{th} c. and the 14^{th} c. are only inferred from the medians, averages
493 (the latter are not shown in Figs. 6c,d) and shape of the 95% confidence intervals of the pdf,
494 which thus leads to rather ambiguous information. When they are taken into account (Fig.
495 6d), the modes of the pdf then become similar to the medians and the averages, showing the
496 same two intensity peaks that are clearly displayed by the method of Thébault and Gallet
497 (2010) whatever the dataset used (Figs. 6a, b).

The example above highlights the fact that a small amount of data can have a significant influence on the statistics of the models derived from the method developed by Livermore et al. (2018), in particular over a time interval wider than that strictly covered by these data. In addition, it should be noted that the 95% credible intervals provided by the AH-RJMCMC method are often wider than those given by the Thébault and Gallet (2010) method (see in particular between c. late 10^{th} c. and early 13^{th} c.), and the individual models are more dispersed inside the credible interval. This comes from two reasons. One arises from the AH-RJMCMC method because of the large a priori intensity range considered in the calculations, which allows for the possibility of fast and ample variations not necessarily seen from the data distribution. The second reason is that the bootstrap approach, on the contrary, uses a regularization defined as the best trade-off between the minimum complexity and the data misfit that reduces the probability of rapid and large variations in the absence of constraints provided by the data. In this way, the philosophy conveyed by the AH-RJMCMC method is very suitable to the detection of very rapid or extreme intensity variations (in this case, each result can have a strong influence on the field intensity evolution; Livermore et al., 2021 in this volume). Indeed, the method admits all possible time-dependence consistent with both the prior information and the dataset, although it returns a higher probability for parsimonious models with the least number of knots.

7. Contributions and limitations of archeointensity dating: case study of Bourges and Chaudry workshops

Two procedures were used to derive chronological constraints based on archeointensity results, and also considering the reference curves established from the two different modeling techniques described in section 6 (Thébault and Gallet, 2010; Livermore et al., 2018). The first method, classical in archeomagnetism (e.g. Pavón-Carrasco et al., 2011) which we refer

523 below as “archeointensity correlation dating”, consists in convolving the pdf of the
524 geomagnetic intensities defining the reference curve with the pdf of the intensity to be dated
525 (i.e. a Gaussian) to form a (normalized) pdf of the age. It should be noted that the true pdf of
526 the reference curves were used in our study and not, for simplification, a series of Gaussian
527 distributions (e.g. Pavón-Carrasco et al., 2011). In this case, the intensity value to be dated is
528 independent of the data used to create the reference curve. The second dating method, referred
529 to as “archeointensity marginalized dating”, was described by Livermore et al (2018) and
530 already used by Gallet et al (2020) and Shaar et al. (2020). Here, in contrast to the first
531 method, the archeointensity value (of a priori poorly known age) to be dated is included in the
532 dataset that constrains the joint age-intensity posterior distribution. The dating is then
533 determined by the posterior age probability distribution derived for this datum by
534 marginalization using the AH-RJMCMC method (see also Schnepp et al., 2015; Hervé and
535 Lanos, 2017). The age distribution of the datum is then constrained by not only its wide prior
536 age interval, but also by the ages of other data which are close in age. For age distributions
537 derived either from the correlation or marginalization methods, we construct the most likely
538 age intervals by calculating the highest density region at a 95.4% threshold (e.g. solid blue
539 filled region in Fig 7). We will see below that the two dating methods give very similar
540 results when using the AH-RJMCMC approach.
541
542 **7.1 Pottery workshop of La Chapelle Saint Ursin (BOUR# groups)**
543 The sampling of fragments associated with the pottery kiln and its production was carried out
544 after an initial ceramological overview. At this moment, it was possible to isolate fragments
545 of lips associated with pots characteristic of the production. The chronological constraints on
546 the period of activity of this small workshop were, however, still rather loose. The objective

547 of our study was therefore to see whether archeointensity analyses could help to better define
548 the period of production, which was perceived as being linked to the 5th century.

549 The two mean intensity values obtained for the pottery (BOUR01/02) and kiln
550 (BOUR03) fragments are very consistent (Table 1), indicating that the pottery wasters found
551 in the kiln filling are most likely associated with the kiln's latest productions. All the results
552 obtained at the fragment level were therefore used to calculate a mean intensity value, which
553 should be characteristic of the ambient field that prevailed at the time the kiln was abandoned
554 (Table 1). The overall mean intensity value was compared to the different intensity variation
555 curves shown in Figure 6, and the results of the archeointensity correlation dating are
556 provided in the first two columns of Table 2. While two age intervals are discriminated during
557 the High Middle Ages with the curves constructed according to the AH-RJMCMC method
558 (Fig. 7a), a single age interval encompassing almost the entire High Medieval Period is
559 isolated using the curves derived from the Thébault and Gallet (2010) approach (Fig. 8a). The
560 fact that the variation curves are respectively (for the two regional field modeling methods)
561 more or less smooth and more or less sensitive to a very small number of data easily explain
562 these differences (see discussion in Section 6). Furthermore, when using the AH-RJMCMC
563 method, one can see the significant effect on the dating results induced by the choice of the
564 database used to build the models, which is much less the case with the method of Thébault
565 and Gallet (2010) (Table 2). On the other hand, the marginal posterior age distribution of the
566 intensity value to be dated derived from the approach developed by Livermore et al 2018 (i.e.,
567 the archeointensity marginalized dating method; last two columns in Table 2; Fig. 7b) gives
568 almost the same dating results as those provided by the archeointensity correlation dating
569 method. Such an agreement can be understood by the fact that the French database is quite
570 dense and the data very coherent, so that the incorporation of a single data point with a wide
571 dating interval (here of 800 years between 400 and 1200) does not have much influence on

572 the calculated models. At this stage, it is fair to say that the results of archeointensity dating
573 indicate that the production of this small workshop may have persisted beyond the 5th century.
574 This possibility was independently confirmed by the complete study of the ceramic
575 material, which now places the production between 450 and 550, and by radiocarbon dating
576 (Fig. 8b). The ceramic dating was first based on the study of the material "out of production"
577 for which was noted the absence of characteristic elements of the 4th c. and early 5th c., and of
578 Merovingian décor with a “molette” (i.e. made by impression with a wood wheel). The kiln
579 production, with a very limited repertoire, also echoes other ensembles discovered in
580 occupation contexts dating from the second half of the 4th c. and the first half of the 5th
581 century. The radiocarbon dating was carried out on charcoal found in a layer associated with
582 the last use of the kiln and should therefore be relevant for dating the end of the production. It
583 gave an uncalibrated age of 1580±30 BP (Lyon-13108 (RICH)) and a calibrated age between
584 420 and 556 calAD (using OxCal 4.4 and IntCal20, Reimer et al. 2020).
585 These different dating elements, archeology, archeomagnetism (archeointensity
586 correlation dating) and radiocarbon, can be combined to better constrain this production.
587 Since the three dating techniques are independent, the product of their pdf is applied, yielding
588 an age interval during the first half of the 6th c. (Fig. 8), whatever the intensity variations
589 curves used or the method considered for deriving the archeomagnetic age intervals. Note that
590 the radiocarbon data contributes little to this dating: combining the radiocarbon data with
591 either the archeological or archeointensity constraints gives an age interval identical or not
592 significantly different from that provided by archeology. In contrast, the archeointensity result
593 in combination with the archeological constraints makes it possible to limit the age interval
594 for the end of the pottery production to ~half a century, which brings a strong constraint for
595 the age of abandonment of the Roman villa associated with this pottery workshop.
596

7.2 Pottery workshop of Chaudry (CHAU# groups)

The archeointensity study was carried out as part of an archeological project aimed at completely re-examining the ceramic material unearthed on this site in the late 1990s (Regnard et al. 2021). Since its discovery, this material has been recognized as dating from the Carolingian period (mid 8th-end 10th century). The re-examination of the material allowed us to detail the production, highlighting in particular the highly standardized nature of the shapes, most of which are closed, and to define several technical groups, the most significant of which have been sampled for archeointensity analyses. The objective was therefore to better define the end of the period of activity of this kiln, certainly associated with a pottery activity extending over a wider spatial area.

The two technical groups associated with the kiln's production (CHAU01/02) yielded very consistent intensity values. The results obtained from two shards (of eleven measured) used in the construction of the kiln (third technical group; group CHAU03) appeared also very close to those obtained for the CHAU01/02 group, and their incorporation does not change the mean, nor its precision (CHAU01/02: 77.3±0.5 versus CHAU01/02/03: 77.4±0.4μT). For the archeomagnetic dating, we used the mean intensity value calculated from the data obtained for the three Chaudry groups, thus assuming that the fragments of CHAU03 were completely refired during the last use of the kiln. The archeointensity dating results obtained from this value are reported in Table 2. We find the same characteristics as before: while a single (long) age interval is obtained by correlation dating using the field evolution given by the Thébault and Gallet (2010) method (Fig. 9a), despite the very low (rather unusual) value of the standard deviation of the archeointensity data point, several distinct intervals (up to three) are observed from the AH-RJMCMC technique. For the latter, this is the case either by performing a correlation dating or by analyzing the marginal

posterior age distribution of this data point (Supp. Fig. 2), again with a significant effect of the database used on the results (Table 2).

The age interval provided by the archeological constraints is rather large, as it encompasses the entire Carolingian period (Fig. 9b). However, based on the recognition of certain regional stylistic elements, Lefèvre and Mahé (2004) proposed to narrow the production period to the first decades of the 10th century. All the results of archeointensity dating imply that the production would not have persisted beyond the very beginning of the 10th century. To test whether this observation is related to the very small standard deviation (0.4µT), we increased its value to 1.5µT. This leads to the same conclusion for the 10th century (Table 2).

Radiocarbon data from charcoal are also available for the kiln (uncalibrated age, 1255±30 BP giving a 95.4%-calibrated age range between 671 and 876; Ref. Lyon-16233 (RICH), Fig. 9b). However, the charcoal was not found at the bottom of the kiln, thus raising the question of the significance of the age obtained. As a result, neither the archeointensity (due to the nature of the intensity variations during the High Middle Ages) nor the radiocarbon data (and their combination) make it possible to constrain the age of the beginning of ceramic production (Fig. 9). In particular, it seems useful to ask whether the stylistic features that led to the early dating of the 10th century could in fact have appeared somewhat earlier (last decades of the 9th c. or first decade of 10th c.) in the Vexin Français area than in other parts of the Ile-de-France region. This issue is still unresolved. Clearly, only additional archeological constraints, from the excavation of other kilns in the Vexin Français or the recognition of this ceramic production in occupation contexts, would further limit the age span of the production.

8. Conclusions

Seven new archeointensity values with accurate dating in the High Middle Ages further improved our knowledge of the variations in geomagnetic intensities in France, and more generally in Western Europe, over the past 1700 years.

Two regional modeling approaches were used to trace these variations, the first derived from the method of Thébault and Gallet (2010), which now considers irregularly spaced knots according to the data distribution, the second developed by Livermore et al. (2018) based on a transdimensional Bayesian technique. In addition, two databases were used that differ according to a criterion of data homogeneity, all of which are located within a 700 km circle around the city of Beaune. This dual approach allowed us to illustrate the sensitivity of the mean curves, based on the distribution of a large set of individual models, to the principles of each of the two modeling approaches. While the first method gives a very regular and smooth evolution in intensity variation, with a weighting of the effects linked to slightly discordant data, the second approach shows more abrupt variations with sometimes stronger amplitudes.

We also illustrated two examples of dating integrating the constraints resulting from the archeointensity results, in addition to those of the available archeological and radiocarbon data. For this, we also used two different dating techniques, either by classically comparing the intensity value to be dated with the reference geomagnetic variation curve, or by analyzing the marginal posterior age distribution of the data point given by the method of Livermore et al (2018). We showed that for France, the two techniques give very similar results. In this respect, the consideration of two different approaches for both regional field modeling and dating strengthens the interpretation of archeointensities for archeological dating.

Finally, beyond the information provided to the archeologists, our study showed that it would certainly be illusory to consider archeointensities as a fully independent "absolute" dating method (e.g. Aitken, 1990; Korte et al., 2019), especially in the absence of direction-based archeomagnetic constraints. On the contrary, archeointensities may provide chronological constraints, which in combination with other archeological and/or radiocarbon dating elements, can be very valuable in refining the dating of the structures/artifacts studied, opening the way to a wide range of complementary research on Medieval pottery production.

Acknowledgment

We are very grateful to Maxime Le Goff for his constant support in the Triaxe measurements and for fruitful discussions around the intensity results. We also thank Caroline Claude from INRAP who was helpful in the selection of medieval groups of pottery fragments. We further thank the two anonymous reviewers and the guest editor Annick Chauvin for their useful comments. This is IPGP contribution no. 4220.

References

Aidona, E., Polymeris, G., Camps, P., Kondopoulou, D., Ioannidis, N., Raptis, K., 2018. Archaeomagnetic versus luminescence methods: the case of an Early Byzantine ceramic workshop in Thessaloniki, Greece. Archaeological and Anthropological Sciences 10. https://doi.org/10.1007/s12520-017-0494-5

Aitken, M., 1990. Science-Based Dating in Archaeology. Taylor & Francis Ltd, 294 pp.

Batt, C.M., Brown, M.C., Clelland, S.-J., Korte, M., Linford, P., Outram, Z., 2017. Advances in archaeomagnetic dating in Britain: new data, new approaches and a new calibration curve. J. Archaeol. Sci. 85, 66–82, https://doi.org/10.1016/j.jas.2017.07.002

694 Biggin, A.J., Poidras, T., 2006. First-order symmetry of weak-field partial thermoremanence
695 in multi-domain ferromagnetic grains. 1. Experimental evidence and physical
696 implications. Earth Planet Sci. Lett. 245, 438–453,
697 https://doi.org/10.1016/j.epsl.2006.02.035

698 Bouillon, J., (Dir.), 2015. Loiret, Saran, Ancienne route de Chartres, au lieu-dit « La
699 Guignace » - (zone sud et zone nord). Une extension nord au complexe artisanal potier de
700 Saran « La Médecinerie » (VIe-Xe siècle), Rapport de fouille, INRAP Centre Île-de-
701 France.

702 Brown, M. C, Hervé, G., Korte, M., Genevey A., Global archaeomagnetic data: the state of
703 the art and future challenges. Phys. Earth Planet. Inter, accepted with minor revisions.

704 Bucur, I., 1994. The direction of the terrestrial magnetic field in France during the last 21
705 centuries. Phys. Earth Planet. Inter. 87, 95–109, https://doi.org/10.1016/0031-
706 9201(94)90024-8

707 Buffett, B., Knezek, N., Holme, R., 2016. Evidence for MAC waves at the top of Earth's core
708 and implications for variations in length of day, Geophysical Journal International, 204,
709 3, 1789–1800, https://doi.org/10.1093/gji/ggv552

710 Casas, L., Shaw, J., Gich, M., Share, J.A., 2005. High-quality microwave archaeointensity
711 determinations from an early 18th century AD English brick kiln. Geophys. J. Int. 161,
712 653–661, https://doi.org/10.1111/j.1365-246X.2005.02631.x

713 Casas, L., Tema, E., 2019. Investigating the expected archaeomagnetic dating precision in
714 Europe: A temporal and spatial analysis based on the SCHA.DIF.3K geomagnetic field

model, Journal of Archaeological Science 108, 104972, https://doi.org/10.1016/j.jas.2019.104972

Catanzariti, G., McIntosh, G., Osete, M., Nakamura, T., Rakowski, A., González, I., Lanos, P., 2007. A Comparison of Radiocarbon and Archaeomagnetic Dating from an Archaeological Site in Spain, Radiocarbon 49, 2, 543-550, https://doi.org/10.1017/S0033822200042454

Chaudriller, S., (Dir.), 2019. Hermé, « Les Malletons » (carrière S.P.M.), Rapport de fouille, INRAP Centre - Île-de-France - Seine-et-Marne.

Chauvin, A., Garcia, Y., Lanos, P., Laubenheimer, F., 2000. Paleointensity of the geomagnetic field recovered on archaeomagnetic sites from France. Phys. Earth Planet. Int. 120, 111–136, https://doi.org/10.1016/S0031-9201(00)00148-5

Coe, R. S., 1967. Paleo-intensities of the Earth's magnetic field determined from Tertiary and Quaternary rocks. J. Geophys. Res. 72, 3247–3262, https://doi.org/10.1029/JZ072i012p03247

Dekkers, M.J., Böhnel, H.N., 2006. Reliable absolute palaeointensities independent of magnetic domain state. Earth Planet. Sci. Lett. 248, 508–517. https://doi.org/10.1016/j.epsl.2006.05.040

Donadini, F., Kovacheva, M., Kostadinova, M., Hedley, I.G., Pesonen, L.J., 2008. Palaeointensity determination on an early medieval kiln from Switzerland and the effect of cooling rate. Phys. Earth. Planet. Int. 33, 449–457, https://doi.org/10.1016/j.pce.2008.02.019

736 Donadini, F., Motschi, A., Rösch, C., Hajdas, I., 2012. Combining an archaeomagnetic and
737 radiocarbon study: dating of medieval replaces at the Mühlegasse. Zürich. J. Archaeol.
738 Sci. 39, 2153–2166, https://doi.org/10.1016/j.jas.2012.02.030

739 Ech-Chakrouni, S., Hus, J., Spassov, S., 2013. Constraints of archaeomagnetic dating and
740 field intensity determinations in three ancient tile kilns in Belgium. Stud Geophys
741 Geod 57, 585–604, https://doi.org/10.1007/s11200-012-0779-1

742 Fabian, K., Leonhardt, R., 2010. Multiple-specimen absolute paleointensity determination: an
743 optimal protocol including pTRM normalization, domain-state correction, and alteration
744 test. Earth Planet. Sci. Lett. 297, 84–94, https://doi.org/10.1016/j.epsl.2010.06.006

745 Gallet, Y., Genevey, A., Le Goff, M., 2002. Three millennia of directional variation of the
746 Earth's magnetic field in western Europe as revealed by archeological artifacts. Phys.
747 Earth. Planet. Inter. 131, 81–89, https://doi.org/10.1016/S0031-9201(02)00030-4

748 Gallet, Y, Le Goff, M., 2006. High-temperature archeointensity measurements from
749 Mesopotamia. Earth and Planetary Science Letters. 241, 159-173.,
750 https://doi.org/10.1016/j.epsl.2005.09.058

751 Gallet, Y., Genevey, A., Le Goff, M., Warmé, N., Gran−Aymerich, J., Lefèvre, A., 2009. On
752 the use of archeology in geomagnetism, and vice−versa: Recent developments in
753 archeomagnetism, C. R. Physique 10, 630−648, https://doi.org
754 /10.1016/j.crhy.2009.08.005

755 Gallet, Y., Genevey, A., Margueron, J.-C., Le Goff, M., Thébault, E., Matthiae, P., Butterlin,
756 P, Al Maqdissi, M., 2014a. Exemples de chronologie archéomagnétique à Mari/Tell
757 Hariri, Syria, Mari, ni Est, ni Ouest, suppl. 2, 217-230

758 Gallet, Y., D'Andrea, M., Genevey, A., Pinnock, F., Le Goff, M., Matthiae, P., 2014b.
759 Archaeomagnetism at Ebla (Tell Mardikh, Syria). New data on geomagnetic field
760 intensity variations in the Near East during the Bronze Age. Journal of Archaeological
761 Science. 42. 295–304, https://doi.org /10.1016/j.jas.2013.11.007

762 Gallet, Y., Fortin, M., Fournier, A., Le Goff, M., & Livermore, P., 2020. Analysis of
763 geomagnetic field intensity variations in Mesopotamia during the third millennium BC
764 with archeological implications. Earth and Planetary Science Letters 537, 1–13,
765 https://doi.org/10.1016/j.epsl.2020.116183

766 Genevey, A., Gallet, Y., 2002. Intensity of the geomagnetic field in western Europe over the
767 past 2000 years: new data from ancient French pottery. J. Geophys. Res. 107 (B11),
768 2285, https://doi.org/10.1029/2001JB000701

769 Genevey, A., Gallet, Y., Margueron, J., 2003. Eight thousand years of geomagnetic field
770 intensity variations in the eastern Mediterranean. J. Geophys. Res. B Solid Earth 108 (5).
771 EPM1-1-1-18. https://doi.org/10.1029/2001JB001612

772 Genevey, A., Gallet, Y., Constable, C.G., Korte, M., Hulot, G., 2008. ArcheoInt: an up-
773 graded compilation of geomagnetic field intensity data for the past ten millennia and its
774 application to the recovery of the past dipole moment. Geochem. Geophys. Geosyst. 9,
775 Q04038, https://doi.org/10.1029/2007GC001881

776 Genevey, A., Gallet, Y., Rosen, J., Le Goff, M., 2009. Evidence for rapid geomagnetic field
777 intensity variations in Western Europe over the past 800 years from new archeointensity
778 French data. Earth Planet. Sci. Lett. 284, 132–143,
779 https://doi.org/10.1016/j.epsl.2009.04.024

780 Genevey, A., Gallet, Y., Thébault, E., Jesset, S., Le Goff, M., 2013. Geomagnetic field
781 intensity variations in Western Europe over the past 1100 years. Geochem. Geophys.
782 Geosyst. 14/8, 2858–2872, https://doi.org/10.1002/ggge.20165

783 Genevey, A., Gallet, Y., Jesset, S., Thébault, E., Bouillon, J., Lefèvre, A., Le Goff, M., 2016.
784 New archeointensity data from French early medieval ceramic production (6th-10th
785 century AD). Tracing 1500 years of geomagnetic field intensity variations in Western
786 Europe. Phys. Earth Planet Inter. 257, 205–219,
787 https://doi.org/10.1016/j.pepi.2016.06.001

788 Genevey, A., Principe, C., Gallet, Y., Clemente, G., Le Goff, M., Fournier, A., Pallecchi, P.,
789 2019. Refining the high-fidelity archaeointensity curve for western Europe over the past
790 millennium: analysis of Tuscan architectural bricks (Italy). Geological Society of
791 London. SP497, https://doi.org/10.6084/m9.figshare.c.4728257

792 Gómez-Paccard, M., Beamud, E., 2008. Recent achievements in archaeomagnetic dating in
793 the Iberian Peninsula: application to Roman and Mediaeval Spanish structures, Journal of
794 Archaeological Science 35, 1389-1398, https://doi.org/10.1016/j.jas.2007.10.005

795 Gómez-Paccard, M., Chauvin, A., Lanos, P., Dufresne, P., Kovacheva, M., Hill, M.J.,
796 Beamud, E., Blain, S., Bouvier, A., Guibert, P.Archaeological Working Team, 2012.
797 Improving our knowledge of rapid geomagnetic field intensity changes observed in
798 Europe between 200 and 1400 AD. Earth Planet. Sci. Lett. 355– 356, 131–143,
799 https://doi.org/10.1016/j.epsl.2012.08.037

800 Hartmann, G.A., Genevey, A., Gallet, Y., Trindade, R.I.F., Etchevarne, C., Le Goff, M.,
801 Afonso, M.C., 2010. Archeointensity in Northeast Brazil over the past five centuries.
802 Earth Planet. Sci. Lett. 296, 340–352, https://doi.org/10.1016/j.epsl.2010.05.016

803 Hartmann, G.A., Genevey, A., Gallet, Y., Trindade, R.I.F., Le Goff, M., Najjar, R.,
804 Etchevarne, C., Afonso, M.C., 2011. New historical archeointensity data from Brazil:
805 Evidence for a large regional non-dipole field contribution over the past few centuries.
806 Earth Planet. Sci. Lett. 306, 66–76. https://doi.org/10.1016/j.epsl.2011.03.030

807 Hellio, G., Gillet, N., Bouligand, C., Jault, D., 2014. Stochastic modelling of regional
808 archaeomagnetic series. Geophys. J. Int. 199 (2), 931–943,
809 https://doi.org/10.1093/gji/ggu303

810 Herries, A., Kovacheva, M., Kostadinova-Avramova, M., 2008. Mineral magnetism and
811 archaeomagnetic dating of a mediaeval oven from Zlatna Livada, Bulgaria. Physics and
812 Chemistry of The Earth 33. https://doi.org/10.1016/j.pce.2008.02.021

813 Hervé, G., Lanos, P., 2017. Improvements in Archaeomagnetic Dating in Western Europe
814 from the Late Bronze to the Late Iron Ages: An Alternative to the Problem of the
815 Hallstattian Radiocarbon Plateau: Improvements in archaeomagnetic dating in Western
816 Europe. Archaeometry. https://doi.org/10.1111/arcm.12344

817 Hervé, G., Faßbinder, J., Gilder, S. A., Metzner-Nebelsick, C., Gallet, Y., Genevey, A.,
818 Schnepp, E., Geisweid, L., Pütz, A., Reuß, S., Wittenborn, F., Flontas, A., Linke, R.,
819 Riedel, G., Walter, F., Westhausen, I., 2017. Fast geomagnetic field intensity variations
820 between 1400 and 400 BCE: New archaeointensity data from Germany. Phys. Earth
821 Planet. Inter. 270, 143–156. https://doi.org/10.1016/j.pepi.2017.07.002

822 Hervé, G., Chauvin, A., Lanos, P., Rochette, P., Perrin, M., Perron d'Arc, M., 2019. Cooling
823 rate effect on thermoremanent magnetization in archaeological baked clays: an
824 experimental study on modern bricks. Geophys. J. Int. 217 (2), 1413–1424,
825 https://doi.org/10.1093/gji/ggz076

826 Jesset, S., (dir.), Saran (Loiret), « La Voie Nouvelle », Rapport de fouille, Ville d'Orléans, to
827 be published.

828 Jones, S. A., Tauxe, L., Blinman, E., Genevey, A., 2020. Archeointensity of the Four Corners
829 Region of the American Southwest. Geochem. Geophys. Geosyst. 21 (3),
830 e2018GC007509, https://doi.org/10.1029/2018GC007509

831 Korte, M., Brown, M., Gunnarson, S., Nilsson, A., Panovska, S., & Wardinski, I., Constable,
832 C., 2019. Refining Holocene geochronologies using palaeomagnetic records. Quaternary
833 Geochronology 50. https://doi.org/10.1016/j.quageo.2018.11.004.

834 Kostadinova-Avramova, M., Jordanova, N., 2019. Study of cooling rate effect on baked clay
835 materials and its importance for ar- chaeointensity determinations. Phys. Earth Planet.
836 Inter. 288, 9– 25, https://doi.org/10.1016/j.pepi.2019.02.009

837 Lanos, P., 2004. Bayesian Inference of Calibration Curves: Application to
838 Archaeomagnetism. Springer London, London, 43–82.

839 Lanos, P., 2019. Physique de l'archéomagnétisme pour la datation de bâtiments du haut
840 Moyen Âge, Reflets phys. 63, Physique et matériaux anciens.
841 https://doi.org/10.1051/refdp/201963054

842 Lefèvre, A., Mahé, N., 2004. La céramique du haut Moyen Âge en Île-de-France à travers la
843 fouille des habitats ruraux, Revue Archéologique de Picardie, n°3-4, 105-150.

844 Lefèvre, A., Peixoto, X., 2015. Les ateliers de potiers de la rue Gaudray à Vanves (Hauts-de-
845 Seine). In: Thuillier, F., Louis, E. (Eds.), Tourner autour du pot..., Les ateliers de potiers
846 médiévaux du Ve au XIIe siècle dans l'espace européen. publications du CRAHAM,
847 Caen.

Livermore, P. W., Fournier, A., Gallet, Y., Bodin, T., 2018. Transdimensional inference of archeomagnetic intensity change. Geophys. J. Int. 215 (3), 2008–2034, https://doi.org/10.1093/gji/ggy383

Livermore, P.W., Gallet, Y., Fournier, A., 2021. Archaeomagnetic intensity variations during the era of geomagnetic spikes in the Levant, Phys. Earth Planet. Inter. 312, https://doi.org/10.1016/j.pepi.2021.106657

Le Goff, M., Gallet, Y., Genevey, A., Warmé, N., 2002. On archaeomagnetic secular variation curves and archaeomagnetic dating. Phys. Earth Planet. Inter. 134, 203–211, https://doi.org/10.1016/S0031-9201(02)00161-9

Le Goff, M., Gallet, Y., 2004. A new three-axis vibrating sample magnetometer for continuous high-temperature magnetization measurements: applications to paleo- and archeo-intensity determinations. Earth Planet. Sci. Lett. 229, 31–43, https://doi.org/10.1016/j.epsl.2004.10.025

Le Goff, M., Gallet, Y., Warmé, N., Genevey, A., 2020. An updated archeomagnetic directional variation curve for France over the past two millennia, following 25 years of additional data acquisition, Physics of the Earth and Planetary Interiors, 309, https://doi.org/10.1016/j.pepi.2020.106592

López-Sánchez, J., McIntosh, G., Osete, M. L., Del Campo, A., Villalaín, J. J., Pérez, L., Kovacheva, M., Rodríguez de la Fuente, O., 2017. Epsilon iron oxide: Origin of the high coercivity stable low Curie temperature magnetic phase found in heated archeological materials. Geochemistry, Geophysics, Geosystems. 18. https://doi.org/10.1002/2017GC006929

López-Sánchez, J., Palencia-Ortas, A., Del Campo, A., McIntosh, G., Kovacheva, M., Martín-Hernández, F., Carmona, N., Rodríguez de la Fuente, O., Marín, P., Molina-Cardín, A., Osete, M.L., 2020 Further progress in the study of epsilon iron oxide in archaeological baked clays, Phys. Earth Planet. Inter. 307. https://doi.org/10.1016/j.pepi.2020.106554

Lowrie, W., 1990. Identification of ferromagnetic minerals in a rock by coercivity and unblocking temperatures properties. Geophys. Res. Lett. 17, 159–162. http://dx.doi.org/10.1029/ GL017i002p00159.

Mahé, N., (Dir.), 2020. Chamigny, Rue de la Marne - RD 80 - Lieu-dit « La Grande Maison », Rapport de fouille, INRAP Île-de-France, Seine-et-Marne.

Marot, E., (Dir.), 2017. La Chapelle Saint-Ursin, l'Angoulaire, chemin des vallées aux Fruscades, Trajectoires antique et alto-médiévale d'un établissement agricole de la proche campagne de Bourges-Avaricum, Rapport final d'opération de fouilles archéologiques, Région Centre - Val de Loire - Département du Cher (18), Bourges Plus.

Pavón-Carrasco, F.J., Osete, M.L., Torta, J.M., Gaya-Pique, L.R., 2009. A regional archeomagnetic model for Europe for the last 3000 years, SCHA.DIF.3K: Applications to archeomagnetic dating. Geochem. Geophys. Geosyst. 10, Q03013. https://doi.org/10.1029/2008GC002244

Pavón-Carrasco, F.J., Rodríguez-González, J., Osete, M. L., Torta, J. M., 2011. A MATLAB tool for archaeomagnetic dating. Journal of Archaeological Science 38, 408-419, https://doi.org/10.1016/j.jas.2010.09.021

Pavón-Carrasco, F. J., Campuzano, S. A., Rivero-Montero, M., Molina-Cardín, A., Gómez-Paccard, M., & Osete, M.L., 2021. SCHA.DIF.4k: 4,000 years of paleomagnetic

reconstruction for Europe and its application for dating. Journal of Geophysical Research: Solid Earth, 126, e2020JB021237. https://doi. org/10.1029/2020JB021237

Principe, C., Gogichaishvili, A., Arrighi, S., Devidze, M., La Felice, S., Paolillo, A., Giordano, D., Morales, J., 2018. Archaeomagnetic dating of Copper Age furnaces at Croce di Papa village and relations on Vesuvius and Phlegraean Fields volcanic activity, Journal of Volcanology and Geothermal Research 349, 217-229, https://doi.org/10.1016/j.jvolgeores.2017.11.002

Regnard, S., 1999. Vienne-en-Arthies (Val-d'Oise). Hameau de Chaudry-La Pierre Percée, Archéologie médiévale 29, 372.

Regnard, S., Fayet,F., Genevey, A., Kucab, A., Regnard, A., Mouterde, P., Verasdonck, P. 2021. Un atelier de potier du IXe siècle au hameau de Chaudry à Vienne-en-Arthies (Val-d'Oise), Revue archéologique du Vexin français et du Val-d'Oise, 45,101-157.

Reimer, P., Austin, W., Bard, E., Bayliss, A., Blackwell, P., Ramsey, C., Butzin, M., Cheng, H., Edwards, R., Friedrich, M., Grootes, P., Guilderson, T., Hajdas, I., Heaton, T., Hogg, A., Hughen, K., Kromer, B., Manning, S., Muscheler, R., Palmer, J., Pearson, C., van der Plicht, J., Reimer, R., Richards, D., Scott, E., Southon, J., Turney, C., Wacker, L., Adolphi, F., Büntgen, U., Capano, M., Fahrni, S., Fogtmann-Schulz, A., Friedrich, R., Köhler, P., Kudsk, S., Miyake, F., Olsen, J., Reinig, F., Sakamoto, M., Sookdeo, A., Talamo, S., 2020. The IntCal20 Northern Hemisphere radiocarbon age calibration curve (0-55 Cal kBP). Radiocarbon 62, 725–757.

Schnepp, E., Obenaus, M., Lanos, P., 2015. Posterior archaeomagnetic dating: An example from the Early Medieval site Thunau am Kamp, Austria. Journal of Archaeological Science: Reports 2, 688-698. https://doi.org/10.1016/j.jasrep.2014.12.002

915 Schnepp, E., Thallner, D., Arneitz,P., Leonhardt,R., 2020. New archeomagnetic secular
916 variation data from Central Europe, II: Intensities, Phys. Earth Planet. Inter. 309,
917 https://doi.org/10.1016/j.pepi.2020.106605

918 Shaar, R., Bechar, S., Finkelstein, I., Gallet, Y., Martin, M. A. S., Ebert, Y., Keinan, J.,
919 Gonen, L., 2020. Synchronizing geomagnetic field intensity records in the Levant
920 between the 23rd and 15th Centuries BCE: Chronological and methodological
921 implications. Geochem. Geophys. Geosyst. 21, 12,
922 https://doi.org/10.1029/2020GC009251

923 Shaw, J., 1974. A new method of determining the magnitude of the palaeomagnetic field:
924 Application to five historic lavas and five archaeological samples. Geophys. J. R. Astron.
925 Soc. 39, 133–141. https://doi.org/10.1111/j.1365-246X.1974.tb05443.x

926 Tema, E., Fantino, F., Ferrara, E., Allegretti, S., Giudice, A., Re, A., Barello, F., Vella, S.,
927 Cirillo, L., Gulmini, M., 2014. Archaeological, archaeomagnetic and
928 thermoluminescence investigation of a baked clay kiln excavated at Chieri, northern
929 Italy: contribution to the rescue of our cultural heritage. Annals of Geophysics 57,
930 G0548, https://doi.org/10.4401/ag-6611

931 Thébault, E., Gallet, Y., 2010. A bootstrap algorithm for deriving the archeomagnetic field
932 intensity variation curve in the Middle East over the past 4 millennia BC. Geophys. Res.
933 Lett. 37, L22303, https://doi.org/10.1029/2010GL044788

934 Thellier, E., Thellier, O., 1959. Sur l'intensité du champ magnétique terrestre dans le passé
935 historique et géologique. Ann. Geophys. 15, 285–376.

936 Thellier, E., 1981. Sur la direction du champ magnétique terrestre en France durant les deux
937 derniers millénaires. Phys. Earth Planet. Inter. 24, 89–132, https://doi.org/10.1016/0031-
938 9201(81)90136-9

939 Troyano, M., Gallet, Y., Genevey, A., Pavlov, V., Fournier, A., Lagroix, F., Niyazova, M.,
940 Mirzaakhmedov, D., 2021. Analyzing the geomagnetic axial dipole field moment over
941 the historical period from new archeointensity results at Bukhara (Uzbekistan, Central
942 Asia). Phys. Earth Planet. Inter. 310, https://doi.org/10.1016/j.pepi.2020.106633.

943

944 **Figure captions:**

945 Figure 1: (a) Location of the archeological sites discussed in this paper. The pink circles
946 indicate the sites associated with the seven new precisely-dated archeointensity results. The
947 two pink circles bordered with purple indicate the sites where groups were collected for
948 dating (the yellow area represents the so-called “Vexin Français” region). The blue circles
949 indicate the geographical distribution of our intensity dataset (Genevey et Gallet, 2002; Gallet
950 et al. 2009; Genevey et al., 2009, 2013, 2016, 2019). The green squares correspond to the
951 sites of the selected data obtained by Chauvin et al. (2000), Donadini et al. (2008), Gómez
952 Paccard et al. (2012) and Schnepp et al. (2020 in this volume). The circle with a radius of
953 700km is centered on the city of Beaune (Burgundy) to where the different intensity results
954 were reduced. (b) Kiln 3060 unearthed at Hermé. Sampling for direction and intensity was
955 concentrated on the central tongue of the Kiln (Group HERME04) ©N. Warmé, Inrap (c)
956 Close-up of the pottery fragments found in kiln 2629 unearthed in Chamigny (Group
957 CHAM03) ©C. Seng, Inrap.

958

Figure 2: Archeointensity results obtained for six groups (or pairs of groups) of fragments. Each curve corresponds to the analysis of a specimen and represents the intensity values (i.e. the R'(Ti) data) obtained over the temperature range Tmin-Tmax where the primary TRM component was isolated (given in Supp Tab. 1). These examples show that for each specimen, the R'(Ti) data are nearly constant over the Tmin-Tmax temperature interval, indicating that the magnetic mineralogy has maintained the same acquisition capability for both the NRM and the laboratory-TRM. Enhanced scatter observed at low temperatures, when the running temperature Ti is close to Tmin, is due to the small NRM and laboratory-TRM fractions involved in the R'(Ti) ratios.

Figure 3: Examples of magnetic behavior for rejected fragments. (a, b) Two fragments for which a major alteration of the magnetic mineralogy was detected from low-field magnetic susceptibility versus temperature measurements. (c, d) Fragment for which the primary TRM component could not be reliably isolated in the thermal demagnetization diagram (c) and corresponding intensity diagram with non-constant intensity values (d). (e, f) Fragment with a single magnetization component observed between 100°C and 520°C in the thermal demagnetization diagram (e) but with decreasing intensity values over the same temperature range (f). In the demagnetization diagrams (c, e), the solid (resp. empty) circles represent the declinations (resp. inclinations) in specimen coordinates.

Figure 4: Thermal demagnetization of three-axis IRM components acquired in fields of 1.25, 0.4 and 0.2 T for six different fragments successfully analyzed in intensity and low-field magnetic susceptibility versus temperature curves (up to 500-520°C) for the same fragments.

983 Figure 5: Archeointensity data available within a 700 km radius around Beaune combining
984 our dataset and other selected results (see details in the figure). The results of Donadini et al
985 (2008) and Gómez Paccard et al. (2012) were modified as discussed in the text. Direct
986 measurements are from http://www.bcmt.fr/. All data were reduced to the latitude of Beaune
987 (47.03°N, 4.83°E)
988
989 Figure 6: Intensity variations curves in Western Europe over the past 1700 years. (a,b)
990 Variation curves obtained using the Thébault and Gallet (2010) method considering our
991 dataset only (a) and our data combined with the other selected data (b). The curve in pink
992 indicates the probability maxima and the pink dotted lines the 95% credible interval. (c,d)
993 Variation curves obtained using the AH-RJMCMC method (Livermore et al., 2018)
994 considering only our data (c) and together with the other selected data (d). The curves in red
995 and blue show the probability maxima and the median values, respectively; the thin dotted
996 lines in blue show the 95% credible interval. More details are given in the text and in supp
997 Table 2. In all diagrams, the density distribution of individual models is shown according to a
998 grey colour code scale (maximum probability of 0.15). Direct measurements are from
999 http://www.bcmt.fr/. All data were reduced to the latitude of Beaune (47.03°N, 4.83°E).
1000
1001 Figure 7: Archeomagnetic dating obtained for the pottery workshop discovered at La Chapelle
1002 Saint Ursin site (BOUR# groups). (a) Archeointensity correlation dating: The variation curve
1003 is calculated using the AH-RJMCMC method developed by Livermore et al (2018) method
1004 and taking into account all the selected data (see text) available within 700 km radius of the
1005 city of Beaune (see Fig. 6d). The horizontal area in orange shows the intensity value ($\pm 2\sigma$) to
1006 be dated. The dating is carried out by direct comparison with the calculated models ensemble.
1007 The age intervals (light blue area, right y-scale; see Table 2) are determined according to a

95.4% threshold value (horizontal blue line) which defines a highest density region. (b) Archeointensity marginalized dating (Livermore et al., 2018): The intensity value to be dated is incorporated with a large age interval (here between 400 and 1200) into the database used for the construction of the models using AH-RJMCMC. The diagram presents the marginal posterior age distribution derived for the data point concerned. As previously, different age intervals (light blue area; Table 2) are obtained according to a 95.4% threshold (horizontal blue line). The picture shows the kiln once excavated © E. Marot, Bourges plus.

Figure 8: Dating elements available for the pottery workshop discovered at La Chapelle Saint Ursin. (a) Archeointensity correlation dating. The variations curve displayed is calculated using the Thébault and Gallet (2010) method and all the data selected within the 700 km radius of the city of Beaune (see Fig. 6b). The Gaussian curve in red next to the intensity axis represents the intensity value to be dated. The age probability derived from the comparison of the BOUR overall mean value with the reference curve, taking into account their error bars, is represented both directly on the variation curve using a colour code and by a probability density curve reported along the age axis. The age interval shown between brackets is the most likely age range at a 95.4% threshold. The drawing represents a characteristic form of the production to be dated (©E. Marot, Bourges Plus). (b) This panel presents the archeological age interval, with a uniform probability density considered for the pottery production (black line), the probability density of the C14 data after calibration (in red) and the final age probability (in green) derived by combining the pdfs of the three dating elements (archeomagnetism of figure (a), archeological and C14).

Figure 9: Same legend as in Fig. 8 but the archeointensity value to be dated was obtained for the pottery workshop discovered at Chaudry. The drawing represents a characteristic form of this production ©S. Regnard, CRAVF.

Table captions

Table 1: New archeointensity results obtained for the seven dated groups of fragments and for the two series of groups investigated for dating.

Table 2: Results of archeomagnetic dating obtained for the pottery workshops discovered at La Chapelle Saint Ursin (BOUR#) and Chaudry (CHAU#). Dating is carried out using two field modeling techniques, according to Thébault and Gallet (2010) and Livermore et al. (2018), two databases and two different dating approaches, here referred to as "archeointensity correlation dating" and "archeointensity marginalized dating". For Chaudry, the calculations are performed using the standard error of mean intensity value and by artificially increasing this error up to 1.5 μT. See the text for more explanation. All age intervals are given with a 95.4% confidence level.

Supplementary information

Supp. Figure 1: Cooling rate (CR) effect on the intensity data obtained by Donadini et al. (2008) and Gómez- Paccard et al. (2012). The results are reported at the site location, both at the specimen (spec.) and group levels. The description of the different symbols is given in the Figure. The "Nblue/Npink" numbers for the data obtained by Gómez- Paccard et al. (2012) indicate the number of results used to derive the mean value when using all the data, i.e. combining CR corrected and uncorrected values (Nblue), and the number of CR-corrected values used to derive the mean (Npink). The "Ngrey/Nyellow" number for the result of

1056 Donadini et al. (2012) indicates the number of results obtained from small samples (volume
1057 1cm^3) analyzed at the Helsinki paleomagnetic laboratory (Ngrey) and the number of large
1058 samples (volume 8 cm^3) analyzed in the paleomagnetic laboratory at Sofia (Nyellow).
1059
1060 Supp. Figure 2: Archeomagnetic dating obtained for the pottery workshop discovered at the
1061 Chaudry site (CHAU# groups). (a) Archeointensity correlation dating: The variation curve is
1062 calculated using the AH-RJMCMC method developed by Livermore et al (2018) method and
1063 taking into account all the selected data (see text) available within the 700 km radius of the
1064 city of Beaune (see Fig. 6d). The horizontal area in orange shows the intensity value (±2σ) to
1065 be dated. The dating is carried out by direct comparison with the calculated models. The age
1066 intervals (light blue area, right y-scale; see Table 2) are determined according to a 95.4%
1067 threshold value (horizontal blue line). (b) Archeointensity marginalized dating (Livermore et
1068 al. 2018): The intensity value to be dated is incorporated with a large age interval (here
1069 between 400 and 1200) in the database used for the construction of the models. The diagram
1070 presents the marginal posterior age distribution derived for the data point concerned. As
1071 previously, different age intervals (light blue area; Table 2) are obtained according to a 95.4%
1072 threshold (horizontal blue line). The picture shows the kiln being excavated with its filling. ©
1073 S. Regnard, CRAVF.
1074
1075 Supp. Table 1: Intensity results obtained at the specimen level and mean values obtained at
1076 the fragment level. 'Natural magnetic moment': Magnetic moment before demagnetization
1077 for each specimen in A.m^2. The volume of each specimen is of the order of 0.75 cm^3 or
1078 slightly less. 'Tmin-Tmax': Interval of temperature involved for the intensity computation. 'F
1079 lab': Intensity of the laboratory field in μT. 'NRM T1 (T1')': Fraction in % between the
1080 magnetization unblocked between Tmin and Tmax, thus used for intensity determination, and

1081 the magnetization with unblocking temperatures ≥ Tmin. 'Slope R': Slope of the straight line
1082 computed by linear regression from the R'(Ti) data between Tmin and Tmax. It is calculated
1083 as follows (see also Gallet and Le Goff 2006): Slope R'=(R'(Tmax)-R'(TMin))/(Mean
1084 (R'(Ti) data) where R'(Tmax) and R'(Tmin) are here the values at Tmax and Tmin deriving
1085 from the linear regression of the R'(Ti) data. It is expressed in %. 'F Triaxe': Intensity values
1086 obtained at the specimen level in μT. It is estimated by computing the arithmetic mean from
1087 all R'(Ti) ratios obtained for a specimen over the Tmin-Tmax temperature range. 'F Triaxe
1088 mean value per fragment ± σF': Mean intensity value obtained at the fragment level with its
1089 standard error when computed from 2 values or its standard deviation when computed from 3
1090 values. (N1/N2/N3/N4)* indicates respectively the number of fragments collected, the
1091 number of fragments whose magnetization was strong enough relative to the Triaxe
1092 sensitivity, the number of fragments measured on the Triaxe for which no sign of magnetic
1093 mineralogy alteration was observed during the susceptibility measurements and the number of
1094 fragments retained to estimate a mean value at the group level. (n1/n2)** indicates
1095 respectively the number of specimens measured using the Triaxe and the number of retained
1096 specimens. Note that we usually test two to three specimens per fragment to reject or retain
1097 the fragment based on our set of quality criteria.
1098
1099 Supp. Table 2: Intensity values derived from the method of Thébault and Gallet (2010;
1100 maximum probability and 95% credible interval) and that of Livermore et al (2018; maximum
1101 probability, median, 95% credible interval). For the latter technique, the following
1102 computational parameters were considered: σ_{move}=30 years, σ_{change}= 5 μT, σ_{birth}=5 μT,
1103 K_{max}=150, prior intensities between 35 μT and 95 μT and a chain length of 200 million
1104 samples. One datum age is perturbed per age-resampling. All the calculations are carried out

using our data alone or our dataset combined with a selection of other results (see text). These values trace the different curves shown in Fig. 6.

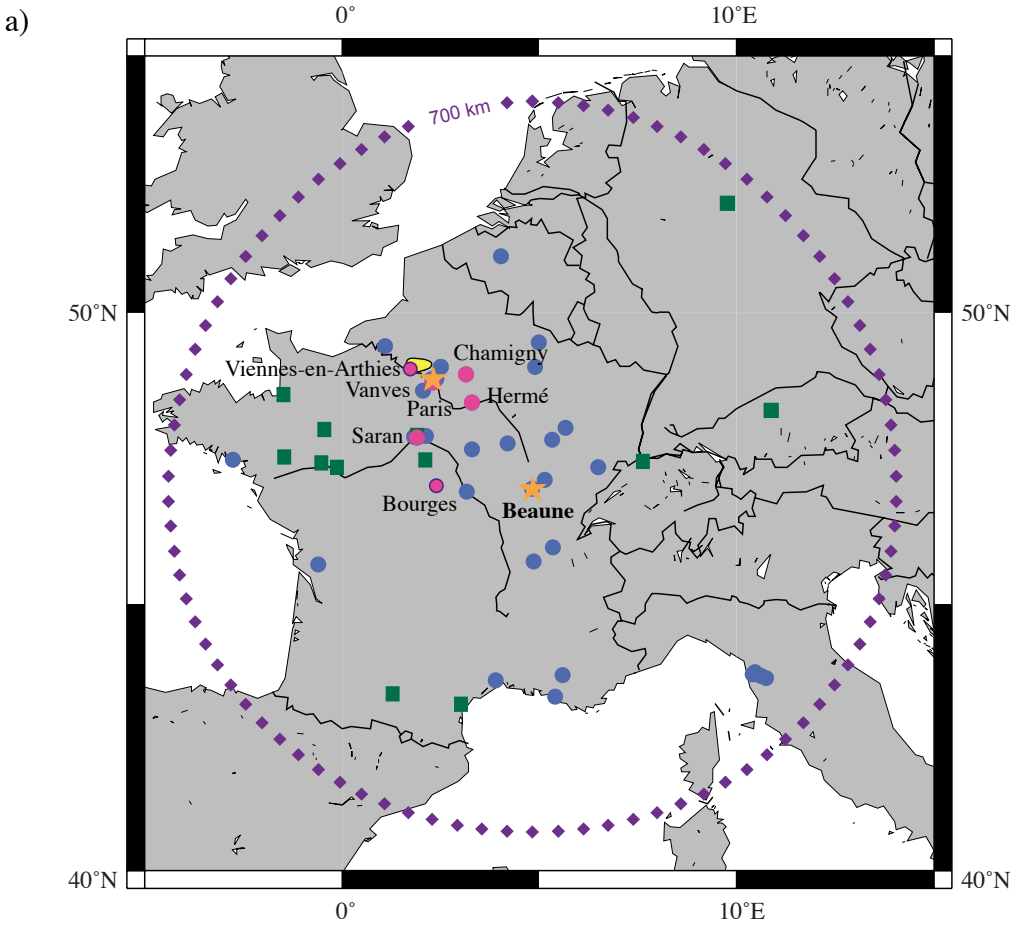
a)
0°
10°E
700 km
50°N
50°N
Chamigny
Viennes-en-Arthies
Vanves
Hermé
Paris
Saran
Bourges
Beaune
40°N
40°N
0°
10°E
b)
c)

Figure 1.

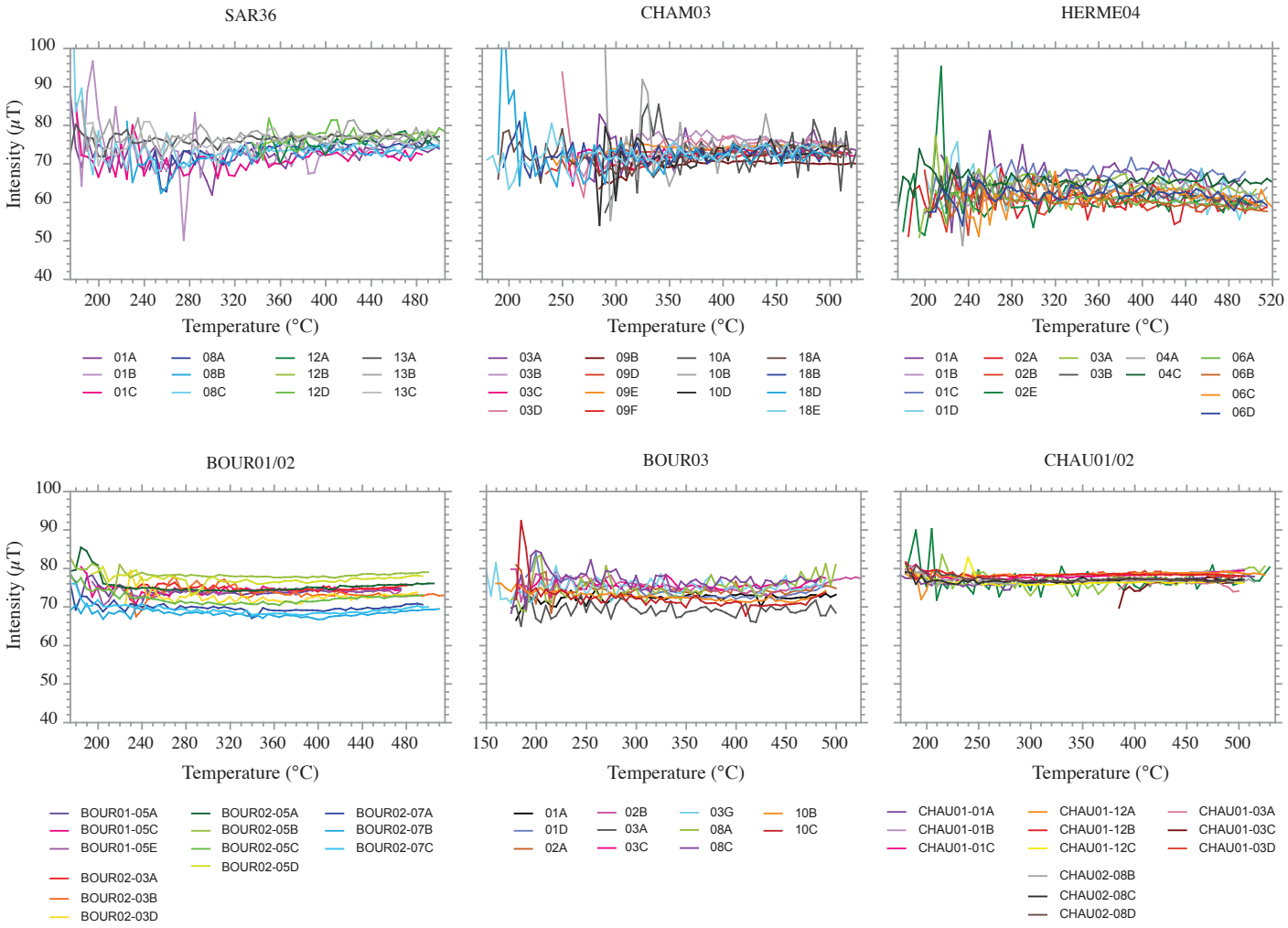
SAR36
CHAM03
HERME04
BOUR01/02
BOUR03
CHAU01/02
Intensity (μT)
Temperature (°C)
01A 01B 01C 08A 08B 08C 12A 12B 12D 13A 13B 13C
03A 03B 03C 03D 09B 09D 09E 09F 10A 10B 10D 18A 18B 18D 18E
01A 01B 01C 01D 02A 02B 02E 03A 03B 04A 04C 06A 06B 06C 06D
BOUR01-05A BOUR01-05C BOUR01-05E BOUR02-03A BOUR02-03B BOUR02-03D BOUR02-05A BOUR02-05B BOUR02-05C BOUR02-05D BOUR02-07A BOUR02-07B BOUR02-07C
01A 01D 02A 02B 03A 03C 03G 08A 08C 10B 10C
CHAU01-01A CHAU01-01B CHAU01-01C CHAU01-12A CHAU01-12B CHAU01-12C CHAU01-03A CHAU01-03C CHAU01-03D CHAU02-08B CHAU02-08C CHAU02-08D

Figure 2.

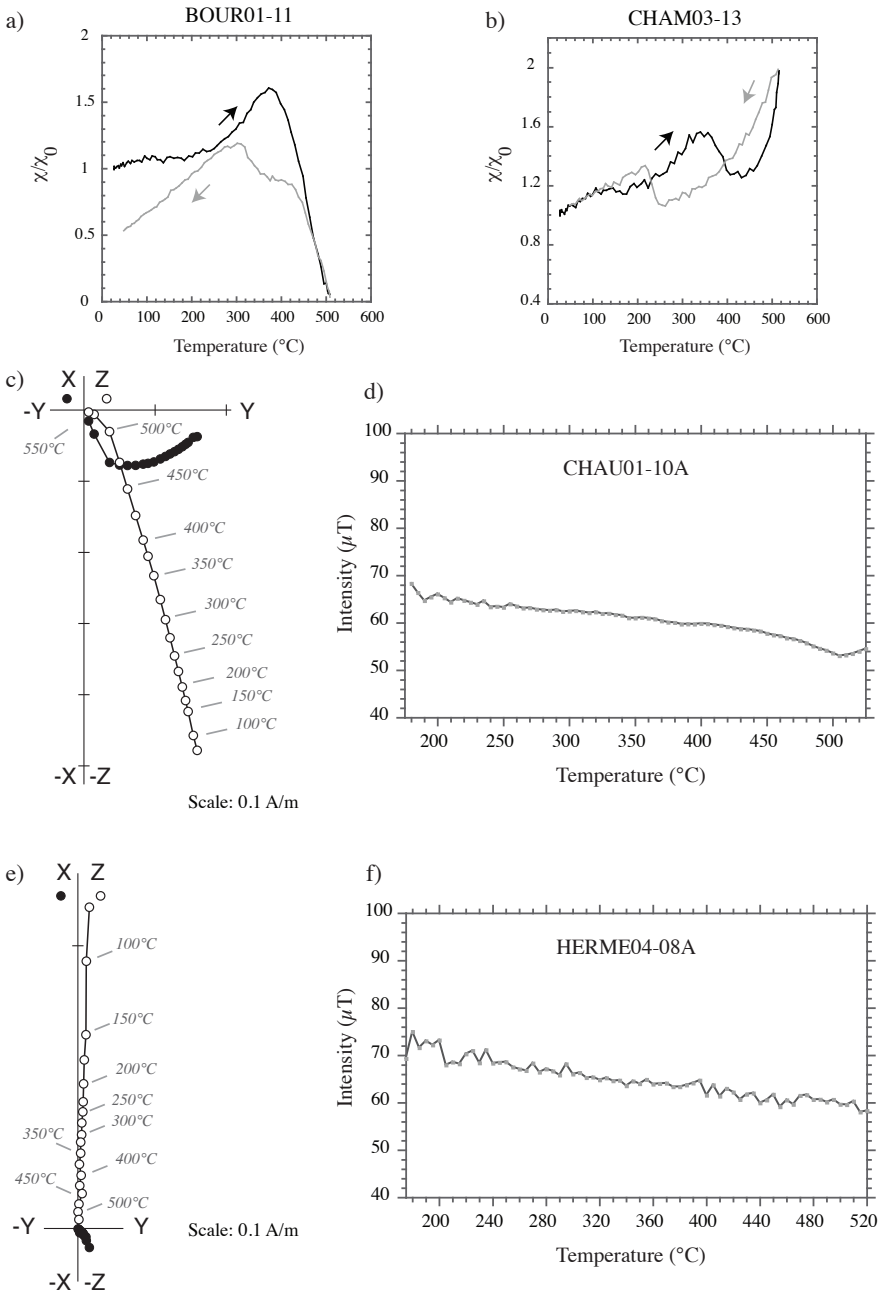
a)
BOUR01-11
χ/χ0
Temperature (°C)
b)
CHAM03-13
χ/χ0
Temperature (°C)
c)
X
Z
-Y
Y
550°C
500°C
450°C
400°C
350°C
300°C
250°C
200°C
150°C
100°C
-X
-Z
Scale: 0.1 A/m
d)
CHAU01-10A
Intensity (μT)
Temperature (°C)
e)
X
Z
100°C
150°C
200°C
250°C
300°C
350°C
400°C
450°C
500°C
-Y
Y
-X
-Z
Scale: 0.1 A/m
f)
HERME04-08A
Intensity (μT)
Temperature (°C)

Figure 3.

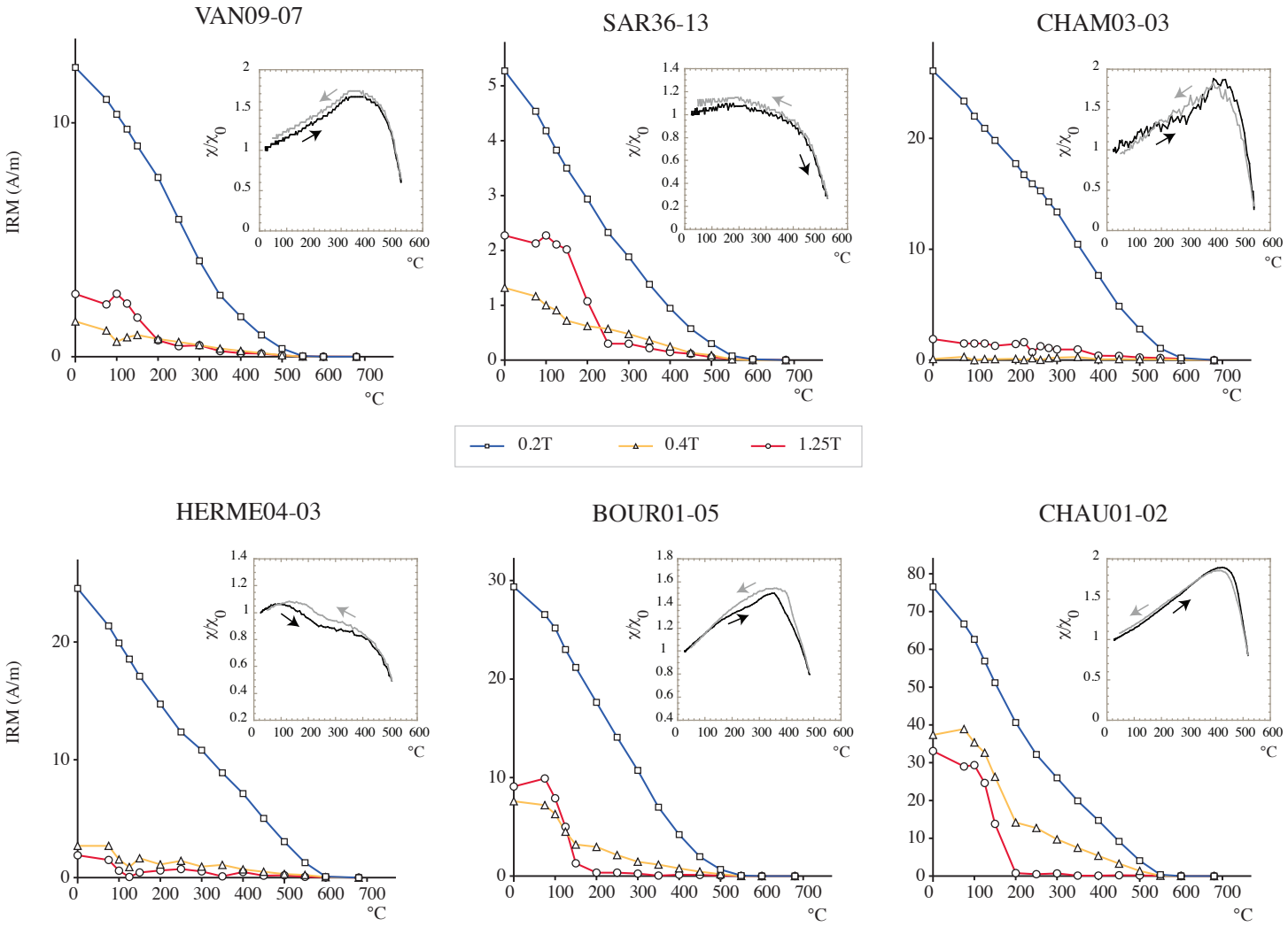
VAN09-07
SAR36-13
CHAM03-03
HERME04-03
BOUR01-05
CHAU01-02
IRM (A/m)
χ/χ0
°C
0.2T
0.4T
1.25T

Figure 4.

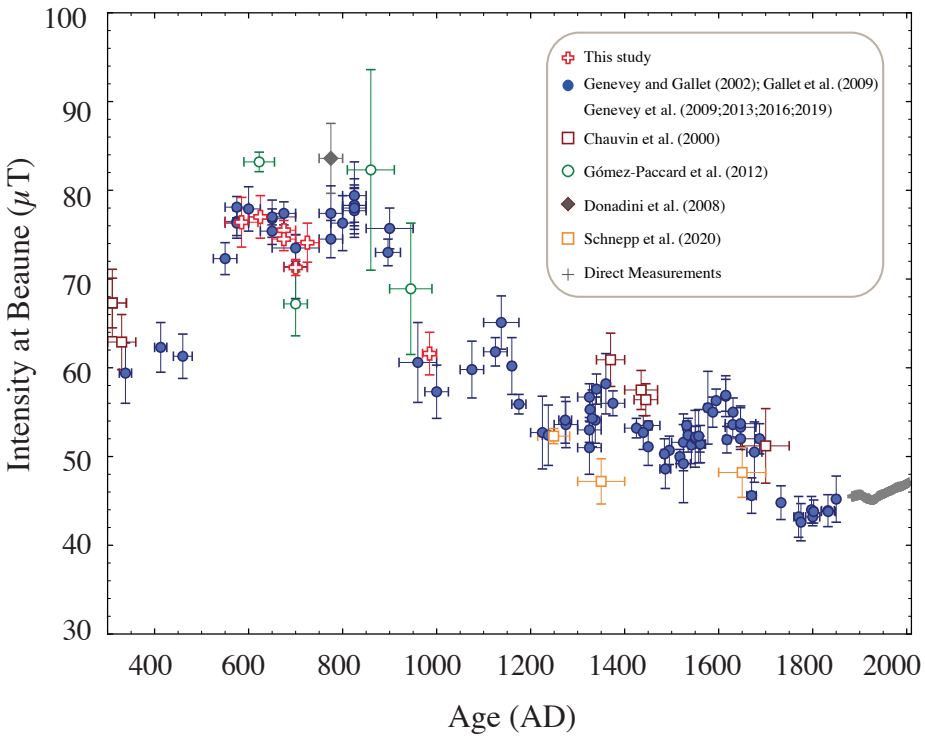
This study
Genevey and Gallet (2002); Gallet et al. (2009)
Genevey et al. (2009;2013;2016;2019)
Chauvin et al. (2000)
Gómez-Paccard et al. (2012)
Donadini et al. (2008)
Schnepp et al. (2020)
Direct Measurements
Intensity at Beaune (μT)
Age (AD)
100
90
80
70
60
50
40
30
400
600
800
1000
1200
1400
1600
1800
2000

Figure 5.

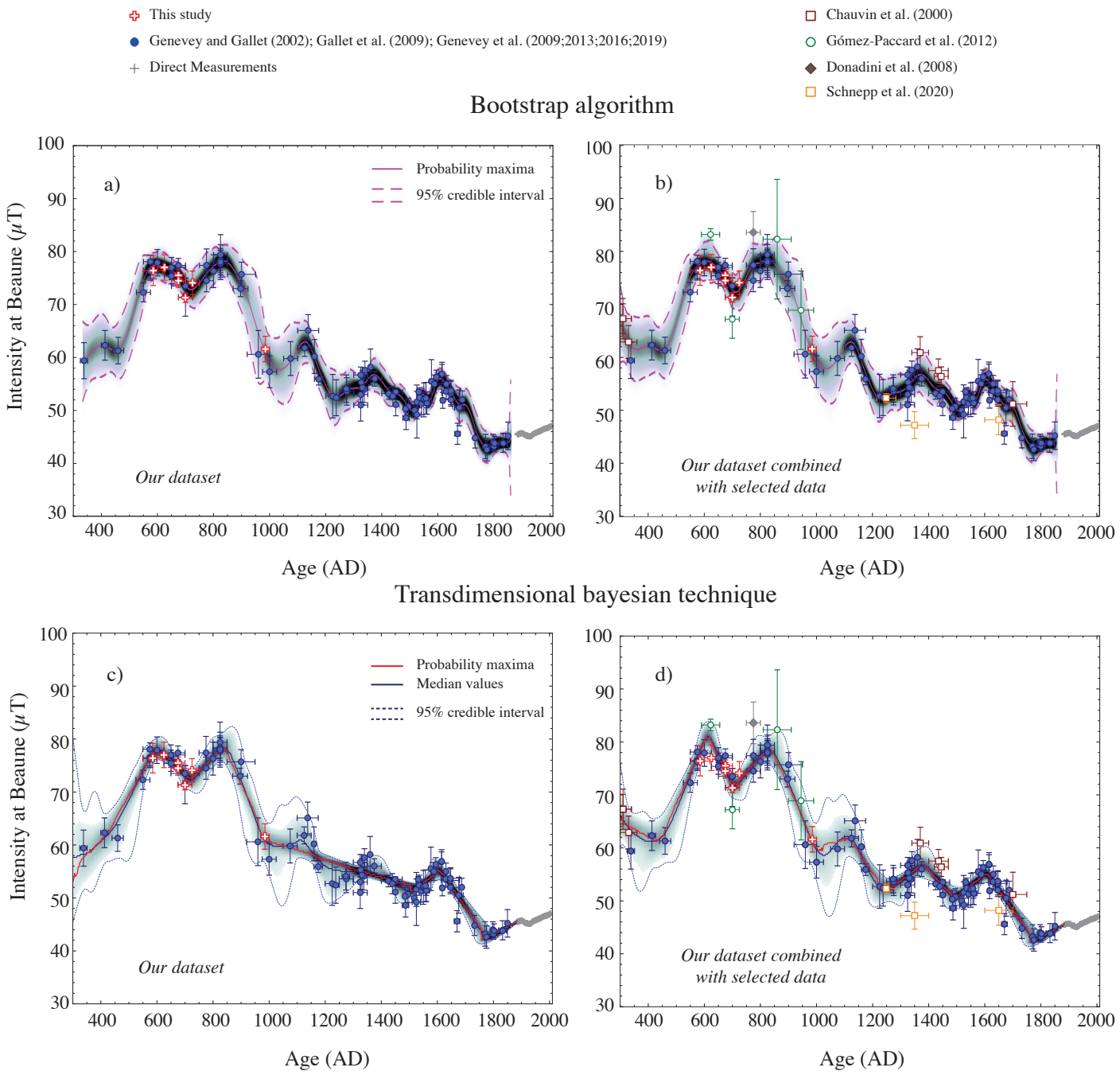
This study
Genevey and Gallet (2002); Gallet et al. (2009); Genevey et al. (2009;2013;2016;2019)
Direct Measurements
Chauvin et al. (2000)
Gómez-Paccard et al. (2012)
Donadini et al. (2008)
Schnepp et al. (2020)
Bootstrap algorithm
a)
b)
Probability maxima
95% credible interval
Our dataset
Our dataset combined with selected data
Intensity at Beaune (μT)
Age (AD)
Transdimensional bayesian technique
c)
d)
Probability maxima
Median values
95% credible interval
Our dataset
Our dataset combined with selected data
Intensity at Beaune (μT)
Age (AD)

Figure 6.

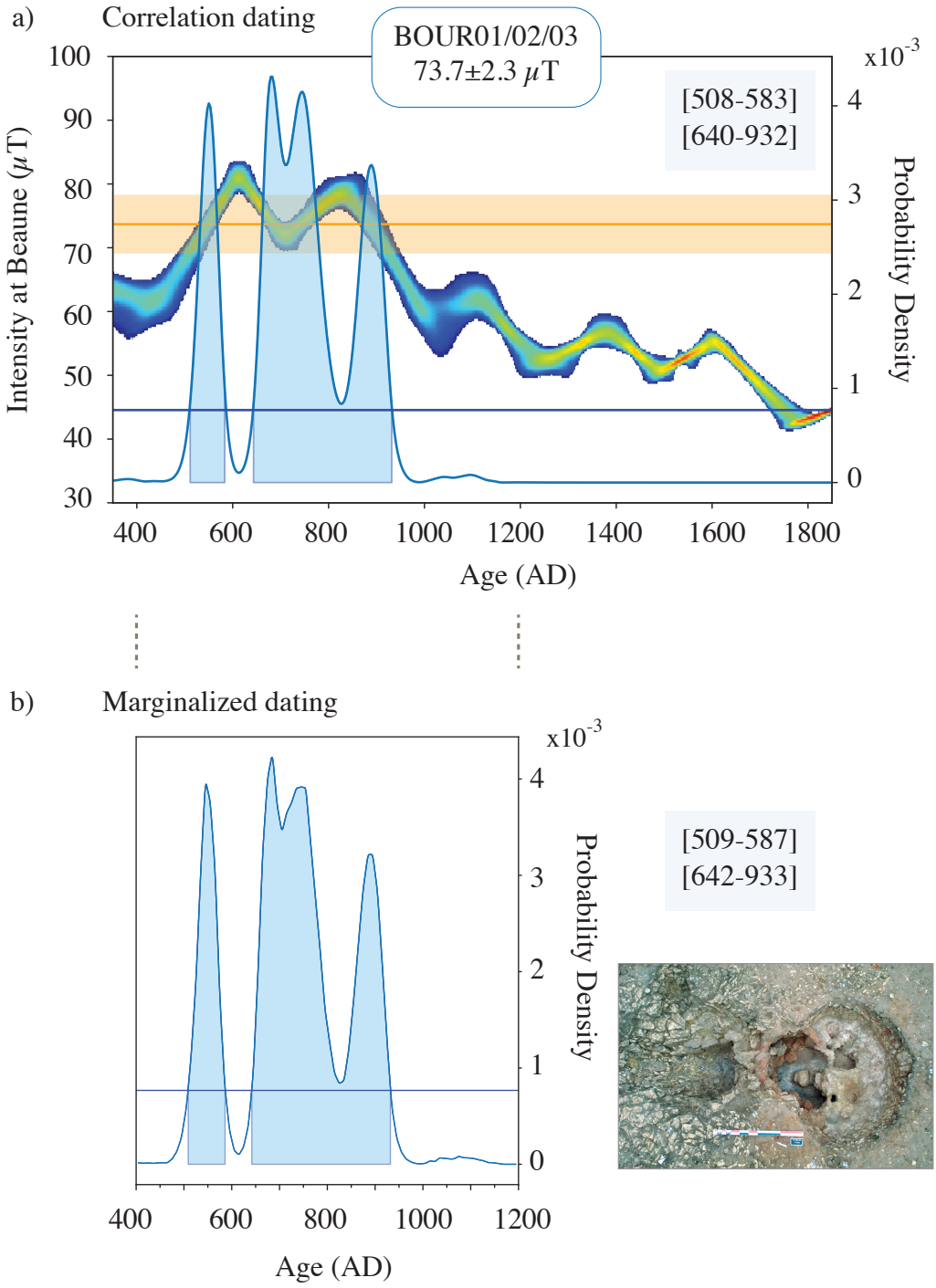
a)
Correlation dating
BOUR01/02/03
73.7±2.3 μT
[508-583]
[640-932]
Intensity at Beaune (μT)
Probability Density
x10-3
Age (AD)
b)
Marginalized dating
[509-587]
[642-933]
Probability Density
x10-3
Age (AD)

Figure 7

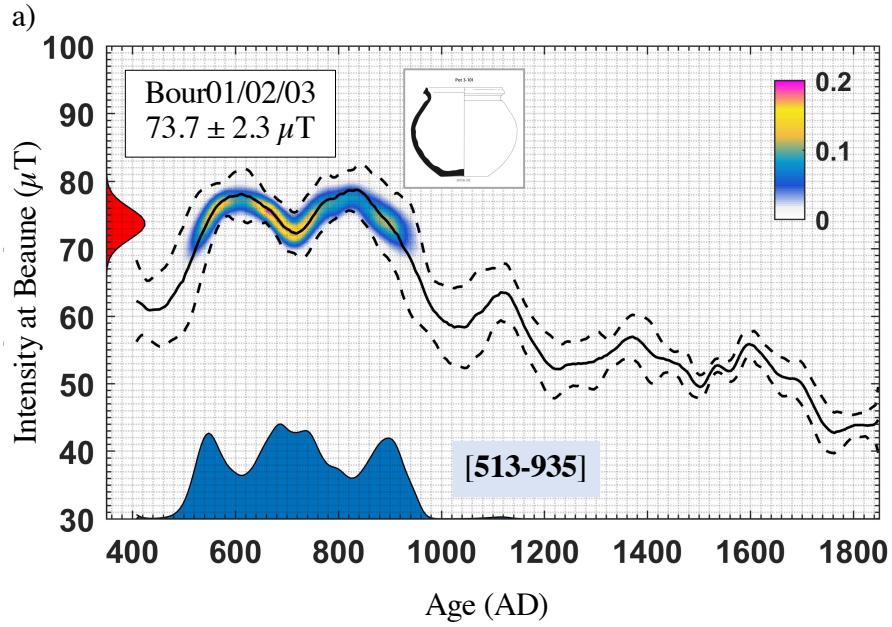
a)
Bour01/02/03
73.7 ± 2.3 μT
0.2
0.1
0
[513-935]
Intensity at Beaune (μT)
100
90
80
70
60
50
40
30
400
600
800
1000
1200
1400
1600
1800
Age (AD)

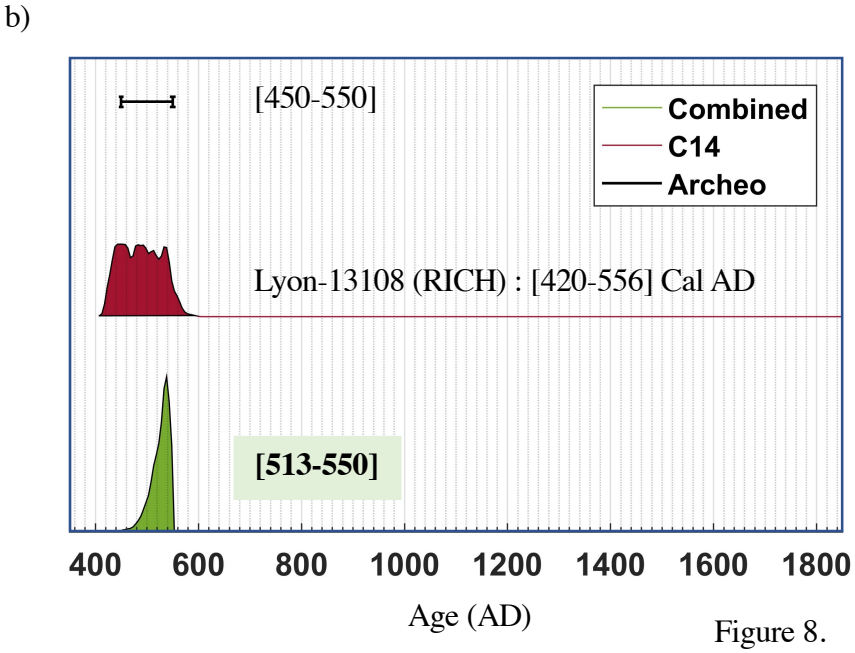
b)
[450-550]
Combined
C14
Archeo
Lyon-13108 (RICH) : [420-556] Cal AD
[513-550]
400
600
800
1000
1200
1400
1600
1800
Age (AD)

Figure 8.

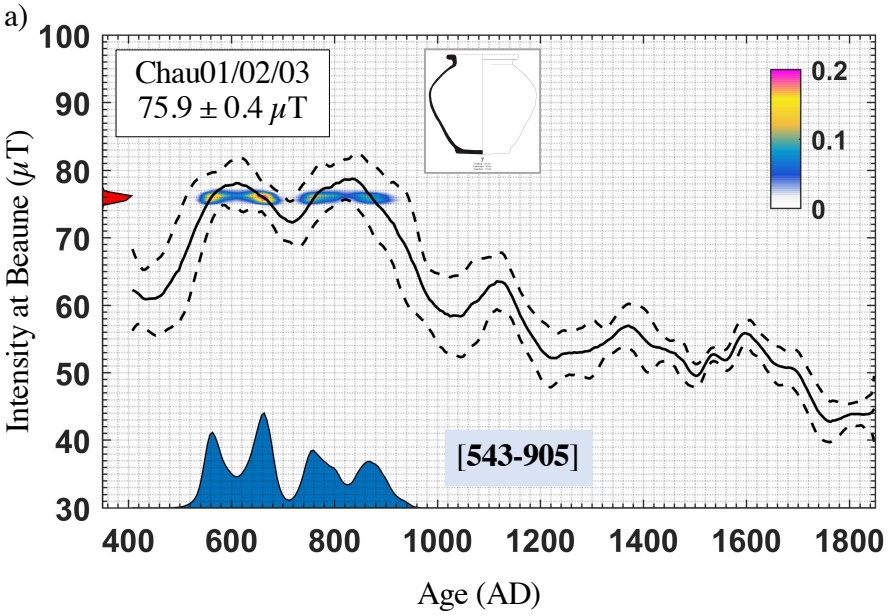
a)
Chau01/02/03
75.9 ± 0.4 μT
0.2
0.1
0
[543-905]
Intensity at Beaune (μT)
100
90
80
70
60
50
40
30
400
600
800
1000
1200
1400
1600
1800
Age (AD)

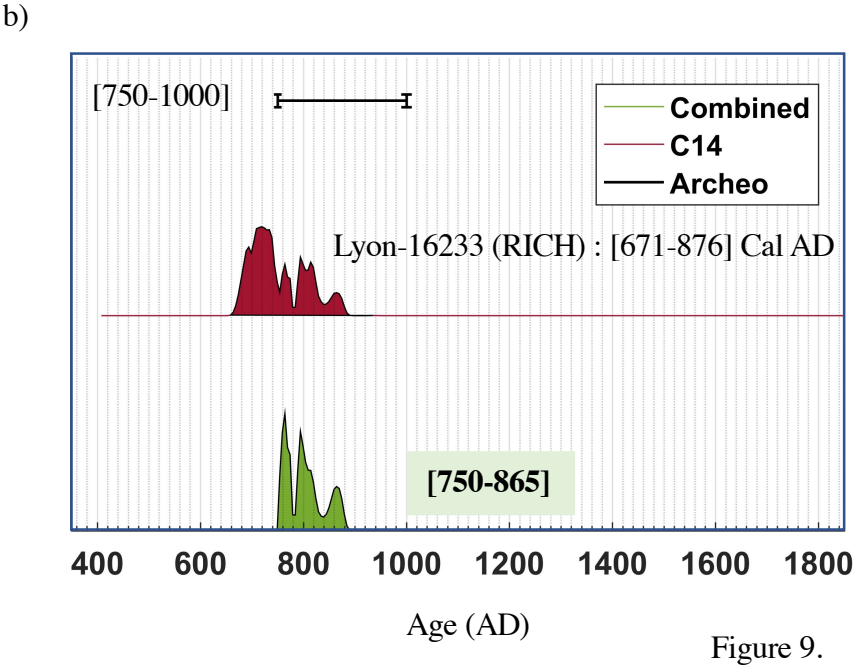
b)
[750-1000]
Combined
C14
Archeo
Lyon-16233 (RICH) : [671-876] Cal AD
[750-865]
400
600
800
1000
1200
1400
1600
1800
Age (AD)

Figure 9.

Table 1

# Group	Site (Location, Archeological excavation)	Archeological description	Type of material	Age (AD.)	N Thermal unit(s) (n specimens)	F ± σF (μT)	F $_{Beaune}$ (μT)
► *Groups analyzed to provide new reference intensity values*							
SAR19	Saran, La Guignace (47.9°N, 1.9°E)	Kiln 10 (SU 2761)	Potsherd	[550-620]	N=12 (n=26)	77.1±2.8	76.4
SAR21	Saran, La Guignace (47.9°N, 1.9°E)	Kiln 5 (SU 2064)	Potsherd	[600-650]	N=5 (n=16)	77.7±2.4	77.0
VAN03	Vanves, rue Gaudray (48.83°N, 2.30°E)	Kiln 3039 (SU 3304 & SU 3305)	Potsherd	[650-700]	N=4 (n=10)	76.9±1.1	75.5
VAN09	Vanves, rue Gaudray (48.83°N, 2.30°E)	Kiln 1138 (SU 1141)	Potsherd	[650-700]	N=4 (n=9)	75.8±1.3	74.5
CHAM03	Chamigny, La Grande Maison (48.97°N, 3.15°E)	Kiln 2629 (Structure 2116)	Potsherd	[675-725]	N=4 (n=15)	72.7±0.9	71.3
SAR36	Saran, Voie Nouvelle (47.9°N, 1.9°E)	F 24 (SU 1073)	Potsherd	[700-750]	N=4 (n=12)	74.7±2.2	74.1
HERME04	Hermé, Les Malletons carrière SPM (48.5°N,3.3°E)	Kiln 3060; fragments from the central (and elongated) support of the floor in the firing chamber	Baked clay fragment	[970-1000]	N=1 (n=15)	62.5±2.4	61.6
► *Groups analyzed for dating*							
BOUR01/02	La Chapelle Saint-Ursin, L'angoulaire, chemin des vallées aux fruscades (47.08°N, 2.4°E)	Kiln 3004 (SU 30121 & SU 30145)	Potsherd		N=4 (n=13)	73.2±2.9	73.2
BOUR03	La Chapelle Saint-Ursin, L'angoulaire, chemin des vallées aux fruscades (47.08°N, 2.4°E)	Kiln 3004, fragments from the kiln floor in the firing chamber	Baked clay fragment		N=1 (n=11)	73.9±2.2	73.9
BOUR01/02/03	La Chapelle Saint-Ursin, L'angoulaire, chemin des vallées aux fruscades (47.08°N, 2.4°E)				N=5 (n=24)	73.7±2.3	73.7
CHAU01/02	Viennes-en-Arthies, Chaudry (49.07°N, 1.73°E)	Filling unit of the kiln	Potsherd		N=4 (n=12)	77.3±0.5	75.8
CHAU03	Viennes-en-Arthies, Chaudry (49.07°N, 1.73°E)	Pottery fragments associated with debris of the kiln walls	Potsherd		N=2 (n=6)	77.6±0.3	76.1
CHAU01/02/03	Viennes-en-Arthies, Chaudry (49.07°N, 1.73°E)				N=6 (n=18)	77.4±0.4	75.9

Table 2

	Archeointensity correlation dating		Archeointensity marginalized dating	
	Our dataset	All selected data	Our dataset	All selected data
► *BOUR01/02/03 : 73.7 ± 2.3 µT*				
Bootstrap algorithm Thébault and Gallet (2010)	[513 – 930]	[513 – 935]	X	X
AH-RJMCMC method Livermore et al. (2018)	[502 – 824] & [839– 926]	[508 – 583] & [640– 932]	[505 – 826] & [844 – 926]	[509 – 587] & [642 – 933]
► *CHAU01/02/03 : 75.9 ± 0.4 µT*				
Bootstrap algorithm Thébault and Gallet (2010)	[543 – 895]	[543 – 905]	X	X
AH-RJMCMC method Livermore et al. (2018)	[541 – 683] & [752 – 899]	[544 – 586] & [643 – 683] & [740 – 902]	[543 – 686] & [752 – 899]	[545 – 589] & [642 – 685] & [742 – 907]
► *CHAU01/02/03 : 75.9 ± 1.5 µT*				
Bootstrap algorithm Thébault and Gallet (2010)	[538 – 905]	[538 – 915]	X	X
AH-RJMCMC method Livermore et al. (2018)	[535 – 707] & [731 – 905]	[535 – 595] & [628 – 698] & [722 – 911]	[535 – 708] & [732 – 905]	[536 – 598] & [631 – 700] & [720 – 913]

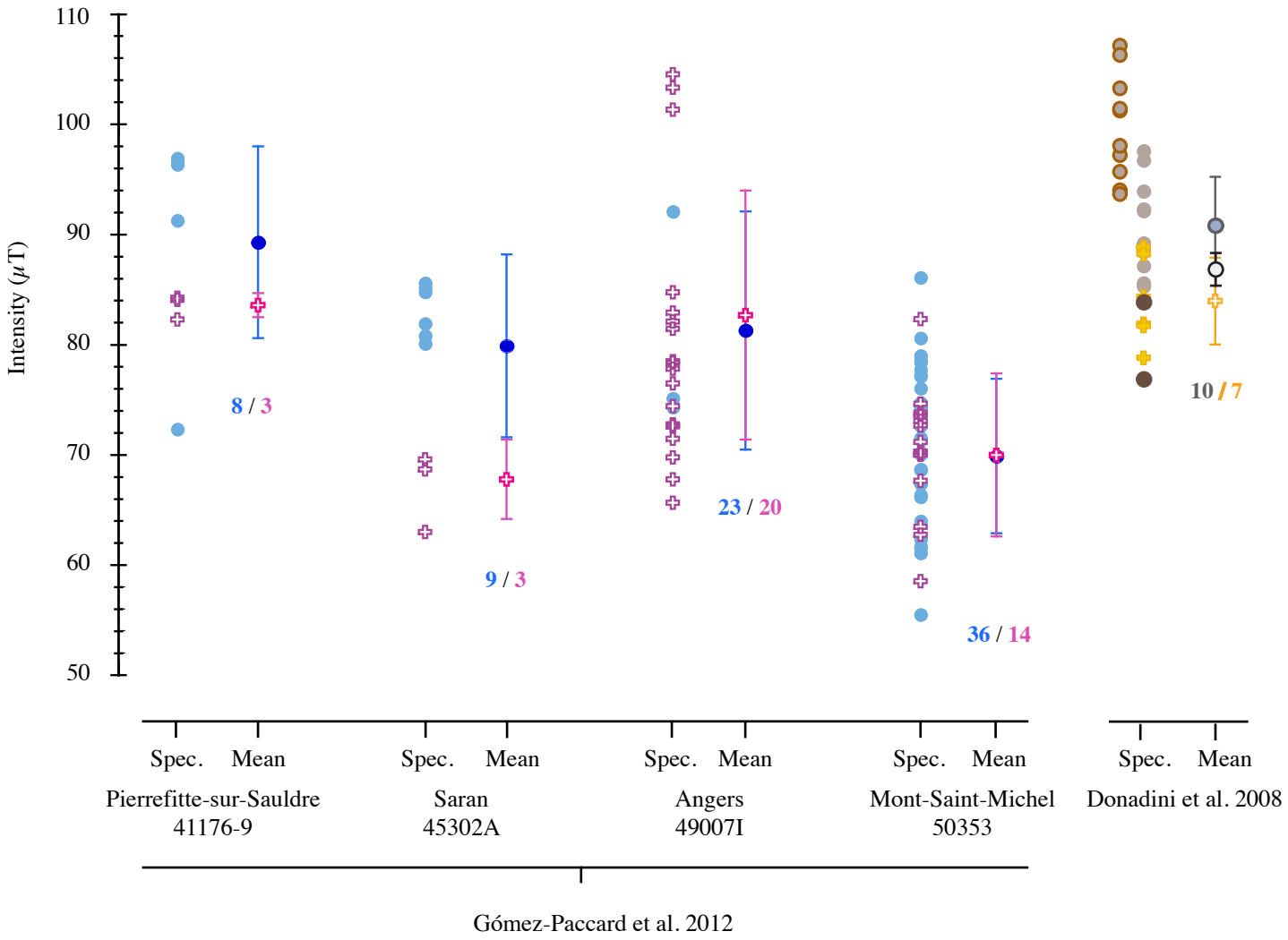

Gómez-Paccard et al. 2012

=> Specimen level

- Non corrected
- Corrected

from cooling rate effect

=> Mean level

- site/group weighted mean computed by Gomez-Paccard et al. 2012 (mixing fragments corrected and non corrected from cooling rate effect)
- site/group weighted mean computed using only fragments for which cooling rate effect was corrected

Donadini et al. 2008

=> Specimen level

- Mini samples
- Mini samples + 10% arbitary cooling rate effect
- Big samples
- Big samples Sofia lab. (no fan)

Heslsinki lab.

=> Mean level

- Weighted mean and weighted error computed by Donadini et al. 2008
- Mean from the mini samples values, + 10% arbitary cooling rate effect
- Mean derived from values obtained for the big samples analyzed in Sofia

Supp. Figure1

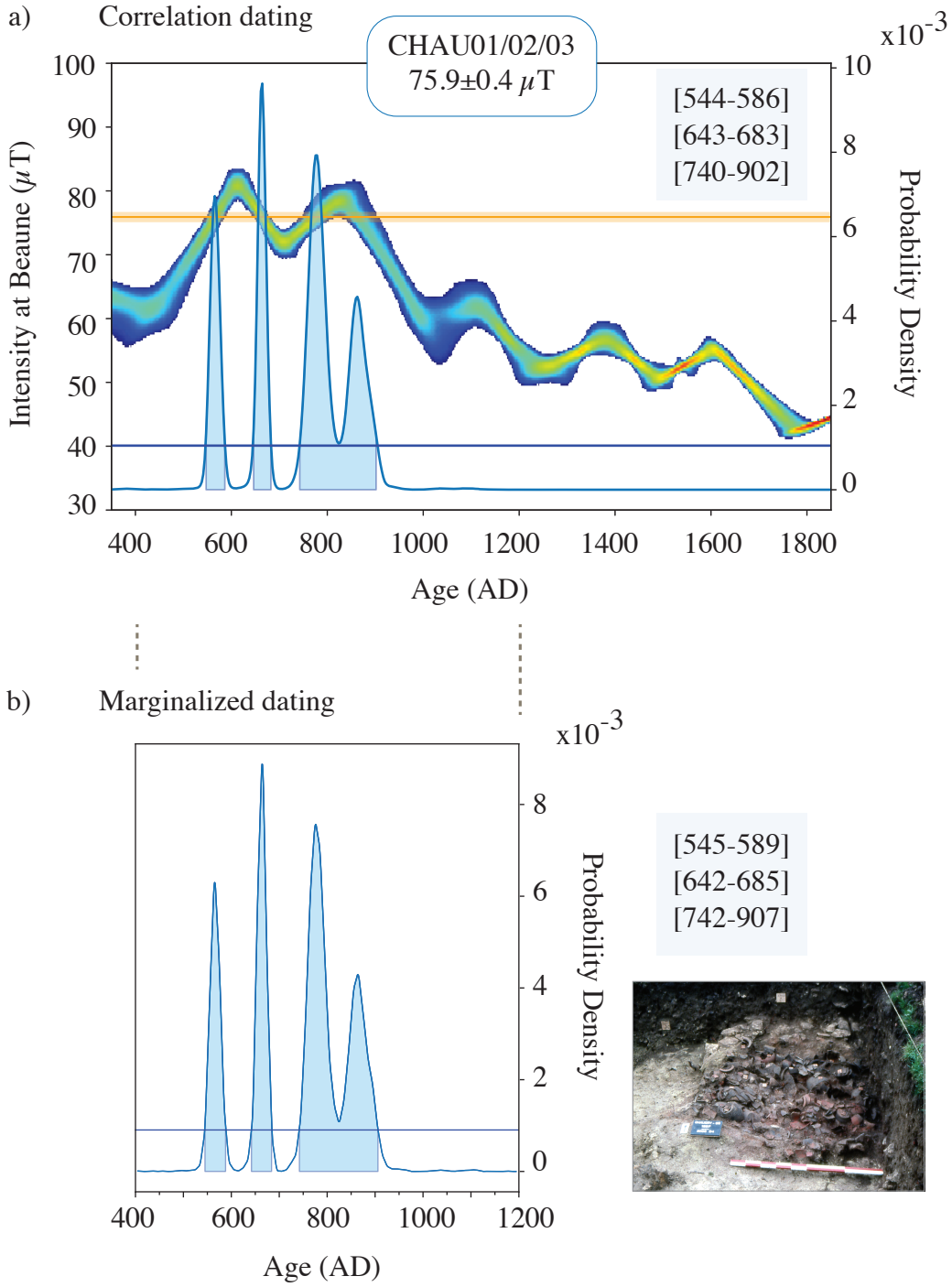
a)
Correlation dating
CHAU01/02/03
75.9±0.4 μT
[544-586]
[643-683]
[740-902]
Intensity at Beaune (μT)
Probability Density
x10-3
Age (AD)
b)
Marginalized dating
[545-589]
[642-685]
[742-907]
Probability Density
x10-3
Age (AD)

Figure S2.

Supp. Table 1

Fragment	Specimen	Natural magnetic moment	Tmin-Tmax	F Lab	NRM T1 (T1')	Slope R'	F Triaxe	F Triaxe mean value per fragment ± σF
		10^{-8} A.m^2	(°C)	(μT)	(%)	(%)	(μT)	(μT)
SAR19, Saran - La Guignace [550-620] AD, (23/20/18/12)*, (42/26)**								
SAR19-02	SAR19-02A	52	315-495	75	87	0	80.7	80.2±0.5
	SAR19-02B	85	350-495	75	89	1	79.6	
SAR19-04	SAR19-04A	43	210-495	75	88	0	78.4	78.9±0.5
	SAR19-04C	49	180-485	75	86	-2	79.4	
SAR19-05	SAR19-05A	49	195-495	75	89	0	78.3	76.4±1.4
	SAR19-05B	37	180-485	75	86	0	75.5	
SAR19-06	SAR19-06A	87	180-495	75	94	-3	76.3	74.8±1.7
	SAR19-06B	94	180-485	75	90	6	74.1	
	SAR19-06C	101	180-485	75	92	1	72.8	
	SAR19-06D	71	180-470	75	84	-2	76.1	
SAR19-07	SAR19-07A	102	180-495	75	90	-1	74.6	76.2±1.6
	SAR19-07B	116	180-485	75	91	-2	77.8	
SAR19-12	SAR19-12A	54	180-495	75	90	3	72.8	72.5±0.4
	SAR19-12B	59	175-480	75	90	3	72.1	
SAR19-13	SAR19-13A	122	180-485	75	91	4	76.0	76.7±0.7
	SAR19-13B	130	180-475	75	89	5	77.3	
SAR19-14	SAR19-14A	117	225-485	75	80	5	75.1	74.6±0.5
	SAR19-14B	96	235-485	75	86	3	74.1	
SAR19-16	SAR19-16A	268	180-485	75	91	1	78.6	78.2±0.4
	SAR19-16B	227	180-470	75	88	1	77.7	
SAR19-18	SAR19-18A	67	265-485	75	86	-6	74.6	75.3±0.7
	SAR19-18B	69	245-490	75	84	1	76.0	
SAR19-21	SAR19-21A	200	180-485	75	78	4	82.1	82.6±0.5
	SAR19-21B	195	180-485	75	81	-2	83.1	
SAR19-23	SAR19-23A	212	180-485	75	91	-2	77.9	78.4±0.5
	SAR19-23C	210	190-470	75	86	-3	78.9	
SAR21, Saran - La Guignace [600-650] AD, (16/10/10/5)*, (28/16)**								
SAR21-02	SAR21-02A	73	200-495	75	92	4	78.3	77.8±1.1
	SAR21-02B	65	200-495	75	79	1	76.5	
	SAR21-02C	57	180-490	75	84	0	78.6	
SAR21-03	SAR21-03A	72	260-495	75	90	6	74.6	76.0±1.3
	SAR21-03B	50	260-495	75	83	0	77.3	
SAR21-05	SAR21-05B	62	220-505	75	83	2	77.6	76.1±2.1
	SAR21-05C	71	190-495	75	90	3	73.7	
	SAR21-05E	95	200-505	75	91	-1	77.0	
SAR21-11	SAR21-11A	52	180-480	75	80	5	80.8	81.7±1.9
	SAR21-11B	61	180-485	75	85	1	84.6	
	SAR21-11C	37	205-485	75	81	1	80.5	
	SAR21-11D	40	195-480	75	90	-3	80.9	
SAR21-15	SAR21-15A	43	280-480	75	71	-6	76.4	77.0±1.3
	SAR21-15B	39	265-505	75	80	-4	77.5	
	SAR21-15C	47	270-505	75	79	3	78.4	
	SAR21-15D	50	270-505	75	81	0	75.5	

VAN03, Vanves - rue Gaudray [650-700] AD, (13/11/10/4)*, (25/10)**

VAN03-23	VAN03-23A	547	265-510	75	99	4	76.7	77.7±1.0
	VAN03-23B	668	265-490	75	98	4	78.7	
VAN03-28	VAN03-28A	145	285-490	75	90	7	77.1	77.6±1.2
	VAN03-28C	138	260-475	75	81	4	79.0	
	VAN03-28D	115	275-490	75	84	6	76.7	
VAN03-30	VAN03-30A	134	225-490	75	86	5	77.5	77.1±0.5
	VAN03-30D	95	200-500	75	81	1	76.6	
VAN03-31	VAN03-31B	56	175-485	75	78	0	76.1	75.3±0.7
	VAN03-31C	75	180-500	75	82	5	75.1	
	VAN03-31D	84	190-500	75	79	3	74.8	

VAN09, Vanves - rue Gaudray [650-700] AD, (11/11/10/4)*, (22/9)**

VAN09-06	VAN09-06A	65	250-510	75	90	3	75.7	75.9±0.2
	VAN09-06C	60	250-500	75	80	3	76.1	
VAN09-07	VAN09-07A	103	185-510	75	94	1	76.3	75.9±0.4
	VAN09-07B	90	175-495	75	91	3	75.5	
VAN09-08	VAN09-08A	161	195-510	75	95	5	76.0	77.3±1.3
	VAN09-08B	108	175-495	75	94	1	78.6	
VAN09-11	VAN09-11A	89	175-510	75	91	7	73.5	74.1±0.7
	VAN09-11B	94	175-495	75	85	-4	74.9	
	VAN09-11C	52	175-495	75	81	3	74.0	

CHAM03, Chamigny - La Grande Maison [675-725] AD, (19/12/9/4)*, (24/15)**

CHAM03-03	CHAM03-03A	70	275-525	75	73	3	73.2	73.7±1.3
	CHAM03-03B	131	250-515	75	73	8	75	
	CHAM03-03C	89	255-525	75	78	5	72.1	
	CHAM03-03D	126	250-510	75	72	4	74.3	
CHAM03-09	CHAM03-09B	319	285-525	75	85	4	69.6	71.8±1.8
	CHAM03-09D	191	235-515	75	82	-3	72.3	
	CHAM03-09E	257	250-515	75	91	4	73.9	
	CHAM03-09F	204	280-505	75	75	5	71.3	
CHAM03-10	CHAM03-10A	36	290-520	75	78	3	72.8	73.1±1.0
	CHAM03-10B	34	290-515	75	75	0	74.3	
	CHAM03-10D	39	280-515	75	80	6	72.3	
CHAM03-18	CHAM03-18A	67	190-520	75	89	3	71.6	72.2±0.5
	CHAM03-18B	76	195-500	75	85	1	72.5	
	CHAM03-18D	47	190-500	75	84	-6	72.6	
	CHAM03-18E	66	180-500	75	84	5	72.2	

SAR36, Saran - Voie nouvelle [700-750] AD, (12/7/7/4)*, (30/12)**

SAR36-01	SAR36-01A	41	175-500	75	92	1	72.5	72.3±1.1
	SAR36-01B	32	180-485	75	88	-5	73.3	
	SAR36-01C	37	180-485	75	86	-2	71.2	
SAR36-08	SAR36-08A	48	245-500	75	92	9	73.5	73.4±1.2
	SAR36-08B	43	225-500	75	89	8	72.2	
	SAR36-08C	39	175-500	75	90	-7	74.5	
SAR36-12	SAR36-12A	39	340-500	75	85	5	75.7	76.5±0.7
	SAR36-12B	155	340-500	75	86	3	76.9	
	SAR36-12D	69	330-500	75	89	3	76.9	
SAR36-13	SAR36-13A	120	175-500	75	87	2	76.4	76.5±0.6
	SAR36-13B	68	185-490	75	78	0	77.1	
	SAR36-13C	42	190-500	75	89	2	76.0	

HERME04, Hermé - Les Malletons carrière SPM [970-1000] AD, (30/15)**

	HERME04-01A	76	215-490	65	66	-1	66.8	
	HERME04-01B	143	220-515	65	84	-2	60.4	
	HERME04-01C	145	200-495	60	75	7	66.6	
	HERME04-01D	61	200-515	60	74	-7	62.9	
	HERME04-02A	74	185-500	65	73	-2	60.8	
	HERME04-02B	56	200-515	65	76	-3	60.5	
	HERME04-02E	61	180-500	60	75	-3	60.7	
	HERME04-03A	113	195-505	65	74	-2	64.7	
	HERME04-03B	82	205-510	65	76	-6	62.5	
	HERME04-04A	91	225-520	65	82	0	63.3	
	HERME04-04C	103	175-520	65	79	-1	65.5	
	HERME04-06A	145	210-520	65	76	-4	60.3	
	HERME04-06B	129	220-515	65	74	-5	59.9	
	HERME04-06C	110	235-520	60	69	3	61.3	
	HERME04-06D	98	205-515	60	66	0	61.8	

BOUR01/02, La Chapelle Saint-Ursin, L'angoulaire, chemin des vallées aux fruscades, (26/20/17/4)*, (29/13)**

BOUR01-05	BOUR01-05A	243	175-475	70	88	-1	74.0	74.1±0.3
	BOUR01-05C	135	185-475	75	93	0	74.4	
	BOUR01-05E	227	195-475	75	93	-1	73.9	
BOUR02-03	BOUR02-03A	743	225-485	75	57	-1	74.8	73.6±1.1
	BOUR02-03B	515	225-510	75	86	-2	73.5	
	BOUR02-03D	479	225-490	75	58	-1	72.6	
BOUR02-05	BOUR02-05A	702	175-505	75	94	-4	75.5	75.8±2.6
	BOUR02-05B	610	175-500	75	84	-1	78.3	
	BOUR02-05C	449	175-495	75	94	-3	72.2	
	BOUR02-05D	646	195-495	75	76	-1	77.1	
BOUR02-07	BOUR02-07A	785	175-495	75	66	-2	69.8	69.1±0.8
	BOUR02-07B	805	175-510	75	75	4	68.2	
	BOUR02-07C	810	175-500	75	81	-1	69.3	

BOUR03, La Chapelle Saint-Ursin, L'angoulaire, chemin des vallées aux fruscades, (33/11)**

BOUR03-01A	236	180-500	75	68	3	72.3	
BOUR03-01D	172	190-490	75	82	-7	74.2	
BOUR03-02A	265	180-500	75	88	-1	74.4	
BOUR03-02B	318	175-525	75	94	-3	75.7	
BOUR03-03A	143	175-505	75	72	-1	69.2	
BOUR03-03C	380	180-490	75	81	-1	75.5	
BOUR03-03G	200	150-490	75	68	1	75.2	
BOUR03-08A	175	175-500	75	66	5	75.0	
BOUR03-08C	120	180-490	75	79	-2	76.9	
BOUR03-10B	550	160-490	75	59	-5	72.8	
BOUR03-10C	200	180-490	75	79	-8	72.2	

CHAU01/02, Viennes-en-Arthies - Chaudry, (25/25/24/4)*, (48/12)**

CHAU01-01	CHAU01-01A	891	175-515	75	90	2	76.7	77.7±0.8
	CHAU01-01B	900	180-505	75	83	3	78.2	
	CHAU01-01C	840	180-505	75	83	1	78.1	
CHAU01-03	CHAU01-03A	438	385-500	75	80	2	76.0	76.8±1.4
	CHAU01-03C	342	385-505	75	88	6	76.0	
	CHAU01-03D	496	365-495	75	81	-2	78.4	
CHAU01-12	CHAU01-12A	751	180-525	75	97	2	78.3	77.7±1.1
	CHAU01-12B	840	180-505	75	92	-1	78.4	
	CHAU01-12C	658	185-505	75	93	-2	76.5	
CHAU02-08	CHAU02-08B	385	180-515	75	95	-1	76.8	77.0±0.3
	CHAU02-08C	441	180-505	75	89	0	76.8	
	CHAU02-08D	316	180-495	75	88	-3	77.3	

CHAU03, Viennes-en-Arthies - Chaudry, (12/11/9/2)*, (20/6)**

CHAU03-05	CHAU03-05A	85	180-530	75	81	3	77.1	77.8±0.9
	CHAU03-05B	276	180-525	75	88	0	78.9	
	CHAU03-05C	123	175-505	75	73	3	77.5	
CHAU03-08	CHAU03-08A	87	180-535	75	81	-6	77.7	77.3±0.3
	CHAU03-08B	42	185-525	75	70	2	77.1	
	CHAU03-08C	124	210-525	75	83	3	77.2	

Supp. Table 2

	Bootstrap algorithm						Transdimensional bayesian technique							
	Fig. 6a			Fig. 6b			Fig. 6c				Fig. 6d			
Age (AD)	Probability Maximum (μT)	Lower Limit (μT)	Upper Limit (μT)	Probability Maximum (μT)	Lower Limit (μT)	Upper Limit (μT)	Age (AD)	Probability Maximum (μT)	Median (μT)	Lower Limit (μT)	Upper Limit (μT)	Probability Maximum (μT)	Median (μT)	Lower Limit (μT)	Upper Limit (μT)
300.00				66.70	74.87	58.61	298.02	52.85	57.65	44.91	81.16	65.45	66.05	59.76	76.93
303.00				66.38	73.99	58.77	301.03	53.15	57.65	45.58	79.92	65.75	66.05	60.24	75.73
306.00				66.04	73.13	58.94	304.03	53.75	57.65	46.24	78.68	65.15	65.75	60.50	74.58
309.00				65.68	72.29	59.07	307.03	54.65	57.65	46.82	77.44	65.45	65.45	60.60	73.51
312.00				65.30	71.45	59.14	310.04	54.05	57.65	47.41	76.22	65.15	65.15	60.56	72.46
315.00				64.91	70.65	59.17	313.04	54.35	57.65	47.96	74.96	64.85	65.15	60.43	71.46
318.00				64.53	69.93	59.13	316.05	54.65	57.95	48.48	73.62	64.85	64.85	60.20	70.55
321.00				64.16	69.31	59.02	319.05	55.85	57.95	49.00	72.30	64.55	64.55	59.90	69.70
324.00				63.78	68.79	58.75	322.05	55.85	57.95	49.49	70.94	64.55	64.25	59.54	68.97
327.00				63.42	68.44	58.41	325.06	56.75	57.95	49.98	69.64	64.25	64.25	59.07	68.35
330.00				63.09	68.19	57.98	328.06	56.75	58.25	50.42	68.50	64.25	63.95	58.54	67.87
333.00				62.80	68.06	57.55	331.06	57.35	58.25	50.82	67.63	63.95	63.65	57.96	67.48
336.00				62.54	67.96	57.12	334.07	57.35	58.25	51.13	66.98	63.95	63.65	57.36	67.17
339.00				62.30	67.89	56.71	337.07	57.65	58.25	51.38	66.58	63.95	63.35	56.75	66.95
342.00				62.09	67.83	56.35	340.08	57.65	58.25	51.57	66.36	63.95	63.05	56.10	66.78
345.00				61.91	67.77	56.04	343.08	57.95	58.25	51.66	66.29	63.65	63.05	55.45	66.66
348.00				61.76	67.72	55.79	346.08	57.95	58.25	51.66	66.36	63.65	62.75	54.80	66.58
351.00	60.18	54.39	65.99	61.64	67.66	55.61	349.09	58.25	58.55	51.63	66.53	63.65	62.75	54.16	66.51
354.00	60.37	54.75	65.99	61.55	67.61	55.48	352.09	58.55	58.55	51.51	66.91	63.65	62.45	53.57	66.50
357.00	60.56	55.06	66.06	61.49	67.56	55.41	355.09	58.55	58.55	51.34	67.42	63.35	62.45	53.03	66.49
360.00	60.74	55.32	66.15	61.45	67.52	55.38	358.10	58.55	58.55	51.21	67.98	63.05	62.45	52.61	66.53
363.00	60.91	55.53	66.29	61.42	67.46	55.39	361.10	59.15	58.85	51.10	68.54	63.35	62.15	52.26	66.57
366.00	61.06	55.68	66.44	61.42	67.43	55.41	364.11	58.55	58.85	51.09	69.01	63.05	62.15	52.01	66.61
369.00	61.21	55.80	66.62	61.45	67.42	55.48	367.11	58.85	59.15	51.12	69.45	63.05	62.15	51.86	66.64
372.00	61.35	55.88	66.81	61.50	67.43	55.58	370.11	59.15	59.15	51.22	69.73	62.75	61.85	51.80	66.71
375.00	61.49	55.95	67.02	61.57	67.45	55.69	373.12	59.15	59.45	51.39	70.02	62.75	61.85	51.79	66.81
378.00	61.63	56.01	67.25	61.62	67.47	55.78	376.12	59.45	59.45	51.67	70.10	62.75	61.85	51.86	66.83
381.00	61.75	56.05	67.46	61.68	67.49	55.87	379.12	59.75	59.75	52.00	70.09	62.75	61.55	52.01	66.88
384.00	61.86	56.07	67.65	61.74	67.53	55.96	382.13	60.05	59.75	52.37	69.99	62.75	61.55	52.20	66.89
387.00	61.96	56.09	67.82	61.81	67.58	56.05	385.13	60.05	60.05	52.79	69.76	62.45	61.55	52.47	66.84
390.00	62.03	56.11	67.96	61.88	67.63	56.13	388.14	60.35	60.05	53.21	69.42	62.45	61.25	52.80	66.75
393.00	62.10	56.14	68.06	61.93	67.67	56.19	391.14	60.35	60.35	53.66	68.97	62.45	61.25	53.17	66.62
396.00	62.16	56.18	68.13	61.98	67.70	56.26	394.14	60.35	60.35	54.12	68.39	62.15	61.25	53.57	66.47
399.00	62.19	56.23	68.15	62.02	67.72	56.33	397.15	60.35	60.65	54.60	67.81	62.15	61.25	53.99	66.26
402.00	62.21	56.29	68.13	62.06	67.71	56.40	400.15	60.65	60.65	55.04	67.21	61.85	61.25	54.41	66.05
405.00	62.21	56.36	68.07	62.08	67.68	56.48	403.15	61.25	60.95	55.45	66.74	61.85	61.25	54.81	65.89
408.00	62.20	56.46	67.94	62.08	67.61	56.56	406.16	61.25	60.95	55.82	66.40	61.85	61.25	55.20	65.75
411.00	62.16	56.56	67.76	62.06	67.48	56.65	409.16	61.55	61.25	56.13	66.14	61.85	61.25	55.52	65.64
414.00	62.10	56.67	67.53	62.02	67.30	56.74	412.17	61.55	61.25	56.37	65.98	61.85	61.25	55.78	65.57
417.00	62.03	56.80	67.26	61.96	67.09	56.84	415.17	61.85	61.55	56.56	65.90	61.55	61.25	55.99	65.52
420.00	61.94	56.93	66.96	61.89	66.84	56.94	418.17	62.15	61.55	56.72	65.89	61.55	61.25	56.13	65.47
423.00	61.84	57.03	66.65	61.80	66.56	57.03	421.18	62.15	61.85	56.84	65.92	61.55	61.25	56.23	65.45
426.00	61.72	57.12	66.33	61.70	66.30	57.10	424.18	62.15	61.85	56.89	66.02	61.25	61.25	56.27	65.46
429.00	61.61	57.16	66.06	61.60	66.05	57.16	427.18	62.45	62.15	56.92	66.16	61.55	61.25	56.27	65.51
432.00	61.50	57.17	65.82	61.51	65.84	57.16	430.19	62.75	62.15	56.92	66.33	61.55	61.25	56.27	65.57
435.00	61.40	57.15	65.66	61.42	65.69	57.15	433.19	63.05	62.45	56.95	66.50	61.25	61.55	56.27	65.65
438.00	61.31	57.06	65.56	61.33	65.59	57.08	436.20	63.05	62.75	56.99	66.66	61.55	61.55	56.32	65.73
441.00	61.23	56.93	65.56	61.25	65.57	56.95	439.20	63.65	62.75	57.08	66.83	61.85	61.55	56.40	65.83
444.00	61.17	56.76	65.57	61.18	65.60	56.78	442.20	63.65	63.05	57.16	67.00	61.85	61.85	56.49	65.95
447.00	61.12	56.56	65.68	61.13	65.67	56.59	445.21	64.25	63.35	57.25	67.18	62.15	61.85	56.63	66.09
450.00	61.10	56.35	65.82	61.09	65.81	56.38	448.21	64.25	63.35	57.31	67.38	62.15	62.15	56.73	66.26
453.00	61.09	56.15	66.02	61.11	66.00	56.20	451.21	64.85	63.65	57.38	67.59	62.15	62.15	56.84	66.45
456.00	61.12	55.99	66.24	61.15	66.24	56.06	454.22	65.15	63.95	57.43	67.80	62.15	62.45	56.93	66.66
459.00	61.20	55.90	66.50	61.24	66.51	55.96	457.22	65.45	64.25	57.48	68.03	63.05	62.45	57.04	66.88
462.00	61.31	55.86	66.78	61.36	66.80	55.95	460.23	65.75	64.55	57.48	68.26	63.35	62.75	57.13	67.13
465.00	61.47	55.87	67.06	61.53	67.10	55.96	463.23	66.05	64.85	57.50	68.51	63.65	63.05	57.19	67.38
468.00	61.66	55.96	67.35	61.73	67.42	56.05	466.23	66.35	65.15	57.50	68.77	63.95	63.35	57.25	67.64
471.00	61.90	56.11	67.68	61.98	67.76	56.21	469.24	66.65	65.45	57.48	69.03	64.55	63.65	57.29	67.91
474.00	62.18	56.34	68.02	62.29	68.13	56.45	472.24	66.95	65.75	57.45	69.30	64.85	63.95	57.31	68.20
477.00	62.50	56.62	68.39	62.60	68.50	56.71	475.24	67.25	66.05	57.40	69.60	65.45	64.25	57.29	68.50
480.00	62.86	56.95	68.78	62.94	68.88	57.01	478.25	67.55	66.35	57.28	69.90	65.75	64.55	57.27	68.81
483.00	63.25	57.32	69.19	63.33	69.31	57.36	481.25	67.55	66.65	57.13	70.22	66.05	64.85	57.25	69.11
486.00	63.66	57.71	69.61	63.75	69.75	57.75	484.26	67.85	66.95	57.02	70.54	66.35	65.15	57.26	69.42
489.00	64.09	58.12	70.06	64.19	70.22	58.16	487.26	68.15	67.25	56.96	70.86	66.65	65.45	57.30	69.73
492.00	64.55	58.57	70.53	64.66	70.72	58.60	490.26	68.45	67.55	56.92	71.21	67.25	66.05	57.36	70.04
495.00	65.04	59.04	71.04	65.17	71.26	59.07	493.27	68.75	67.85	56.92	71.59	67.85	66.35	57.46	70.34
498.00	65.56	59.54	71.58	65.67	71.79	59.54	496.27	69.05	68.15	57.00	71.97	68.15	66.65	57.60	70.65
501.00	66.07	60.02	72.12	66.18	72.35	60.01	499.27	69.35	68.45	57.14	72.35	68.45	66.95	57.80	70.94
504.00	66.60	60.52	72.67	66.72	72.93	60.51	502.28	69.65	68.75	57.35	72.73	68.45	67.55	58.04	71.24
507.00	67.15	61.04	73.26	67.27	73.52	61.02	505.28	69.95	69.05	57.63	73.10	69.35	67.85	58.35	71.54
510.00	67.71	61.57	73.85	67.83	74.12	61.54	508.29	70.25	69.35	57.99	73.45	69.35	68.15	58.72	71.84
513.00	68.28	62.11	74.45	68.39	74.72	62.07	511.29	70.25	69.65	58.41	73.79	69.65	68.75	59.14	72.14
516.00	68.85	62.66	75.04	68.96	75.31	62.61	514.29	70.55	70.25	58.93	74.13	69.95	69.05	59.58	72.43
519.00	69.42	63.22	75.62	69.52	75.88	63.17	517.30	70.85	70.55	59.55	74.41	70.25	69.35	60.13	72.72
522.00	69.97	63.78	76.17	70.09	76.44	63.74	520.30	71.15	70.85	60.23	74.68	70.55	69.95	60.79	73.01
525.00	70.53	64.37	76.69	70.65	76.97	64.33	523.30	71.45	71.15	60.96	74.93	70.85	70.25	61.50	73.30
528.00	71.09	64.98	77.19	71.18	77.44	64.92	526.31	71.75	71.45	61.85	75.17	71.45	70.55	62.31	73.60
531.00	71.63	65.61	77.65	71.71	77.88	65.54	529.31	72.05	71.75	62.84	75.50	71.75	71.15	63.13	73.90
534.00	72.16	66.26	78.05	72.24	78.28	66.20	532.32	72.35	72.05	63.84	75.85	72.05	71.45	64.02	74.22
537.00	72.67	66.94	78.41	72.75	78.62	66.88	535.32	72.65	72.35	64.94	76.21	72.35	71.75	64.89	74.53
540.00	73.18	67.65	78.71	73.24	78.89	67.59	538.32	72.95	72.65	66.04	76.55	72.65	72.35	65.77	74.86
543.00	73.66	68.38	78.94	73.70	79.09	68.32	541.33	73.25	73.25	67.15	76.91	72.95	72.65	66.64	75.20
546.00	74.12	69.14	79.11	74.15	79.22	69.08	544.33	73.25	73.55	68.18	77.26	73.25	72.95	67.47	75.55
549.00	74.56	69.93	79.20	74.59	79.31	69.87	547.33	73.55	73.85	69.16	77.58	73.85	73.55	68.30	75.92
552.00	74.97	70.71	79.22	74.99	79.31	70.66	550.34	73.85	74.15	70.05	77.88	74.15	73.85	69.10	76.29
555.00	75.34	71.47	79.22	75.36	79.28	71.43	553.34	74.15	74.45	70.86	78.13	74.45	74.15	69.84	76.68
558.00	75.68	72.18	79.19	75.68	79.23	72.12	556.35	74.45	74.75	71.58	78.34	74.75	74.75	70.56	77.09
561.00	75.96	72.76	79.19	75.96	79.21	72.70	559.35	75.05	75.05	72.21	78.53	75.05	75.05	71.26	77.51
564.00	76.21	73.23	79.19	76.21	79.25	73.18	562.35	75.35	75.35	72.74	78.70	75.65	75.35	71.94	77.97
567.00	76.45	73.61	79.28	76.43	79.32	73.53	565.36	75.35	75.65	73.20	78.84	75.95	75.95	72.55	78.44
570.00	76.65	73.89	79.41	76.64	79.47	73.81	568.36	75.65	75.95	73.62	78.99	76.25	76.25	73.15	78.95
573.00	76.82	74.11	79.53	76.86	79.64	74.07	571.36	75.95	76.25	73.99	79.11	76.55	76.55	73.72	79.48
576.00	76.97	74.33	79.61	77.05	79.81	74.30	574.37	76.25	76.55	74.34	79.23	76.85	77.15	74.24	80.05
579.00	77.09	74.53	79.64	77.22	79.94	74.51	577.37	76.55	76.85	74.65	79.36	77.45	77.45	74.72	80.65
582.00	77.17	74.72	79.63	77.37	80.10	74.63	580.38	76.85	77.15	74.94	79.48	77.45	77.75	75.18	81.25
585.00	77.23	74.83	79.62	77.48	80.28	74.68	583.38	77.15	77.15	75.21	79.59	78.05	78.35	75.61	81.82
588.00	77.26	74.87	79.65	77.59	80.54	74.63	586.38	77.45	77.45	75.45	79.72	78.35	78.65	76.00	82.29
591.00	77.27	74.84	79.70	77.67	80.82	74.53	589.39	77.45	77.45	75.66	79.85	78.65	78.95	76.37	82.69
594.00	77.27	74.75	79.80	77.74	81.10	74.37	592.39	77.45	77.75	75.84	79.96	78.95	79.55	76.72	82.99

597.00	77.26	74.63	79.91	77.82	81.35	74.31
600.00	77.25	74.54	79.94	77.91	81.54	74.28
603.00	77.22	74.49	79.94	77.99	81.63	74.34
606.00	77.18	74.46	79.91	78.05	81.68	74.42
609.00	77.15	74.45	79.85	78.11	81.72	74.48
612.00	77.10	74.40	79.79	78.11	81.77	74.45
615.00	77.04	74.32	79.76	78.09	81.84	74.33
618.00	76.97	74.21	79.74	78.02	81.88	74.15
621.00	76.91	74.11	79.71	77.94	81.89	74.00
624.00	76.85	74.04	79.67	77.85	81.79	73.90
627.00	76.78	74.01	79.56	77.76	81.62	73.92
630.00	76.70	74.00	79.41	77.66	81.34	73.98
633.00	76.62	74.01	79.23	77.53	81.02	74.05
636.00	76.54	74.01	79.07	77.39	80.70	74.08
639.00	76.45	73.97	78.94	77.24	80.41	74.06
642.00	76.37	73.89	78.84	77.06	80.14	73.99
645.00	76.28	73.81	78.75	76.87	79.90	73.84
648.00	76.20	73.74	78.66	76.68	79.65	73.69
651.00	76.12	73.74	78.51	76.49	79.38	73.61
654.00	76.04	73.75	78.32	76.32	79.05	73.59
657.00	75.95	73.78	78.11	76.16	78.72	73.59
660.00	75.88	73.78	77.99	76.01	78.44	73.59
663.00	75.80	73.68	77.93	75.87	78.25	73.50
666.00	75.72	73.51	77.95	75.72	78.14	73.31
669.00	75.63	73.26	78.00	75.54	78.08	73.01
672.00	75.50	72.99	77.99	75.33	77.98	72.68
675.00	75.34	72.74	77.95	75.09	77.84	72.33
678.00	75.12	72.51	77.74	74.81	77.59	72.04
681.00	74.89	72.28	77.49	74.51	77.27	71.74
684.00	74.63	72.03	77.23	74.18	76.94	71.41
687.00	74.36	71.70	77.02	73.87	76.68	71.05
690.00	74.09	71.32	76.87	73.57	76.49	70.65
693.00	73.82	70.87	76.77	73.27	76.34	70.19
696.00	73.56	70.45	76.67	72.98	76.20	69.77
699.00	73.33	70.08	76.57	72.74	76.06	69.40
702.00	73.13	69.85	76.41	72.54	75.89	69.19
705.00	72.97	69.72	76.22	72.39	75.69	69.08
708.00	72.84	69.66	76.03	72.28	75.50	69.06
711.00	72.76	69.61	75.91	72.23	75.43	69.03
714.00	72.71	69.57	75.85	72.21	75.43	69.00
717.00	72.70	69.47	75.91	72.22	75.51	68.92
720.00	72.70	69.35	76.05	72.28	75.76	68.81
723.00	72.76	69.23	76.28	72.40	76.08	68.72
726.00	72.84	69.19	76.52	72.57	76.44	68.70
729.00	72.96	69.17	76.75	72.79	76.81	68.78
732.00	73.09	69.23	76.95	73.05	77.16	68.92
735.00	73.24	69.34	77.13	73.33	77.49	69.16
738.00	73.40	69.52	77.28	73.64	77.83	69.46
741.00	73.58	69.72	77.45	73.98	78.16	69.81
744.00	73.78	69.95	77.62	74.33	78.49	70.17
747.00	73.98	70.17	77.80	74.69	78.84	70.55
750.00	74.19	70.38	77.99	75.06	79.20	70.92
753.00	74.41	70.59	78.23	75.40	79.56	71.25
756.00	74.63	70.79	78.48	75.74	79.92	71.57
759.00	74.85	70.97	78.74	76.08	80.29	71.87
762.00	75.07	71.14	79.00	76.40	80.63	72.16
765.00	75.29	71.33	79.24	76.69	80.94	72.44
768.00	75.50	71.53	79.46	76.93	81.17	72.70
771.00	75.69	71.76	79.63	77.14	81.32	72.96
774.00	75.88	72.01	79.75	77.32	81.41	73.24
777.00	76.07	72.31	79.82	77.45	81.40	73.51
780.00	76.24	72.61	79.87	77.54	81.34	73.75
783.00	76.40	72.88	79.92	77.59	81.25	73.93
786.00	76.56	73.12	80.00	77.62	81.21	74.03
789.00	76.73	73.32	80.14	77.64	81.20	74.08
792.00	76.89	73.46	80.31	77.65	81.22	74.06
795.00	77.04	73.59	80.49	77.65	81.28	74.03
798.00	77.18	73.72	80.65	77.68	81.32	74.05
801.00	77.32	73.90	80.73	77.72	81.33	74.10
804.00	77.45	74.14	80.76	77.79	81.29	74.29
807.00	77.59	74.44	80.74	77.88	81.22	74.53
810.00	77.73	74.76	80.70	77.97	81.14	74.79
813.00	77.86	75.06	80.65	78.06	81.10	75.03
816.00	77.96	75.29	80.64	78.15	81.09	75.20
819.00	78.04	75.43	80.67	78.23	81.15	75.32
822.00	78.10	75.44	80.74	78.29	81.22	75.33
825.00	78.15	75.43	80.86	78.32	81.32	75.32
828.00	78.18	75.37	81.00	78.33	81.40	75.28
831.00	78.18	75.27	81.10	78.33	81.47	75.19
834.00	78.16	75.15	81.18	78.29	81.55	75.03
837.00	78.13	75.04	81.21	78.22	81.66	74.79
840.00	78.07	74.91	81.23	78.12	81.80	74.45
843.00	77.98	74.76	81.20	78.00	81.97	74.02
846.00	77.86	74.58	81.14	77.85	82.16	73.54
849.00	77.73	74.39	81.07	77.66	82.33	72.99
852.00	77.57	74.16	80.98	77.47	82.49	72.46
855.00	77.39	73.90	80.88	77.28	82.59	71.96
858.00	77.20	73.61	80.78	77.06	82.58	71.50
861.00	76.98	73.28	80.67	76.82	82.55	71.11
864.00	76.73	72.92	80.55	76.57	82.35	70.79
867.00	76.48	72.53	80.43	76.32	82.11	70.53
870.00	76.21	72.12	80.30	76.07	81.82	70.32
873.00	75.93	71.70	80.17	75.81	81.49	70.13
876.00	75.64	71.27	80.02	75.56	81.18	69.94
879.00	75.34	70.83	79.85	75.33	80.89	69.76
882.00	75.04	70.41	79.67	75.10	80.64	69.56
885.00	74.73	69.99	79.48	74.86	80.40	69.32
888.00	74.41	69.57	79.25	74.62	80.19	69.05
891.00	74.09	69.17	79.01	74.37	79.99	68.76
894.00	73.77	68.78	78.76	74.11	79.79	68.44
897.00	73.45	68.40	78.50	73.83	79.56	68.11
900.00	73.13	68.00	78.25	73.55	79.32	67.77
903.00	72.80	67.58	78.02	73.28	79.12	67.43
906.00	72.46	67.10	77.81	72.99	78.94	67.05
909.00	72.09	66.55	77.63	72.68	78.77	66.58
912.00	71.70	65.92	77.49	72.34	78.65	66.03
915.00	71.29	65.21	77.37	71.98	78.57	65.40
918.00	70.85	64.43	77.27	71.59	78.51	64.67

595.39	77.45	77.75	75.98	80.08	79.25	79.85	77.05	83.23
598.40	77.45	77.75	76.06	80.18	79.85	80.15	77.36	83.42
601.40	77.75	77.75	76.11	80.27	80.45	80.45	77.66	83.56
604.40	77.45	77.75	76.12	80.34	80.75	80.75	77.95	83.69
607.41	77.45	77.75	76.10	80.39	80.75	80.75	78.21	83.78
610.41	77.45	77.75	76.07	80.42	80.75	80.75	78.39	83.84
613.42	77.15	77.75	76.02	80.43	80.75	81.05	78.45	83.87
616.42	77.15	77.75	75.96	80.41	80.75	80.75	78.37	83.87
619.42	76.85	77.45	75.90	80.38	80.75	80.75	78.20	83.84
622.43	76.85	77.45	75.83	80.30	80.45	80.75	77.96	83.78
625.43	76.85	77.15	75.75	80.20	80.15	80.45	77.71	83.67
628.43	76.85	77.15	75.66	80.06	79.55	80.15	77.46	83.51
631.44	76.55	77.15	75.57	79.90	79.25	79.85	77.22	83.34
634.44	76.55	76.85	75.48	79.69	78.95	79.25	76.98	83.11
637.45	76.55	76.85	75.37	79.45	78.65	78.95	76.75	82.83
640.45	76.25	76.55	75.27	79.19	78.35	78.65	76.51	82.46
643.45	76.25	76.55	75.15	78.89	78.05	78.35	76.27	81.98
646.46	76.25	76.25	75.03	78.58	77.75	78.05	76.03	81.42
649.46	75.95	76.25	74.91	78.29	77.45	77.45	75.76	80.78
652.46	75.95	75.95	74.78	78.00	77.15	77.15	75.47	80.11
655.47	75.65	75.95	74.63	77.74	76.85	76.85	75.15	79.47
658.47	75.65	75.65	74.48	77.49	76.25	76.55	74.78	78.88
661.48	75.35	75.65	74.30	77.26	76.25	76.25	74.36	78.34
664.48	75.35	75.35	74.11	77.06	75.95	75.95	73.88	77.84
667.48	75.05	75.05	73.88	76.88	75.35	75.35	73.36	77.39
670.49	75.05	75.05	73.62	76.71	75.05	75.05	72.80	76.97
673.49	74.75	74.75	73.33	76.56	75.05	74.75	72.22	76.59
676.49	74.75	74.75	72.99	76.40	74.75	74.45	71.66	76.24
679.50	74.45	74.45	72.61	76.25	74.45	74.15	71.18	75.92
682.50	74.45	74.15	72.22	76.08	74.15	73.85	70.77	75.60
685.51	74.15	74.15	71.86	75.89	73.85	73.55	70.43	75.30
688.51	73.85	73.85	71.52	75.68	73.55	72.95	70.13	75.01
691.51	73.85	73.85	71.25	75.45	73.25	72.65	69.90	74.74
694.52	73.55	73.55	71.03	75.21	72.65	72.65	69.71	74.47
697.52	73.55	73.25	70.85	74.98	72.65	72.35	69.57	74.23
700.52	73.25	73.25	70.72	74.77	72.35	72.05	69.45	74.02
703.53	73.25	72.95	70.62	74.61	72.05	72.05	69.35	73.86
706.53	72.95	72.95	70.55	74.47	72.05	72.05	69.27	73.78
709.54	72.95	72.65	70.49	74.36	72.05	71.75	69.21	73.78
712.54	72.65	72.65	70.43	74.29	72.05	72.05	69.17	73.88
715.54	72.65	72.65	70.37	74.26	72.05	72.05	69.14	74.01
718.55	72.65	72.65	70.29	74.27	72.05	72.05	69.10	74.20
721.55	72.65	72.65	70.20	74.32	72.35	72.05	69.06	74.39
724.55	72.65	72.65	70.09	74.41	72.65	72.35	69.03	74.62
727.56	72.65	72.65	69.97	74.54	72.95	72.65	69.00	74.88
730.56	72.95	72.65	69.88	74.68	72.95	72.65	68.98	75.18
733.57	72.95	72.65	69.81	74.85	73.25	72.95	69.01	75.50
736.57	73.25	72.95	69.77	75.02	73.55	73.25	69.05	75.86
739.57	73.25	72.95	69.74	75.21	73.55	73.55	69.14	76.25
742.58	73.55	73.25	69.75	75.41	73.85	73.55	69.30	76.63
745.58	73.85	73.25	69.79	75.63	73.85	73.85	69.52	76.99
748.58	73.85	73.55	69.85	75.87	74.15	74.15	69.85	77.36
751.59	74.15	73.85	69.95	76.12	74.15	74.45	70.33	77.74
754.59	74.15	73.85	70.06	76.40	74.45	74.45	70.89	78.09
757.60	74.45	74.15	70.22	76.69	74.75	74.75	71.45	78.46
760.60	74.45	74.45	70.42	76.98	74.75	75.05	71.99	78.81
763.60	74.75	74.45	70.65	77.27	75.05	75.05	72.47	79.16
766.61	74.75	74.75	70.93	77.56	75.35	75.35	72.89	79.47
769.61	75.05	74.75	71.24	77.84	75.35	75.65	73.24	79.79
772.61	75.05	75.05	71.59	78.13	75.65	75.65	73.57	80.06
775.62	75.35	75.35	71.98	78.42	75.65	75.95	73.86	80.31
778.62	75.35	75.35	72.38	78.68	75.95	76.25	74.11	80.53
781.63	75.65	75.65	72.79	78.95	75.95	76.25	74.34	80.74
784.63	75.65	75.95	73.18	79.21	76.25	76.55	74.54	80.93
787.63	75.95	75.95	73.55	79.47	76.55	76.85	74.74	81.07
790.64	76.25	76.25	73.88	79.71	76.55	76.85	74.92	81.16
793.64	76.25	76.55	74.18	79.91	76.85	77.15	75.08	81.22
796.64	76.55	76.55	74.44	80.08	76.85	77.45	75.24	81.23
799.65	76.55	76.85	74.66	80.21	77.15	77.45	75.39	81.22
802.65	76.85	76.85	74.86	80.32	77.45	77.75	75.53	81.19
805.66	76.85	77.15	75.04	80.41	77.45	77.75	75.66	81.15
808.66	77.15	77.45	75.21	80.47	77.75	78.05	75.78	81.11
811.66	77.45	77.45	75.35	80.53	77.75	78.05	75.88	81.07
814.67	77.45	77.75	75.48	80.60	78.05	78.05	75.97	81.04
817.67	77.75	77.75	75.60	80.68	78.05	78.35	76.05	81.02
820.67	77.75	78.05	75.70	80.75	78.05	78.35	76.09	81.02
823.68	78.05	78.05	75.78	80.82	78.35	78.35	76.10	81.04
826.68	78.05	78.05	75.83	80.89	78.35	78.35	76.07	81.06
829.69	78.35	78.35	75.85	80.98	78.35	78.35	76.00	81.11
832.69	78.05	78.35	75.82	81.09	78.35	78.35	75.89	81.17
835.69	78.35	78.35	75.74	81.21	78.35	78.35	75.75	81.25
838.70	78.05	78.35	75.62	81.34	78.35	78.35	75.58	81.36
841.70	78.35	78.35	75.44	81.47	78.35	78.35	75.37	81.46
844.70	78.35	78.35	75.23	81.61	78.35	78.05	75.14	81.58
847.71	77.75	78.05	74.99	81.77	77.75	78.05	74.90	81.71
850.71	77.75	78.05	74.71	81.93	77.15	77.75	74.63	81.83
853.72	77.45	77.75	74.42	82.07	76.55	77.45	74.34	81.93
856.72	76.55	77.45	74.10	82.18	76.25	77.15	74.05	82.00
859.72	76.25	77.45	73.75	82.27	76.25	76.85	73.74	82.07
862.73	75.65	77.15	73.41	82.34	75.95	76.55	73.42	82.10
865.73	75.65	76.85	73.04	82.37	75.65	76.25	73.08	82.11
868.73	75.05	76.25	72.65	82.35	75.05	75.95	72.74	82.06
871.74	75.05	75.95	72.23	82.31	75.05	75.65	72.39	81.96
874.74	74.45	75.65	71.76	82.20	74.75	75.35	72.02	81.83
877.75	74.15	75.35	71.25	82.05	74.45	75.05	71.62	81.70
880.75	73.85	74.75	70.68	81.85	74.15	74.75	71.21	81.47
883.75	73.25	74.45	70.02	81.63	73.55	74.45	70.77	81.20
886.76	73.25	74.15	69.31	81.32	73.25	74.15	70.31	80.84
889.76	72.65	73.55	68.51	80.95	72.95	73.85	69.83	80.42
892.76	72.35	73.25	67.63	80.50	72.35	73.25	69.30	79.91
895.77	71.75	72.95	66.63	79.96	72.05	72.95	68.74	79.31
898.77	71.45	72.35	65.62	79.34	71.75	72.65	68.10	78.66
901.78	71.45	72.05	64.59	78.63	71.45	72.35	67.40	78.01
904.78	71.15	71.45	63.60	77.88	71.15	71.75	66.64	77.35
907.78	70.85	71.15	62.73	77.18	70.85	71.45	65.84	76.73
910.79	70.25	70.85	62.02	76.52	70.55	71.15	65.00	76.18
913.79	69.95	70.25	61.36	75.89	69.95	70.55	64.14	75.67
916.79	69.65	69.95	60.73	75.34	69.65	70.25	63.30	75.22

921.00	70.39	63.59	77.20	71.16	78.46	63.86
924.00	69.92	62.71	77.13	70.69	78.41	62.97
927.00	69.43	61.80	77.05	70.21	78.35	62.07
930.00	68.91	60.87	76.95	69.71	78.26	61.16
933.00	68.38	59.94	76.81	69.21	78.12	60.29
936.00	67.84	59.05	76.64	68.69	77.92	59.46
939.00	67.30	58.20	76.41	68.15	77.61	58.69
942.00	66.78	57.43	76.13	67.63	77.22	58.05
945.00	66.26	56.75	75.78	67.12	76.71	57.53
948.00	65.75	56.15	75.35	66.58	76.04	57.12
951.00	65.24	55.65	74.83	66.04	75.26	56.84
954.00	64.72	55.24	74.18	65.51	74.36	56.65
957.00	64.21	54.99	73.43	64.97	73.39	56.56
960.00	63.72	54.87	72.58	64.43	72.34	56.52
963.00	63.22	54.88	71.58	63.90	71.27	56.54
966.00	62.73	54.93	70.51	63.39	70.20	56.58
969.00	62.24	55.09	69.39	62.89	69.16	56.63
972.00	61.79	55.28	68.30	62.41	68.18	56.63
975.00	61.36	55.46	67.27	61.94	67.28	56.59
978.00	60.95	55.54	66.33	61.50	66.51	56.49
981.00	60.56	55.56	65.56	61.10	65.88	56.32
984.00	60.21	55.45	64.95	60.73	65.39	56.07
987.00	59.89	55.26	64.53	60.38	65.00	55.76
990.00	59.60	54.97	64.23	60.04	64.69	55.39
993.00	59.33	54.64	64.02	59.74	64.46	55.02
996.00	59.07	54.27	63.88	59.46	64.26	54.65
999.00	58.84	53.90	63.77	59.19	64.10	54.28
1002.00	58.63	53.55	63.71	58.95	63.96	53.94
1005.00	58.44	53.23	63.65	58.73	63.85	53.61
1008.00	58.25	52.90	63.59	58.53	63.75	53.31
1011.00	58.08	52.61	63.55	58.35	63.68	53.03
1014.00	57.94	52.35	63.53	58.20	63.63	52.78
1017.00	57.82	52.13	63.53	58.08	63.63	52.55
1020.00	57.73	51.92	63.54	57.99	63.63	52.34
1023.00	57.66	51.75	63.58	57.91	63.67	52.15
1026.00	57.62	51.60	63.65	57.85	63.73	51.97
1029.00	57.60	51.46	63.74	57.80	63.81	51.80
1032.00	57.60	51.35	63.85	57.79	63.93	51.64
1035.00	57.62	51.25	63.99	57.79	64.07	51.51
1038.00	57.67	51.17	64.16	57.81	64.24	51.39
1041.00	57.73	51.12	64.35	57.86	64.43	51.30
1044.00	57.81	51.07	64.55	57.94	64.64	51.23
1047.00	57.92	51.07	64.77	58.03	64.86	51.22
1050.00	58.04	51.09	65.00	58.15	65.09	51.21
1053.00	58.18	51.14	65.22	58.27	65.31	51.23
1056.00	58.33	51.22	65.45	58.40	65.52	51.29
1059.00	58.51	51.36	65.67	58.56	65.72	51.40
1062.00	58.70	51.53	65.86	58.74	65.92	51.57
1065.00	58.89	51.74	66.03	58.95	66.10	51.79
1068.00	59.12	52.03	66.20	59.16	66.26	52.07
1071.00	59.36	52.38	66.34	59.39	66.38	52.40
1074.00	59.60	52.78	66.43	59.64	66.48	52.80
1077.00	59.87	53.25	66.48	59.89	66.52	53.26
1080.00	60.15	53.78	66.52	60.15	66.54	53.76
1083.00	60.43	54.34	66.51	60.43	66.54	54.31
1086.00	60.71	54.93	66.50	60.70	66.53	54.88
1089.00	60.99	55.51	66.47	60.98	66.50	55.46
1092.00	61.26	56.08	66.44	61.25	66.48	56.03
1095.00	61.53	56.63	66.43	61.51	66.46	56.56
1098.00	61.78	57.13	66.43	61.75	66.47	57.04
1101.00	62.02	57.57	66.46	61.98	66.48	57.48
1104.00	62.24	57.96	66.53	62.21	66.55	57.87
1107.00	62.43	58.26	66.61	62.41	66.64	58.18
1110.00	62.59	58.49	66.70	62.58	66.73	58.42
1113.00	62.71	58.64	66.78	62.70	66.81	58.60
1116.00	62.79	58.74	66.84	62.79	66.86	58.71
1119.00	62.84	58.82	66.86	62.84	66.87	58.79
1122.00	62.84	58.85	66.84	62.83	66.84	58.84
1125.00	62.78	58.86	66.71	62.80	66.72	58.87
1128.00	62.68	58.85	66.50	62.69	66.51	58.86
1131.00	62.51	58.81	66.20	62.53	66.22	58.83
1134.00	62.31	58.75	65.86	62.30	65.86	58.74
1137.00	62.06	58.64	65.48	62.04	65.47	58.61
1140.00	61.76	58.45	65.06	61.73	65.06	58.40
1143.00	61.41	58.18	64.65	61.38	64.65	58.12
1146.00	61.04	57.84	64.24	61.00	64.25	57.76
1149.00	60.64	57.41	63.86	60.59	63.86	57.31
1152.00	60.21	56.93	63.49	60.16	63.49	56.83
1155.00	59.75	56.38	63.12	59.71	63.11	56.30
1158.00	59.30	55.85	62.75	59.24	62.72	55.76
1161.00	58.85	55.33	62.38	58.77	62.30	55.24
1164.00	58.41	54.83	61.98	58.30	61.86	54.74
1167.00	57.97	54.37	61.57	57.85	61.41	54.29
1170.00	57.54	53.94	61.14	57.41	60.95	53.87
1173.00	57.12	53.53	60.71	56.98	60.48	53.48
1176.00	56.72	53.14	60.29	56.57	60.04	53.10
1179.00	56.34	52.77	59.90	56.18	59.63	52.73
1182.00	55.96	52.38	59.53	55.79	59.24	52.34
1185.00	55.58	51.96	59.19	55.40	58.88	51.93
1188.00	55.21	51.53	58.90	55.02	58.56	51.48
1191.00	54.86	51.08	58.64	54.64	58.27	51.01
1194.00	54.51	50.60	58.43	54.27	58.03	50.52
1197.00	54.18	50.10	58.25	53.93	57.82	50.04
1200.00	53.85	49.60	58.11	53.60	57.64	49.57
1203.00	53.56	49.12	58.00	53.31	57.49	49.12
1206.00	53.29	48.66	57.92	53.03	57.35	48.72
1209.00	53.06	48.25	57.87	52.79	57.21	48.37
1212.00	52.84	47.88	57.81	52.58	57.07	48.09
1215.00	52.66	47.56	57.75	52.41	56.93	47.90
1218.00	52.50	47.31	57.69	52.29	56.78	47.81
1221.00	52.38	47.15	57.62	52.20	56.61	47.79
1224.00	52.30	47.10	57.53	52.13	56.41	47.87
1227.00	52.27	47.10	57.42	52.13	56.21	48.03
1230.00	52.26	47.23	57.29	52.15	56.03	48.27
1233.00	52.27	47.40	57.15	52.19	55.87	48.51
1236.00	52.32	47.65	57.00	52.25	55.79	48.72
1239.00	52.40	47.93	56.86	52.33	55.76	48.90
1242.00	52.49	48.24	56.74	52.42	55.79	49.05

919.80	69.35	69.35	60.06	74.88	69.35	69.95	62.46	74.83
922.80	69.05	69.05	59.38	74.47	69.05	69.35	61.67	74.48
925.81	68.75	68.45	58.80	74.10	68.75	69.05	60.97	74.19
928.81	68.45	68.15	58.30	73.77	68.45	68.45	60.30	73.94
931.81	68.15	67.55	57.88	73.41	68.15	68.15	59.74	73.67
934.82	67.85	67.25	57.55	73.07	67.85	67.85	59.25	73.41
937.82	67.25	66.95	57.24	72.68	67.25	67.25	58.84	73.12
940.82	67.25	66.35	56.98	72.26	66.95	66.95	58.49	72.80
943.83	66.65	66.05	56.76	71.77	66.65	66.35	58.22	72.41
946.83	66.35	65.45	56.62	71.27	66.35	66.05	57.99	71.98
949.84	65.75	65.15	56.51	70.72	65.75	65.75	57.78	71.50
952.84	65.45	64.55	56.48	70.12	65.45	65.15	57.61	70.99
955.84	65.15	64.25	56.51	69.52	64.85	64.85	57.47	70.40
958.85	64.55	63.65	56.54	68.91	64.55	64.25	57.38	69.78
961.85	63.95	63.35	56.62	68.33	64.25	63.95	57.32	69.21
964.85	63.05	63.05	56.73	67.78	63.95	63.65	57.32	68.62
967.86	62.45	62.75	56.85	67.25	63.35	63.05	57.32	68.03
970.86	62.15	62.15	56.96	66.76	63.05	62.75	57.32	67.45
973.87	61.85	61.85	57.03	66.30	62.45	62.45	57.27	66.93
976.87	61.55	61.55	57.04	65.89	61.85	61.85	57.18	66.44
979.87	61.55	61.55	56.97	65.49	61.55	61.55	57.01	65.99
982.88	60.95	61.25	56.81	65.14	61.25	61.25	56.77	65.60
985.88	60.95	60.95	56.57	64.83	60.95	60.95	56.43	65.25
988.88	60.95	60.65	56.26	64.56	60.65	60.65	55.99	64.97
991.89	60.65	60.65	55.84	64.34	60.35	60.35	55.48	64.76
994.89	60.65	60.35	55.36	64.19	60.35	60.05	54.90	64.64
997.90	60.65	60.35	54.84	64.10	60.05	59.75	54.29	64.62
1000.90	60.65	60.05	54.27	64.07	60.05	59.75	53.66	64.71
1003.90	60.65	60.05	53.71	64.13	59.75	59.45	53.03	64.92
1006.91	60.65	60.05	53.17	64.20	59.45	59.15	52.41	65.21
1009.91	60.35	60.05	52.64	64.37	59.45	59.15	51.77	65.59
1012.91	60.35	59.75	52.11	64.58	59.75	58.85	51.17	65.96
1015.92	60.35	59.75	51.59	64.87	59.45	58.85	50.54	66.35
1018.92	60.35	59.75	51.10	65.25	60.05	58.85	49.95	66.90
1021.93	60.35	59.75	50.61	65.65	59.45	58.55	49.35	67.50
1024.93	60.35	59.75	50.13	66.12	60.35	58.55	48.79	68.05
1027.93	60.05	59.75	49.70	66.49	60.65	58.55	48.30	68.56
1030.94	60.05	59.75	49.30	66.89	60.65	58.55	47.85	68.95
1033.94	60.05	59.75	49.01	67.19	60.65	58.85	47.52	69.28
1036.94	60.05	59.75	48.80	67.34	60.65	58.85	47.28	69.49
1039.95	60.05	59.75	48.61	67.50	60.95	58.85	47.13	69.52
1042.95	60.05	59.75	48.50	67.61	60.95	59.15	47.07	69.48
1045.96	60.05	59.75	48.48	67.64	60.95	59.15	47.04	69.38
1048.96	59.75	59.75	48.53	67.58	60.95	59.45	47.05	69.25
1051.96	59.75	59.75	48.66	67.53	60.95	59.75	47.23	69.08
1054.97	59.75	59.75	48.87	67.47	60.95	59.75	47.40	68.90
1057.97	59.75	59.75	49.13	67.46	60.95	60.05	47.67	68.76
1060.97	59.75	59.75	49.46	67.50	60.95	60.35	48.01	68.71
1063.98	59.75	60.05	49.90	67.56	60.95	60.35	48.40	68.74
1066.98	59.75	60.05	50.36	67.71	60.95	60.65	48.87	68.82
1069.99	59.75	60.05	50.92	67.88	60.95	60.65	49.51	68.97
1072.99	59.45	60.05	51.57	68.05	60.95	60.95	50.18	69.11
1075.99	59.45	60.05	52.25	68.22	61.25	61.25	50.91	69.25
1079.00	59.45	60.05	52.96	68.42	61.25	61.25	51.65	69.45
1082.00	59.45	60.05	53.71	68.60	61.25	61.55	52.39	69.64
1085.00	59.45	60.35	54.46	68.79	61.25	61.55	53.21	69.81
1088.01	59.45	60.35	55.26	68.92	61.25	61.55	54.07	69.91
1091.01	59.15	60.35	56.03	69.07	61.55	61.85	54.89	70.04
1094.02	59.15	60.35	56.75	69.13	61.55	61.85	55.73	70.09
1097.02	59.15	60.65	57.21	69.14	61.55	61.85	56.56	70.03
1100.02	59.15	60.65	57.43	69.10	61.85	62.15	57.25	69.93
1103.03	59.15	60.65	57.53	68.96	61.55	62.15	57.77	69.74
1106.03	58.85	60.95	57.58	68.85	61.55	62.15	58.06	69.52
1109.03	58.85	60.95	57.60	68.66	61.55	62.15	58.24	69.26
1112.04	58.85	60.95	57.59	68.44	61.85	62.15	58.34	68.94
1115.04	58.85	60.95	57.57	68.21	61.55	61.85	58.37	68.63
1118.05	58.85	60.65	57.55	67.98	61.55	61.85	58.37	68.34
1121.05	58.85	60.65	57.51	67.74	61.55	61.85	58.32	68.08
1124.05	58.55	60.65	57.46	67.47	61.55	61.85	58.25	67.73
1127.06	58.55	60.35	57.41	67.17	61.25	61.55	58.15	67.39
1130.06	58.55	60.35	57.35	66.88	60.65	61.25	58.04	67.10
1133.06	58.55	60.05	57.29	66.59	60.65	61.25	57.91	66.78
1136.07	58.55	59.75	57.21	66.29	60.35	60.95	57.77	66.48
1139.07	58.55	59.75	57.12	65.98	60.05	60.65	57.61	66.17
1142.08	58.55	59.45	57.02	65.67	59.75	60.35	57.44	65.85
1145.08	58.25	59.15	56.91	65.27	59.75	60.05	57.26	65.52
1148.08	58.25	58.85	56.78	64.89	59.45	59.75	57.07	65.17
1151.09	58.25	58.85	56.63	64.49	59.15	59.45	56.86	64.75
1154.09	58.25	58.55	56.45	64.00	58.85	59.15	56.63	64.26
1157.09	58.25	58.55	56.23	63.43	58.55	58.85	56.36	63.73
1160.10	57.95	58.25	55.95	62.80	58.25	58.55	56.02	63.15
1163.10	57.95	57.95	55.58	62.13	57.95	58.25	55.57	62.54
1166.11	57.95	57.95	55.14	61.43	57.95	57.95	54.98	61.90
1169.11	57.65	57.65	54.61	60.65	57.65	57.65	54.24	61.19
1172.11	57.65	57.35	54.05	59.91	57.35	57.05	53.40	60.41
1175.12	57.65	57.35	53.38	59.37	57.05	56.75	52.48	59.69
1178.12	57.65	57.05	52.68	58.98	56.75	56.45	51.60	59.09
1181.12	57.35	57.05	52.00	58.75	56.45	56.15	50.88	58.62
1184.13	57.35	56.75	51.39	58.58	56.15	55.85	50.31	58.22
1187.13	57.35	56.45	50.85	58.47	56.15	55.55	49.87	57.89
1190.14	57.35	56.45	50.37	58.39	55.85	55.25	49.55	57.63
1193.14	57.35	56.15	49.95	58.32	55.55	54.95	49.30	57.41
1196.14	57.35	56.15	49.66	58.25	55.55	54.65	49.10	57.20
1199.15	57.35	56.15	49.41	58.18	55.25	54.35	48.97	56.99
1202.15	57.05	55.85	49.24	58.12	55.25	54.05	48.88	56.79
1205.15	57.05	55.85	49.12	58.05	54.95	53.75	48.84	56.59
1208.16	57.05	55.85	49.04	57.99	54.95	53.75	48.83	56.40
1211.16	57.05	55.55	49.01	57.93	54.65	53.45	48.85	56.21
1214.17	57.05	55.55	48.99	57.86	54.35	53.15	48.89	56.03
1217.17	57.05	55.55	49.01	57.80	54.35	52.85	48.95	55.85
1220.17	56.75	55.55	49.04	57.73	52.25	52.85	49.03	55.67
1223.18	56.75	55.55	49.10	57.67	52.25	52.55	49.12	55.50
1226.18	56.75	55.25	49.17	57.60	52.25	52.55	49.23	55.33
1229.18	56.75	55.25	49.25	57.54	52.25	52.55	49.32	55.17
1232.19	56.75	55.25	49.34	57.48	52.25	52.55	49.42	55.01
1235.19	56.75	55.25	49.44	57.41	52.25	52.55	49.51	54.86
1238.20	56.45	55.25	49.53	57.35	52.55	52.25	49.58	54.72
1241.20	56.45	55.25	49.64	57.29	52.55	52.25	49.64	54.59

1245.00	52.60	48.55	56.65	52.52	55.86	49.17
1248.00	52.73	48.86	56.62	52.61	55.93	49.31
1251.00	52.87	49.14	56.61	52.71	55.95	49.46
1254.00	53.02	49.38	56.66	52.80	55.94	49.66
1257.00	53.16	49.57	56.75	52.88	55.93	49.84
1260.00	53.30	49.71	56.88	52.95	55.92	49.99
1263.00	53.43	49.82	57.04	53.02	55.96	50.07
1266.00	53.56	49.91	57.22	53.07	56.04	50.09
1269.00	53.67	49.97	57.38	53.10	56.18	50.02
1272.00	53.77	50.03	57.51	53.13	56.33	49.93
1275.00	53.86	50.12	57.61	53.16	56.48	49.85
1278.00	53.93	50.22	57.62	53.20	56.60	49.81
1281.00	53.97	50.33	57.61	53.25	56.69	49.81
1284.00	54.01	50.47	57.55	53.30	56.75	49.85
1287.00	54.04	50.62	57.45	53.34	56.76	49.92
1290.00	54.05	50.78	57.33	53.39	56.76	50.01
1293.00	54.07	50.95	57.19	53.44	56.75	50.13
1296.00	54.08	51.12	57.04	53.50	56.74	50.25
1299.00	54.10	51.29	56.90	53.56	56.73	50.39
1302.00	54.11	51.45	56.77	53.63	56.73	50.52
1305.00	54.13	51.60	56.66	53.70	56.74	50.66
1308.00	54.16	51.74	56.58	53.78	56.75	50.81
1311.00	54.21	51.88	56.54	53.88	56.77	50.99
1314.00	54.27	52.02	56.53	53.99	56.78	51.19
1317.00	54.35	52.17	56.52	54.10	56.78	51.43
1320.00	54.45	52.34	56.56	54.24	56.76	51.71
1323.00	54.57	52.54	56.60	54.40	56.75	52.05
1326.00	54.71	52.76	56.66	54.58	56.75	52.41
1329.00	54.88	53.01	56.74	54.77	56.81	52.76
1332.00	55.06	53.26	56.86	54.98	56.97	52.98
1335.00	55.25	53.49	57.03	55.20	57.31	53.09
1338.00	55.46	53.66	57.25	55.42	57.76	53.06
1341.00	55.66	53.79	57.54	55.63	58.27	53.00
1344.00	55.86	53.83	57.88	55.85	58.77	52.93
1347.00	56.04	53.84	58.24	56.05	59.18	52.94
1350.00	56.21	53.81	58.62	56.23	59.48	52.99
1353.00	56.36	53.76	58.97	56.39	59.62	53.14
1356.00	56.48	53.69	59.28	56.50	59.70	53.30
1359.00	56.57	53.62	59.51	56.58	59.74	53.43
1362.00	56.61	53.56	59.66	56.65	59.83	53.43
1365.00	56.62	53.51	59.74	56.68	59.99	53.38
1368.00	56.60	53.45	59.74	56.68	60.18	53.21
1371.00	56.52	53.39	59.65	56.67	60.36	52.98
1374.00	56.43	53.32	59.53	56.62	60.49	52.76
1377.00	56.31	53.25	59.36	56.54	60.50	52.55
1380.00	56.15	53.15	59.15	56.43	60.49	52.37
1383.00	55.97	53.02	58.92	56.30	60.39	52.21
1386.00	55.77	52.87	58.68	56.15	60.22	52.07
1389.00	55.57	52.69	58.45	55.98	60.02	51.94
1392.00	55.36	52.49	58.23	55.79	59.77	51.81
1395.00	55.14	52.27	58.02	55.58	59.50	51.66
1398.00	54.92	52.02	57.81	55.37	59.22	51.52
1401.00	54.69	51.76	57.61	55.16	58.94	51.37
1404.00	54.47	51.51	57.43	54.95	58.68	51.22
1407.00	54.26	51.28	57.24	54.75	58.43	51.08
1410.00	54.06	51.07	57.04	54.57	58.18	50.96
1413.00	53.87	50.91	56.83	54.39	57.93	50.86
1416.00	53.70	50.79	56.61	54.24	57.66	50.82
1419.00	53.55	50.76	56.35	54.09	57.37	50.83
1422.00	53.41	50.75	56.07	53.98	57.06	50.89
1425.00	53.30	50.84	55.77	53.88	56.71	51.05
1428.00	53.22	50.98	55.45	53.81	56.32	51.29
1431.00	53.15	51.16	55.13	53.77	55.96	51.57
1434.00	53.10	51.32	54.87	53.75	55.65	51.85
1437.00	53.06	51.40	54.72	53.72	55.48	51.95
1440.00	53.03	51.38	54.68	53.69	55.40	51.98
1443.00	53.00	51.32	54.69	53.64	55.44	51.86
1446.00	52.98	51.15	54.81	53.57	55.47	51.66
1449.00	52.93	50.97	54.90	53.46	55.48	51.44
1452.00	52.86	50.78	54.94	53.33	55.45	51.22
1455.00	52.75	50.61	54.89	53.18	55.33	51.02
1458.00	52.62	50.43	54.81	53.00	55.18	50.81
1461.00	52.45	50.24	54.66	52.80	54.99	50.60
1464.00	52.27	50.04	54.51	52.58	54.79	50.37
1467.00	52.07	49.81	54.34	52.35	54.58	50.11
1470.00	51.84	49.53	54.15	52.10	54.37	49.83
1473.00	51.59	49.24	53.95	51.83	54.15	49.52
1476.00	51.34	48.93	53.74	51.56	53.91	49.21
1479.00	51.08	48.64	53.52	51.28	53.66	48.91
1482.00	50.84	48.40	53.28	51.02	53.39	48.65
1485.00	50.61	48.21	53.01	50.76	53.09	48.43
1488.00	50.39	48.09	52.70	50.52	52.75	48.29
1491.00	50.19	48.01	52.36	50.30	52.41	48.19
1494.00	50.01	47.99	52.04	50.11	52.07	48.14
1497.00	49.88	47.99	51.77	49.95	51.79	48.13
1500.00	49.78	48.01	51.55	49.85	51.57	48.13
1503.00	49.76	48.06	51.46	49.81	51.44	48.16
1506.00	49.78	48.13	51.42	49.80	51.40	48.22
1509.00	49.85	48.24	51.47	49.90	51.46	48.33
1512.00	50.03	48.44	51.62	50.05	51.57	48.53
1515.00	50.29	48.77	51.82	50.30	51.77	48.84
1518.00	50.64	49.22	52.06	50.65	52.00	49.31
1521.00	51.10	49.84	52.36	51.08	52.29	49.88
1524.00	51.58	50.47	52.69	51.57	52.62	50.53
1527.00	52.06	51.05	53.07	52.04	53.00	51.09
1530.00	52.50	51.49	53.50	52.46	53.41	51.51
1533.00	52.78	51.73	53.83	52.79	53.80	51.78
1536.00	52.94	51.83	54.04	52.89	53.95	51.85
1539.00	52.90	51.79	54.02	52.87	53.97	51.79
1542.00	52.75	51.61	53.90	52.77	53.90	51.64
1545.00	52.51	51.32	53.70	52.52	53.69	51.34
1548.00	52.24	50.98	53.49	52.25	53.50	50.99
1551.00	51.97	50.61	53.32	51.99	53.34	50.65
1554.00	51.79	50.34	53.24	51.77	53.22	50.35
1557.00	51.70	50.18	53.21	51.75	53.23	50.23
1560.00	51.77	50.19	53.35	51.76	53.33	50.19
1563.00	51.93	50.23	53.63	51.93	53.63	50.25
1566.00	52.26	50.36	54.15	52.22	54.09	50.35

1244.20	56.45	55.25	49.74	57.24	52.55	52.25	49.71	54.46
1247.21	56.45	55.25	49.85	57.18	52.55	52.25	49.76	54.35
1250.21	56.45	55.25	49.97	57.12	52.55	52.25	49.80	54.27
1253.21	56.45	55.25	50.09	57.07	52.55	52.25	49.84	54.21
1256.22	56.15	54.95	50.22	57.01	52.55	52.25	49.85	54.16
1259.22	56.15	54.95	50.35	56.95	52.55	52.25	49.87	54.15
1262.23	56.15	54.95	50.50	56.89	52.55	52.55	49.87	54.16
1265.23	56.15	54.95	50.64	56.84	52.55	52.55	49.85	54.19
1268.23	56.15	54.95	50.76	56.78	52.55	52.55	49.81	54.23
1271.24	55.85	54.95	50.89	56.73	52.85	52.55	49.75	54.29
1274.24	55.85	54.95	51.02	56.67	52.85	52.55	49.68	54.35
1277.24	55.85	54.95	51.15	56.62	52.85	52.55	49.59	54.42
1280.25	55.85	54.95	51.29	56.57	53.15	52.85	49.50	54.49
1283.25	55.85	54.95	51.43	56.52	53.15	52.85	49.41	54.56
1286.26	55.85	54.95	51.58	56.47	53.45	52.85	49.31	54.63
1289.26	55.55	54.95	51.71	56.42	53.45	53.15	49.22	54.71
1292.26	55.55	54.95	51.87	56.37	53.45	53.15	49.13	54.79
1295.27	55.55	54.95	52.04	56.33	53.75	53.45	49.07	54.87
1298.27	55.55	54.95	52.20	56.28	53.75	53.45	49.07	54.95
1301.27	55.55	54.95	52.39	56.24	53.75	53.45	49.10	55.04
1304.28	55.25	54.95	52.58	56.19	54.05	53.75	49.22	55.13
1307.28	55.25	54.95	52.77	56.16	54.05	53.75	49.42	55.23
1310.29	55.25	54.95	52.98	56.13	54.35	54.05	49.73	55.33
1313.29	55.25	54.95	53.19	56.11	54.35	54.05	50.15	55.44
1316.29	55.25	54.95	53.40	56.11	54.35	54.05	50.73	55.56
1319.30	55.25	54.95	53.58	56.13	54.35	54.35	51.40	55.70
1322.30	54.95	54.95	53.74	56.17	54.65	54.35	52.12	55.85
1325.30	54.95	54.95	53.86	56.23	54.65	54.65	52.77	56.03
1328.31	54.95	54.95	53.93	56.33	54.95	54.95	53.31	56.29
1331.31	54.95	54.95	53.98	56.45	54.95	54.95	53.65	56.66
1334.32	54.95	54.95	54.00	56.60	55.25	55.25	53.87	57.13
1337.32	54.95	54.95	53.99	56.77	55.25	55.25	54.02	57.59
1340.32	54.95	54.95	53.98	56.94	55.25	55.55	54.14	58.02
1343.33	54.95	54.95	53.96	57.11	55.55	55.55	54.23	58.41
1346.33	54.65	54.95	53.94	57.27	55.55	55.85	54.30	58.74
1349.33	54.65	54.95	53.91	57.41	55.85	55.85	54.35	59.01
1352.34	54.65	54.95	53.88	57.54	55.85	56.15	54.40	59.22
1355.34	54.65	54.95	53.84	57.67	56.15	56.15	54.44	59.41
1358.35	54.65	54.95	53.81	57.77	56.15	56.45	54.47	59.55
1361.35	54.35	54.95	53.77	57.85	56.15	56.45	54.48	59.65
1364.35	54.35	54.95	53.73	57.92	56.45	56.45	54.48	59.75
1367.36	54.35	54.65	53.69	57.96	56.45	56.45	54.46	59.84
1370.36	54.35	54.65	53.65	58.01	56.45	56.75	54.43	59.94
1373.36	54.35	54.65	53.61	58.03	56.45	56.75	54.40	60.03
1376.37	54.35	54.65	53.57	58.03	56.45	56.75	54.36	60.11
1379.37	54.05	54.65	53.53	58.03	56.45	56.75	54.31	60.18
1382.38	54.05	54.65	53.48	58.02	56.45	56.75	54.26	60.22
1385.38	54.05	54.35	53.43	58.00	56.45	56.75	54.21	60.25
1388.38	54.05	54.35	53.39	57.96	56.45	56.45	54.16	60.26
1391.39	54.05	54.35	53.34	57.90	56.15	56.45	54.11	60.23
1394.39	54.05	54.35	53.29	57.82	56.15	56.45	54.06	60.19
1397.39	54.05	54.35	53.24	57.73	56.15	56.15	54.01	60.09
1400.40	53.75	54.05	53.19	57.61	55.85	56.15	53.96	59.95
1403.40	53.75	54.05	53.13	57.48	55.55	55.85	53.91	59.78
1406.40	53.75	54.05	53.08	57.30	55.25	55.85	53.84	59.56
1409.41	53.75	54.05	53.02	57.10	55.25	55.55	53.78	59.33
1412.41	53.75	54.05	52.96	56.86	54.95	55.55	53.70	59.04
1415.42	53.75	53.75	52.90	56.57	54.95	55.25	53.62	58.71
1418.42	53.75	53.75	52.84	56.27	54.65	54.95	53.53	58.35
1421.42	53.45	53.75	52.77	55.95	54.35	54.95	53.42	57.93
1424.43	53.45	53.75	52.70	55.61	54.35	54.65	53.30	57.46
1427.43	53.45	53.45	52.62	55.27	54.05	54.35	53.16	56.94
1430.43	53.45	53.45	52.51	54.95	54.05	54.05	52.99	56.41
1433.44	53.45	53.45	52.38	54.65	53.75	54.05	52.78	55.88
1436.44	53.15	53.15	52.21	54.39	53.75	53.75	52.51	55.42
1439.45	53.15	53.15	51.99	54.16	53.45	53.45	52.15	55.01
1442.45	53.15	53.15	51.69	53.97	53.45	53.45	51.70	54.68
1445.45	53.15	52.85	51.33	53.84	53.15	53.15	51.18	54.41
1448.46	53.15	52.85	50.92	53.74	52.85	52.85	50.61	54.18
1451.46	52.85	52.85	50.48	53.65	52.85	52.55	50.06	53.99
1454.46	52.85	52.55	50.05	53.59	52.55	52.55	49.57	53.82
1457.47	52.85	52.55	49.69	53.52	52.55	52.25	49.18	53.67
1460.47	52.85	52.25	49.41	53.47	52.25	51.95	48.90	53.54
1463.48	52.85	52.25	49.23	53.42	52.25	51.95	48.73	53.42
1466.48	52.85	52.25	49.12	53.36	51.95	51.65	48.65	53.31
1469.48	52.85	51.95	49.05	53.31	51.95	51.35	48.62	53.21
1472.49	52.85	51.95	49.03	53.26	51.65	51.35	48.63	53.11
1475.49	52.85	51.95	49.05	53.22	51.35	51.05	48.68	53.02
1478.49	52.85	51.65	49.09	53.17	51.35	51.05	48.75	52.93
1481.50	52.85	51.65	49.13	53.13	51.05	50.75	48.83	52.85
1484.50	52.55	51.65	49.18	53.08	50.75	50.75	48.89	52.78
1487.51	52.55	51.65	49.22	53.04	50.75	50.75	48.94	52.72
1490.51	52.55	51.35	49.25	53.00	50.75	50.75	48.95	52.66
1493.51	52.55	51.35	49.27	52.97	50.75	50.75	48.93	52.61
1496.52	52.55	51.35	49.26	52.93	50.75	50.75	48.86	52.56
1499.52	52.55	51.35	49.22	52.89	50.75	50.75	48.72	52.52
1502.52	52.55	51.35	49.17	52.86	51.05	50.75	48.57	52.48
1505.53	51.35	51.35	49.10	52.82	51.05	51.05	48.48	52.45
1508.53	51.35	51.65	49.08	52.79	51.05	51.05	48.46	52.43
1511.54	51.35	51.65	49.16	52.76	51.35	51.05	48.59	52.42
1514.54	51.65	51.65	49.35	52.73	51.35	51.35	48.91	52.43
1517.54	51.95	51.65	49.73	52.71	51.65	51.35	49.38	52.45
1520.55	51.95	51.95	50.22	52.74	51.65	51.65	49.70	52.60
1523.55	51.95	51.95	50.80	52.86	51.95	51.95	50.21	53.03
1526.55	51.95	51.95	51.19	53.17	51.95	51.95	51.01	53.63
1529.56	52.25	52.25	51.42	53.47	51.95	52.25	51.35	53.75
1532.56	52.25	52.25	51.54	53.55	52.25	52.25	51.55	53.74
1535.57	52.25	52.25	51.57	53.49	52.25	52.25	51.64	53.79
1538.57	52.25	52.25	51.53	53.38	52.55	52.55	51.66	53.66
1541.57	52.55	52.55	51.45	53.34	52.55	52.55	51.56	53.49
1544.58	52.55	52.55	51.38	53.39	52.55	52.55	51.39	53.48
1547.58	52.85	52.55	51.32	53.49	52.85	52.85	51.30	53.55
1550.58	52.85	52.85	51.28	53.62	52.85	52.85	51.23	53.67
1553.59	53.15	52.85	51.22	53.77	53.15	52.85	51.13	53.83
1556.59	53.15	52.85	51.15	53.94	53.15	53.15	51.00	54.01
1559.60	53.15	53.15	51.09	54.13	53.45	53.15	50.88	54.20
1562.60	53.45	53.15	51.05	54.36	53.45	53.45	50.81	54.42
1565.60	53.45	53.45	51.05	54.65	53.45	53.45	50.81	54.67

1569.00	52.64	50.53	54.76	52.60	54.72	50.48
1572.00	53.10	50.75	55.44	53.04	55.38	50.70
1575.00	53.58	51.09	56.08	53.52	56.01	51.03
1578.00	54.06	51.54	56.57	53.99	56.48	51.50
1581.00	54.51	52.11	56.91	54.43	56.81	52.04
1584.00	54.92	52.69	57.15	54.83	57.03	52.64
1587.00	55.28	53.22	57.34	55.19	57.24	53.15
1590.00	55.58	53.62	57.54	55.48	57.43	53.53
1593.00	55.78	53.86	57.69	55.70	57.64	53.75
1596.00	55.91	54.00	57.81	55.79	57.75	53.82
1599.00	55.91	54.01	57.81	55.81	57.79	53.82
1602.00	55.87	54.00	57.75	55.77	57.76	53.78
1605.00	55.77	53.89	57.65	55.64	57.65	53.62
1608.00	55.61	53.70	57.51	55.46	57.51	53.40
1611.00	55.41	53.46	57.36	55.25	57.34	53.15
1614.00	55.20	53.24	57.17	55.02	57.12	52.90
1617.00	54.98	53.03	56.93	54.78	56.85	52.71
1620.00	54.75	52.87	56.62	54.53	56.51	52.55
1623.00	54.51	52.71	56.31	54.28	56.14	52.41
1626.00	54.26	52.53	55.99	54.03	55.81	52.24
1629.00	54.02	52.28	55.76	53.79	55.55	52.02
1632.00	53.76	51.94	55.58	53.54	55.38	51.70
1635.00	53.51	51.53	55.48	53.27	55.28	51.27
1638.00	53.24	51.07	55.40	53.01	55.22	50.80
1641.00	52.96	50.60	55.33	52.74	55.16	50.32
1644.00	52.69	50.15	55.22	52.45	55.06	49.85
1647.00	52.41	49.74	55.07	52.17	54.90	49.44
1650.00	52.12	49.37	54.87	51.89	54.71	49.07
1653.00	51.84	49.02	54.67	51.63	54.51	48.75
1656.00	51.59	48.69	54.49	51.39	54.34	48.44
1659.00	51.36	48.36	54.36	51.16	54.20	48.13
1662.00	51.16	48.07	54.26	50.97	54.09	47.85
1665.00	51.01	47.83	54.18	50.83	54.00	47.65
1668.00	50.92	47.73	54.11	50.73	53.92	47.56
1671.00	50.89	47.76	54.02	50.70	53.83	47.56
1674.00	50.89	47.84	53.94	50.74	53.74	47.73
1677.00	50.94	48.01	53.86	50.80	53.71	47.90
1680.00	50.99	48.10	53.87	50.86	53.70	48.02
1683.00	51.01	48.12	53.90	50.93	53.81	48.01
1686.00	50.98	48.00	53.98	50.94	53.93	47.97
1689.00	50.92	47.82	54.00	50.88	54.02	47.75
1692.00	50.75	47.55	53.95	50.77	54.01	47.51
1695.00	50.52	47.25	53.80	50.57	53.92	47.23
1698.00	50.23	46.91	53.55	50.33	53.73	46.93
1701.00	49.89	46.55	53.22	50.03	53.46	46.61
1704.00	49.50	46.16	52.83	49.68	53.11	46.25
1707.00	49.06	45.74	52.39	49.28	52.70	45.86
1710.00	48.60	45.28	51.92	48.85	52.26	45.43
1713.00	48.12	44.80	51.44	48.40	51.82	44.99
1716.00	47.62	44.29	50.95	47.95	51.38	44.52
1719.00	47.12	43.76	50.48	47.48	50.93	44.03
1722.00	46.62	43.23	50.01	47.01	50.50	43.53
1725.00	46.13	42.72	49.55	46.56	50.07	43.04
1728.00	45.67	42.24	49.10	46.11	49.65	42.58
1731.00	45.24	41.81	48.66	45.69	49.22	42.17
1734.00	44.84	41.46	48.22	45.30	48.79	41.81
1737.00	44.48	41.17	47.79	44.93	48.36	41.51
1740.00	44.17	40.95	47.40	44.59	47.93	41.25
1743.00	43.90	40.76	47.04	44.28	47.53	41.04
1746.00	43.66	40.60	46.72	44.01	47.18	40.85
1749.00	43.46	40.46	46.46	43.78	46.88	40.68
1752.00	43.30	40.34	46.27	43.59	46.64	40.53
1755.00	43.18	40.22	46.13	43.42	46.45	40.38
1758.00	43.08	40.12	46.04	43.27	46.31	40.23
1761.00	42.99	40.02	45.97	43.16	46.19	40.13
1764.00	42.95	40.00	45.91	43.08	46.10	40.06
1767.00	42.93	40.01	45.85	43.04	46.00	40.07
1770.00	42.93	40.09	45.76	43.01	45.89	40.14
1773.00	42.96	40.27	45.65	43.02	45.74	40.29
1776.00	43.00	40.51	45.49	43.04	45.57	40.51
1779.00	43.06	40.79	45.34	43.09	45.39	40.79
1782.00	43.13	41.08	45.18	43.15	45.23	41.08
1785.00	43.21	41.36	45.06	43.24	45.11	41.36
1788.00	43.30	41.60	45.01	43.31	45.02	41.60
1791.00	43.39	41.79	45.01	43.38	45.00	41.78
1794.00	43.47	41.92	45.02	43.47	45.02	41.92
1797.00	43.54	42.01	45.06	43.54	45.06	42.02
1800.00	43.60	42.09	45.10	43.60	45.11	42.10
1803.00	43.65	42.16	45.14	43.66	45.15	42.17
1806.00	43.68	42.20	45.17	43.70	45.20	42.20
1809.00	43.71	42.20	45.22	43.73	45.24	42.22
1812.00	43.74	42.19	45.28	43.75	45.29	42.21
1815.00	43.75	42.16	45.35	43.77	45.35	42.19
1818.00	43.76	42.12	45.41	43.78	45.39	42.17
1821.00	43.78	42.09	45.46	43.79	45.42	42.16
1824.00	43.78	42.07	45.50	43.79	45.43	42.16
1827.00	43.79	42.04	45.53	43.79	45.46	42.13
1830.00	43.78	41.93	45.64	43.78	45.54	42.02
1833.00	43.77	41.68	45.87	43.77	45.84	41.68
1836.00	43.78	41.35	46.19	43.77	46.19	41.35
1839.00	43.80	41.01	46.61	43.81	46.46	41.15
1842.00	43.94	40.70	47.18	43.92	46.92	40.91
1845.00	44.23	38.85	49.61	44.18	47.84	40.53
1848.00	44.77	33.68	55.87	44.71	52.02	37.41

1568.61	53.45	53.45	51.09	55.08	53.75	53.75	50.92	54.99
1571.61	53.75	53.75	51.17	55.99	53.75	53.75	51.15	55.42
1574.61	53.75	53.75	51.29	56.92	53.75	54.05	51.48	56.10
1577.62	54.05	54.05	51.48	57.23	54.05	54.05	51.98	56.64
1580.62	54.05	54.05	51.82	57.31	54.05	54.35	52.57	56.83
1583.63	54.05	54.35	52.53	57.28	54.35	54.35	52.90	56.87
1586.63	54.35	54.65	52.98	57.20	54.35	54.65	53.10	56.86
1589.63	54.65	54.65	53.15	57.16	54.65	54.65	53.23	56.86
1592.64	54.65	54.95	53.25	57.14	54.65	54.95	53.30	56.87
1595.64	54.95	54.95	53.31	57.11	54.95	54.95	53.37	56.86
1598.64	55.25	55.25	53.37	57.06	54.95	54.95	53.42	56.83
1601.65	55.25	55.25	53.42	56.97	54.95	54.95	53.47	56.76
1604.65	55.25	55.25	53.46	56.83	54.95	54.95	53.51	56.65
1607.66	54.95	54.95	53.49	56.66	54.95	54.95	53.52	56.51
1610.66	54.95	54.95	53.49	56.46	54.95	54.95	53.50	56.35
1613.66	54.65	54.65	53.45	56.25	54.65	54.65	53.42	56.16
1616.67	54.65	54.65	53.36	56.03	54.65	54.65	53.31	55.96
1619.67	54.35	54.35	53.22	55.82	54.35	54.35	53.16	55.76
1622.67	54.35	54.35	53.05	55.62	54.05	54.05	52.99	55.57
1625.68	54.05	54.05	52.87	55.44	54.05	54.05	52.80	55.39
1628.68	53.75	53.75	52.67	55.28	53.75	53.75	52.60	55.21
1631.69	53.45	53.75	52.46	55.13	53.45	53.45	52.39	55.04
1634.69	53.45	53.45	52.24	55.00	53.15	53.45	52.18	54.88
1637.69	53.15	53.15	52.01	54.86	53.15	53.15	51.96	54.71
1640.70	52.85	52.85	51.78	54.71	52.85	52.85	51.73	54.51
1643.70	52.55	52.55	51.54	54.52	52.55	52.55	51.50	54.29
1646.70	52.25	52.55	51.29	54.30	52.25	52.25	51.25	54.03
1649.71	52.25	52.25	51.04	54.05	52.25	52.25	51.01	53.77
1652.71	51.95	51.95	50.79	53.77	51.95	51.95	50.75	53.50
1655.72	51.65	51.65	50.52	53.48	51.65	51.65	50.50	53.21
1658.72	51.35	51.65	50.25	53.18	51.35	51.35	50.23	52.94
1661.72	51.35	51.35	49.97	52.88	51.35	51.35	49.96	52.66
1664.73	51.05	51.05	49.69	52.60	51.05	51.05	49.69	52.40
1667.73	50.75	50.75	49.42	52.32	50.75	50.75	49.43	52.14
1670.73	50.45	50.45	49.14	52.06	50.45	50.45	49.16	51.89
1673.74	50.45	50.45	48.86	51.80	50.45	50.45	48.89	51.65
1676.74	50.15	50.15	48.58	51.56	50.15	50.15	48.62	51.43
1679.75	49.85	49.85	48.31	51.33	49.85	49.85	48.35	51.21
1682.75	49.55	49.55	48.04	51.12	49.55	49.55	48.09	51.01
1685.75	49.55	49.25	47.76	50.93	49.55	49.25	47.81	50.81
1688.76	49.25	49.25	47.46	50.74	49.25	49.25	47.52	50.63
1691.76	48.95	48.95	47.14	50.54	48.95	48.95	47.21	50.43
1694.76	48.65	48.65	46.82	50.32	48.65	48.65	46.91	50.23
1697.77	48.35	48.35	46.49	50.10	48.65	48.35	46.59	50.02
1700.77	48.35	48.05	46.17	49.89	48.35	48.35	46.28	49.82
1703.78	48.05	48.05	45.83	49.69	48.05	48.05	45.96	49.62
1706.78	47.75	47.75	45.50	49.48	47.75	47.75	45.64	49.42
1709.78	47.45	47.45	45.16	49.26	47.75	47.45	45.31	49.21
1712.79	47.45	47.15	44.81	49.05	47.45	47.15	44.98	49.01
1715.79	47.15	46.85	44.46	48.84	47.15	47.15	44.65	48.80
1718.79	46.85	46.85	44.11	48.63	46.85	46.85	44.31	48.60
1721.80	46.55	46.55	43.76	48.42	46.85	46.55	43.98	48.39
1724.80	46.25	46.25	43.39	48.20	46.55	46.25	43.63	48.18
1727.81	46.25	45.95	43.03	47.99	46.25	45.95	43.28	47.98
1730.81	45.95	45.65	42.66	47.77	45.95	45.95	42.92	47.77
1733.81	45.65	45.35	42.24	47.56	45.95	45.65	42.53	47.57
1736.82	45.65	45.35	41.87	47.38	45.65	45.35	42.12	47.39
1739.82	45.35	45.05	41.68	47.20	45.35	45.05	41.82	47.21
1742.82	45.05	44.75	41.56	47.01	45.05	44.75	41.66	47.03
1745.83	44.75	44.45	41.47	46.83	45.05	44.75	41.56	46.85
1748.83	44.75	44.15	41.41	46.65	44.75	44.45	41.49	46.67
1751.84	44.45	44.15	41.37	46.47	44.45	44.15	41.43	46.49
1754.84	44.15	43.85	41.34	46.28	44.45	43.85	41.40	46.31
1757.84	42.05	43.55	41.33	46.10	44.15	43.85	41.39	46.13
1760.85	42.35	43.25	41.34	45.92	42.35	43.55	41.40	45.96
1763.85	42.35	43.25	41.36	45.74	42.35	43.25	41.40	45.78
1766.85	42.35	42.95	41.40	45.56	42.35	42.95	41.42	45.60
1769.86	42.35	42.65	41.44	45.39	42.35	42.95	41.46	45.43
1772.86	42.35	42.65	41.48	45.21	42.35	42.65	41.50	45.26
1775.87	42.65	42.65	41.53	45.04	42.65	42.65	41.54	45.09
1778.87	42.65	42.65	41.59	44.88	42.65	42.65	41.60	44.93
1781.87	42.65	42.65	41.65	44.72	42.65	42.65	41.66	44.77
1784.88	42.65	42.65	41.72	44.56	42.65	42.65	41.73	44.62
1787.88	42.95	42.95	41.80	44.41	42.95	42.95	41.80	44.48
1790.88	42.95	42.95	41.88	44.27	42.95	42.95	41.88	44.34
1793.89	42.95	42.95	41.97	44.15	42.95	42.95	41.97	44.21
1796.89	42.95	42.95	42.07	44.03	42.95	42.95	42.07	44.10
1799.90	43.25	42.95	42.16	43.94	43.25	42.95	42.15	44.00
1802.90	43.25	43.25	42.25	43.86	43.25	43.25	42.23	43.92
1805.90	43.25	43.25	42.33	43.81	43.25	43.25	42.31	43.86
1808.91	43.25	43.25	42.41	43.80	43.25	43.25	42.39	43.83
1811.91	43.55	43.25	42.50	43.82	43.55	43.25	42.48	43.84
1814.91	43.55	43.55	42.60	43.87	43.55	43.55	42.57	43.88
1817.92	43.55	43.55	42.70	43.92	43.55	43.55	42.68	43.92
1820.92	43.85	43.55	42.82	43.98	43.85	43.55	42.79	43.98
1823.93	43.85	43.85	42.94	44.05	43.85	43.85	42.91	44.05
1826.93	43.85	43.85	43.07	44.12	43.85	43.85	43.04	44.12
1829.93	43.85	43.85	43.19	44.19	43.85	43.85	43.17	44.19
1832.94	44.15	43.85	43.31	44.27	44.15	43.85	43.29	44.27
1835.94	44.15	44.15	43.43	44.35	44.15	44.15	43.41	44.34
1838.94	44.15	44.15	43.54	44.42	44.15	44.15	43.52	44.42
1841.95	44.15	44.15	43.65	44.50	44.15	44.15	43.63	44.50
1844.95	44.45	44.45	43.75	44.58	44.45	44.45	43.73	44.58
1847.96	44.45	44.45	43.84	44.66	44.45	44.45	43.82	44.66